universität wien

MASTERARBEIT / MASTER'S THESIS

Titel der Masterarbeit / Title of the Master's Thesis

Diagrammatic Quantum Monte Carlo for the Fröhlich Polaron

verfasst von / submitted by

Thomas Hahn BSc

angestrebter akademischer Grad / in partial fulfilment of the requirements for the degree of

Master of Science (MSc)

Wien, 2017 / Vienna, 2017

Studienkennzahl lt. Studienblatt / degree programme code as it appears on the student record sheet:	A 066 910
Studienrichtung lt. Studienblatt / degree programme as it appears on the student record sheet:	Masterstudium Computational Science UG2002
Betreut von / Supervisor:	Assoz. Prof. Dr. Cesare Franchini

Abstract

Thomas HAHN

Diagrammatic Quantum Monte Carlo for the Fröhlich Polaron

The aim of the present thesis is to implement a working Diagrammatic Quantum Monte Carlo (DQMC) code and apply it to the three and two dimensional Fröhlich polaron. The algorithm used is based on the papers by Prokef'ev *et al.* [Physical Review Letters. **81**(1):2514 (1998)] and Mishchenko *et al.* [Physical Review B. **62**(10):6317 (2000)] in which they used the DQMC method successfully to calculate properties of the 3D Fröhlich polaron. To date, there are no DQMC results for the 2D case.

In the first chapters, this thesis introduces the polaron problem with focus on the Fröhlich Hamiltonian. It further gives an overview of Green's functions in many-body physics and their connections to Feynman diagrams as well as a detailed derivation of the diagrammatic expansion of the Green's function for the Fröhlich polaron. Basic principles of Monte Carlo and especially of DQMC simulations are reviewed. The last part of the thesis describes in detail how the DQMC algorithm can be applied to the Fröhlich polaron before presenting and discussing the obtained results.

The results support the expectation that, for Fröhlich polarons, the polaronic effect in two spatial dimensions is greater than in three. They also show the usefulness of the DQMC method and some of its limitations, especially of the implemented code. Further improvement of the code could overcome these limitations and small modifications could be enough to apply it to other interesting physical systems.

Zusammenfassung

Thomas HAHN

Diagrammatic Quantum Monte Carlo for the Fröhlich Polaron

Das Ziel der vorliegenden Arbeit ist es, einen funktionierenden Diagrammatic Quantum Monte Carlo (DQMC) Code zu implementieren und ihn zu verwenden, um Berechnungen am drei- bzw. zweidimensionalen Fröhlich Polaron durchzuführen. Der implementierte DQMC Algorithmus wird in den Studien von Prokef'ev *et al.* [Physical Review Letters. **81**(1):2514 (1998)] und Mishchenko *et al.* [Physical Review B. **62**(10):6317 (2000)] beschrieben, in denen die DQMC Methode erfolgreich angewendet wurde, um Eigenschaften des 3D Fröhlich Polarons zu berechnen. Bis heute sind keine DQMC Resultate für den zweidimensionalen Fall bekannt.

Die ersten Kapitel dieser Arbeit geben eine Einführung in die Polaron Thematik mit besonderem Augenmerk auf dem Fröhlich Hamiltonoperator. Des Weiteren werden Greensche Funktionen in der Vielteilchentheorie und deren Zusammenhang zu Feynman Diagrammen besprochen. Es folgt ein allgemeiner Überblick über Monte Carlo- und DQMC Simulationen. Zum Schluss wird sehr detailiert beschrieben, wie der DQMC Algorithmus für das Fröhlich Polaron verwendet werden kann, und es werden die Resultate presentiert.

Die Ergebnisse bestätigen die Erwartung, dass für das Fröhlich Polaron die polaronischen Effekte in zweidimensionalen Systemen stärker in Erscheinung treten als in dreidimensionalen Systemen. Sie unterstreichen die Nützlichkeit der DQMC Methode, zeigen aber auch ihre Grenzen auf, speziell von der vorliegenden Implementierung. Durch einige Verbesserungen und Änderungen könnte diese auch auf andere interessante Systeme angewendet werden.

Acknowledgements

My special thanks go to my supervisor of this thesis, Assoz. Prof. Dr. Cesare FRANCHINI from the Department of Computational Materials Physics at the University of Vienna, for giving me the opportunity and especially enough time to work in a field and on a subject I wasn't too familiar with. He was always very helpful and supportive and pointed me in the right direction.
Furthermore, I would like to thank Prof. Dr. Jacques TEMPERE and Dr. Sergei KLIMIN from the University of Antwerp for the very informative discussions and the insight they provided.

Contents

List of Figures

List of Tables

List of Symbols

$\langle \dots \rangle$	expectation value
$\hat{q}$	quantum mechanical operator of quantity q
$\bar{q}$	arithmetic mean of quantity q
$\|\phi_0\rangle$, $\|0\rangle$	ground state of the unperturbed Hamiltonian
$\|\Psi_0\rangle$	true ground state of the full Hamiltonian
$\hat{a}_\mu^\dagger$, $\hat{a}_\mu$	creation, annihilation operator of electrons in state μ
$\hat{b}_\mu^\dagger$, $\hat{b}_\mu$	creation, annihilation operator of phonons in state μ
$\hat{c}_\nu^\dagger$, $\hat{c}_\nu$	creation, annihilation operator of particles in state ν
$\mathcal{D}_n$	nth-order Feynman diagram
D	dimensionality
$D(\mathbf{r})$, $D(\mathbf{r}, \mathbf{r}_{el})$	electric displacement field
$D^0(\mathbf{w}, \tau)$	free phonon Green's function
e	elementary charge
$E[\dots]$	expectation value
$E_c(\alpha)$	continuum edge
E_0, $E_0(\mathbf{k})$, $E_0(\mathbf{k}, \alpha)$	lowest energy for a given $\mathbf{k}$ and α
$E(\mathbf{r})$	electric field
$G(\mathbf{k}, \tau)$	one-electron Green's function
$G_N(\mathbf{k}, \tau; \mathbf{q}_N, \dots, \mathbf{q}_1)$	one-electron-N-phonon Green's function
$\tilde{G}_N(\mathbf{k}, \tau; \mathbf{q}_N, \dots, \mathbf{q}_1)$	reduced one-electron-N-phonon Green's function
$G^0(\mathbf{k}, \tau)$	free electron Green's function
H	Fröhlich Hamiltonian
H_0	unperturbed Hamiltonian
H_1 (H_1^I)	interaction Hamiltonian (Interaction picture)
$\hbar$	reduced Planck constant
i	imaginary unit
k	modulus of wave vector $\mathbf{k}$
k_c	wave vector length corresponding to E_c
$\mathbf{k}$	electron/total wave vector
L	Lagrange function
m_e	bare electron mass
m^*	effective electron mass
m_{pol}	polaron effective mass
M_i	mass of nucleus i

n	order of diagram
N	number of external phonons
$\bar{N}$	average number of phonons of the polaron
$p_{\mathcal{A}}$	probability of addressing update $\mathcal{A}$
$\mathbf{p}_{el}$	electron momentum
$\mathbf{P}$	nucleus/ion momentum
$P(\mathbf{k}, \tau)$	function of interest in the DQMC
$\mathbf{P}(\mathbf{r})$	electric polarization field
q_1, q_2	weak-coupling coefficient
$\mathbf{q}$	external phonon wave vector
$\mathbf{r}$	position vector
$\mathbf{r}_{el}$	electron coordinates
R	acceptance ratio
$\mathbf{R}$	nucleus/ion coordinates
$\mathbf{R}_i^{(0)}$	equilibrium position of ion i
s_X	sample standard error of the random variable X
s_X^2	sample variance of the random variable X
t	time
$\hat{T}$, $\hat{T}_\tau$	(imaginary) time-ordering operators
U_S, U_I	time evolution operator
$Var[\dots]$	variance
V_D	volume in D dimensions
w	modulus of the wave vector $\mathbf{w}$
$\mathbf{w}$	(internal) phonon wave vector
$\mathbf{z}_i$	ionic displacement
$Z_0^{(N)}(\mathbf{k})$	polaron Z-factor
α	electron-phonon coupling constant
γ	vibrating mass of the polarization field
$\epsilon_n(\mathbf{k})$, $\epsilon(\mathbf{k})$	dispersion relation of a Bloch electron
η	strong-coupling coefficient
μ	free parameter in DQMC algorithm
ξ	topology index of a Feynman diagram
σ_X	standard deviation of the random variable X
σ_X^2	variance of the random variable X
τ	real variable in imaginary time formalism
ω	constant frequency of longitudinal optical phonons

Chapter 1

Introduction

Theoretical investigations of solids on the microscopic level come with an inherent complexity due to the large number of particles involved. A solid, which is assumed to be a crystal, is composed of many particles (of order $10^{23} - 10^{24}$), all interacting with each other [1]. The particles can be divided into N_N positively charged atomic nuclei, where nucleus i has mass M_i and charge $Z_i e$ (e is the elementary charge), and N_e electrons, each with mass m_e and charge $-e$. In a crystal, atomic nuclei are arranged in a regular fashion giving rise to the crystal lattice. Charge neutrality of the solid requires that

$$N_e = \sum_{i=0}^{N_N} Z_i.$$

The most important force in solid-state physics is the electromagnetic force with the usual Coulomb potential. If we neglect relativistic effects, the full Hamilton operator for the electrons and atomic nuclei in a solid can immediately be written down. In first quantization, it is given by

$$\hat{H}_{full} = \hat{T}_e + \hat{V}_{e-e} + \hat{T}_N + \hat{V}_{N-N} + \hat{V}_{e-N}. \tag{1.1}$$

Here

$$\hat{T}_e = \sum_{i=1}^{N_e} \frac{\hat{\mathbf{p}}_{el,i}^2}{2m_e} \tag{1.2}$$

is the kinetic energy of the electrons,

$$\hat{T}_N = \sum_{i=1}^{N_N} \frac{\hat{\mathbf{P}}_i^2}{2M_i} \tag{1.3}$$

is the kinetic energy of the nuclei,

$$\hat{V}_{e-e} = \frac{1}{2} \sum_{\substack{i,j=1 \\ i \neq j}}^{N_e} v_{e-e}(\hat{\mathbf{r}}_{el,i}, \hat{\mathbf{r}}_{el,j}) = \frac{1}{2} \sum_{\substack{i,j=1 \\ i \neq j}}^{N_e} \frac{e^2}{|\hat{\mathbf{r}}_{el,i} - \hat{\mathbf{r}}_{el,j}|} \tag{1.4}$$

describes the interaction between electrons,

$$\hat{V}_{N-N} = \frac{1}{2} \sum_{\substack{i,j=1 \\ i \neq j}}^{N_N} v_{N-N}(\hat{\mathbf{R}}_i, \hat{\mathbf{R}}_j) = \frac{1}{2} \sum_{\substack{i,j=1 \\ i \neq j}}^{N_N} \frac{Z_i Z_j e^2}{|\hat{\mathbf{R}}_i - \hat{\mathbf{R}}_i|} \tag{1.5}$$

describes the interaction between nuclei and

$$\hat{V}_{e-N} = \sum_{i=1}^{N_e} \sum_{j=1}^{N_N} v_{e-N}(\hat{\mathbf{r}}_{el,i}, \hat{\mathbf{R}}_j) = \sum_{i=1}^{N_e} \sum_{j=1}^{N_N} \frac{-Z_j e^2}{|\hat{\mathbf{r}}_{el,i} - \hat{\mathbf{R}}_j|} \tag{1.6}$$

represents the interaction between electrons and nuclei. The momentum and position operators of the electrons and nuclei are given by $\hat{\mathbf{p}}_{el,i}$, $\hat{\mathbf{r}}_{el,i}$ and $\hat{\mathbf{P}}_i$, $\hat{\mathbf{R}}_i$, respectively [2].

The interaction potentials in Eq. 1.4, 1.5 and 1.6 are the well known Coulomb potentials. Equation 1.1 can also describe the situation where one distinguishes between inner core electrons and outer valence electrons. Core electrons are assumed to be tightly bound to a nucleus and to occupy closed inner electronic shells, while the valence electrons occupy non-closed outer shells and are responsible for the chemical bonds that form the solid. An atomic nucleus together with its cloud of core electrons can be seen as one rigid charge, which will be referred to as an ion. In this case, the Hamiltonian becomes a function of the coordinates and momenta of $N_{e'}$ outer valence electrons and $N_I = N_N$ ions. Thus a solid can also be seen as an interacting system of lattice ions and valence electrons. When this point of view is used, one has to be aware that the interaction potentials $v_{I-I}(\mathbf{R}_i, \mathbf{R}_j)$ and $v_{e-I}(\mathbf{r}_{el,i}, \mathbf{R}_j)$ are no longer given by the simple Coulomb potentials from Eq. 1.5 and 1.6 since the core electrons in the inner shells of the ions screen the positive charge of the nuclei from their surroundings [1, 2, 3].

Due to the large number of ions and electrons in a solid and the long range Coulomb interaction between them, exact solutions to the many-body Schrödinger equation for the full Hamiltonian (Eq. 1.1) seem to be impossible to find. We therefore have to introduce various approximations and model systems. An obvious strategy is to focus on a certain subsystem that can be represented by an effective Hamiltonian which, in contrast to the original problem, can be treated or even solved exactly with known methods. The first obvious approximation is to separate the electronic and ionic motions in Eq. 1.1 which leads to two famous model systems:

1. Bloch electrons [4] describe the motion of independent electrons in a static, periodic potential field created by a rigid ionic lattice. The solutions of the corresponding Schrödinger equation are the well-known Bloch states. This periodic potential can be derived from the general electron-ion interaction

term in Eq. 1.6. The momentary position of ion j can be written as

$$\mathbf{R}_j = \mathbf{R}_j^{(0)} + \mathbf{z}_j, \tag{1.7}$$

where $\mathbf{R}_j^{(0)}$ is the ion's equilibrium position and $\mathbf{z}_j$ is its current deviation from this position. For small $\mathbf{z}_j$, the potential can be expanded around the equilibrium positions of the ions, so that the interaction between electron i and ion j becomes

$$V(\hat{\mathbf{r}}_{el,i} - \hat{\mathbf{R}}_j) = V(\hat{\mathbf{r}}_{el,i} - \hat{\mathbf{R}}_j^{(0)}) - \nabla V(\hat{\mathbf{r}}_{el,i} - \hat{\mathbf{R}}_j^{(0)}) \cdot \hat{\mathbf{z}}_j + \mathcal{O}(z_j^2). \tag{1.8}$$

Considering only the zeroth-order term, the ions are fixed at their equilibrium positions and the two-particle electron-ion interaction operator is approximated by an one-particle operator which depends only on the position of the electron. The ionic equilibrium coordinates enter this operator as fixed parameters. Since the interaction between electrons is neglected, one only has to deal with a one-body Hamiltonian (in position basis)

$$H_{Bloch}(\frac{\hbar}{i}\nabla_{\mathbf{r}_{el}}, \mathbf{r}_{el}) = -\frac{\hbar^2}{2m_e}\nabla^2_{\mathbf{r}_{el}} + V_{\mathbf{R}_1^{(0)},\ldots,\mathbf{R}_{N_N}^{(0)}}(\mathbf{r}_{el}), \tag{1.9}$$

in which $\mathbf{r}_{el}$ are the coordinates of the electron and the potential is periodic with an arbitrary lattice vector $\mathbf{G}$:

$$V_{\mathbf{R}_1^{(0)},\ldots,\mathbf{R}_{N_N}^{(0)}}(\mathbf{r}_{el}) = V_{\mathbf{R}_1^{(0)},\ldots,\mathbf{R}_{N_N}^{(0)}}(\mathbf{r}_{el} + \mathbf{G}).$$

Solutions to this problem are the Bloch functions $\Psi_{n\mathbf{k}}(\mathbf{r}_{el})$:

$$H_{Bloch}\Psi_{n\mathbf{k}}(\mathbf{r}_{el}) = \epsilon_n(\mathbf{k})\Psi_{n\mathbf{k}}(\mathbf{r}_{el}) \rightarrow \Psi_{n\mathbf{k}}(\mathbf{r}_{el}) = \frac{1}{\sqrt{V_D}} e^{i\mathbf{k}\mathbf{r}_{\mathbf{el}}} u_{n\mathbf{k}}(\mathbf{r}_{el}), \tag{1.10}$$

where $\mathbf{k}$ is a wave vector, V_D is the volume of the lattice in D dimensions, n is the so called band index, $u_{n\mathbf{k}}(\mathbf{r}_{el})$ is a periodic function with the same periodicity as the potential field and $\epsilon_n(\mathbf{k})$ is the energy spectrum or band structure of the Bloch electron. This means that for a given wave vector $\mathbf{k}$ there are an infinite number of solutions, $u_{n\mathbf{k}}(\mathbf{r}_{el})$ and $\epsilon_n(\mathbf{k})$, indexed by the band number n. The energy bands are filled up from below by the electrons according to the Pauli principle. The last fully occupied band is usually called valence band and the next higher one, which is either empty or partially filled, is called conduction band. For small $\mathbf{k}$ values and an isotropic energy band, $\epsilon_n(\mathbf{k})$ can be developed around $k = 0$ leading to

$$\epsilon_n(\mathbf{k}) = \epsilon_n(\mathbf{0}) + \frac{\hbar^2 k^2}{2m^*}. \tag{1.11}$$

Equation 1.11 has the form of the dispersion relation of a free electron except that the electron mass m_e is replaced by an effective band mass m^* [1].

2. Phonons describe the motions ions in their own potential field and are derived from the corresponding Hamilton operator:

$$\hat{H}'_{ions} = \hat{T}_I + \hat{V}_{I-I}(\hat{\mathbf{R}}_1, \ldots, \hat{\mathbf{R}}_{N_I}) = \sum_{i=1}^{N_I} \frac{\hat{\mathbf{P}}_i^2}{2M_i} + \frac{1}{2} \sum_{\substack{i,j=1 \\ i \neq j}}^{N_I} v_{I-I}(\hat{\mathbf{R}}_i, \hat{\mathbf{R}}_j). \tag{1.12}$$

The ions in the solid form a crystal lattice but can still move around their equilibrium positions $\mathbf{R}_i^{(0)}$. By expanding $\hat{V}_{I-I}(\hat{\mathbf{R}}_1, \ldots, \hat{\mathbf{R}}_{N_I})$ around these equilibrium positions and neglecting terms higher than 2^{nd}-order, i.e. using a harmonic approximation, one arrives at an effective Hamiltonian describing a set of coupled harmonic oscillators. This Hamiltonian can be diagonalized with a canonical transformation to the normal modes of the lattice, so that in the end the problem has reduced to a set of non-interacting bosonic quasi-particles, called phonons. The final form of the Hamiltonian and its solutions are then usually given in terms of creation ($\hat{b}^\dagger_{\mathbf{w}r}$) and annihilation ($\hat{b}_{\mathbf{w}r}$) operators [3]:

$$\hat{H}_{ions} = \sum_{\mathbf{w}} \sum_{r=1}^{D*n_I} \hbar\omega_r(\mathbf{w}) \left(\hat{b}^\dagger_{\mathbf{w}r} \hat{b}_{\mathbf{w}r} + \frac{1}{2} \right), \tag{1.13}$$

where D is the dimension of the problem, n_I is the number of ions in the unit cell, $\omega_r(\mathbf{w})$ are the eigenfrequencies and

$$E_0 = \sum_{\mathbf{w}} \sum_{r=1}^{D*n_I} \hbar\omega_r(\mathbf{w}) \frac{1}{2} \tag{1.14}$$

is the ground state energy when no phonons are present. The index r represents the phonon branch. There are $D * n_I$ different branches for each wave vector $\mathbf{w}$ in a D-dimensional lattice with n_I ions in the unit cell.

The last example describes a very common approach used in many-body physics where a system of strongly interacting particles is transformed into a system of weakly or non-interacting 'fictitious' particles, also called quasi-particles or elementary excitations. This has the advantage that the new system can be solved either exactly, like in the phonon case, or treated with known methods, e.g. perturbation theory. In general, a Hamiltonian consisting of a one-body operator $\hat{T}$ and a two-body interaction operator $\hat{V}$ is given in second quantization by

$$\hat{H} = \hat{T} + \hat{V} = \sum_{\alpha,\beta} \langle \alpha | T | \beta \rangle \, \hat{c}^\dagger_\alpha \hat{c}_\beta + \sum_{\alpha,\beta,\gamma,\delta} \langle \alpha\beta | V | \gamma\delta \rangle \, \hat{c}^\dagger_\alpha \hat{c}^\dagger_\beta \hat{c}_\delta \hat{c}_\gamma. \tag{1.15}$$

Using a canonical transformation, it can be turned into a system of weakly interacting elementary excitations above the ground state E_0

$$\hat{H} = E_0 + \sum_{\mu} \epsilon_\mu \hat{d}^\dagger_\mu \hat{d}_\mu + f(\ldots, \hat{d}_\mu, \ldots, \hat{d}^\dagger_\mu, \ldots), \tag{1.16}$$

where $\hat{d}^\dagger_\mu$ and $\hat{d}_\mu$ are the creation and annihilation operators for the elementary excitations, ϵ_μ is their dispersion relation and $f(\ldots, \hat{d}_\mu, \ldots, \hat{d}^\dagger_\mu, \ldots)$ represents the remaining small interaction between them [5].

This thesis will be concerned with a quasi-particle used in condensed matter physics, called polaron. A polaron can be described as an electron in a crystal that 'dresses' itself with phonons due to interactions with the dynamic ionic lattice (cf. Bloch electrons, where the lattice is considered to be static). Mathematically this interaction corresponds to the first order term in Eq. 1.8. When the electron moves through the lattice, the phonon cloud gets carried with it and so modifies the electron's properties (effective mass, energy spectrum, responses to external electrical and magnetic fields, etc.). The complex, consisting of the electron together with the lattice distortion induced by it, is seen as one entity. The polaron problem consists in calculating the properties of this entity.

One of the most famous model Hamiltonian, describing an electron coupled to a dynamic lattice, is the Fröhlich Hamiltonian [6]. It considers a conduction electron interacting with a dielectric medium. The Fröhlich Hamiltonian has been of great interest ever since its emergence in the middle of the 20^{th} century. Especially as a non-relativistic quantum field theoretical model that couples a fermionic particle to a scalar boson field and as a simple mathematical problem, it got the attention of a lot of famous physicists. For example, Richard Feynman calculated the ground state energy and effective mass of the Fröhlich polaron to a very high accuracy using his path integral approach [7]. To this day it serves as a testing ground for new analytical and numerical methods [8]. In 1998 Prokof'ev *et al.* [9] developed a new Quantum Monte Carlo method that allows one to sample Feynman diagrams stochastically. This method is called Diagrammatic Quantum Monte Carlo and has also been tested on the Fröhlich polaron [9, 10]. Ever since then, the DQMC has been further improved and applied successfully to more sophisticated problems (see e.g. [11, 12, 13, 14, 15]).

As part of this thesis, the Diagrammatic Quantum Monte Carlo algorithm is implemented as described by Prokf'ev *et al.* [9] and Mishchenko *et al.* [10] to obtain ground state energies, effective masses and other properties of the Fröhlich polaron in 3 dimensions as well as 2 dimensions. The results are then compared to [9, 10] and to other numerical and analytical treatments.

1.1 Outline

- Chapter 2 introduces the polaron problem in more detail and gives some historical remarks on how it originated. Then follows a complete derivation of the Fröhlich Hamiltonian in 3 dimensions and a short overview of some analytical methods to treat this Hamiltonian. The changes, which have to be made to go from 3D to 2D, are also mentioned.

- Chapter 3 reviews some important aspects of many-body physics and quantum field theory, like Green's functions and Feynman diagrams. These will be later necessary for the DQMC technique.

- Chapter 4 starts with some general notes on Monte Carlo methods, what they are, how they are used and how one samples results and estimates errors. After that, the Diagrammatic Quantum Monte Carlo method is introduced.

- Chapter 5 gives instructions on how the Diagrammatic Quantum Monte Carlo method can be used for the Fröhlich Hamiltonian. It is to a large extent based on [9, 10]. Since literature on DQMC implementations is rather scarce, this thesis tries to go into great detail and to explain every step of the algorithm.

- Chapter 6 presents the results obtained from the DQMC implementation. They are compared to analytical methods (exactly known expansions, Feynman's path integral) and the difference between 3D and 2D is discussed. At the end, some conclusive remarks are given and possible modifications and future projects are pointed out.

Chapter 2

The polaron problem

2.1 Historical remarks

Electronic motion in crystals has been of enormous interest ever since the beginning of solid-state physics in the 1920s and 1930s. As already mentioned in Eq. 1.10, electrons in the periodic potential field of a rigid crystal lattice have an energy spectrum consisting of allowed and forbidden bands [4]. An electron at the bottom of such an allowed band behaves as a free particle but with a mass different from the bare electron mass (Eq. 1.11).

The concept of the polaron arose a few years later in 1933 from the famous paper by L. Landau "Über die Bewegung der Elektronen im Kristallgitter" in which he tried to explain F-centres in NaCl [16]. In this very short paper, Landau argued that for a system consisting of an electron in a crystal lattice the energetically most favourable state is either the state, where the electron is moving freely in an undistorted or only slightly distorted lattice, or the state, where the electron is trapped in a strongly distorted lattice. The latter can be associated with a localized polaron state in the strong-coupling limit [17].

Pekar picked up Landau's concept and developed the idea further for an electron coupled to lattice distortions in an ideal (no defects) ionic crystal [18, 19]. He was the first to introduce the term "polaron" for a local quantum state of an electron. This state arises because the electron polarizes its surrounding ionic lattice dielectrically with its own electric field, thus creating small dipole moments. The interaction between the electron and the dipole moments can produce a potential well in which the electron can become localized [18, 20].

To describe the polaron state, Pekar developed a macroscopic semiclassical model for a free electron coupled to a polarizable dielectric continuum. The continuum approximation, i.e. ignoring the discreteness of the lattice, is valid if coupling to long-wavelength optical phonons dominates the interaction and if the radius of the localized state is large compared to the lattice constant. In this model, the dielectric medium is characterized by its static and high frequency dielectric constants. Such

approximations are appropriate for an electron interacting with optical phonons [17, 8]. Pekar calculated the ground state energy and wave function for this self-trapped electron state by using a variational method [20].

In a perfect lattice, the self-trapping is never complete and hence the electron plus its surrounding polarization can move through the medium. The electron has to move slowly, i.e. with low kinetic energy, so that the ionic polarization can follow the electron. In that case, the polaron behaves as a free electron but with an enhanced effective mass [8]. Landau and Pekar were the first to calculate the effective mass of a polaron [21]. Fröhlich later showed that the results obtained by Pekar and Landau can be obtained with a variational method in the strong-coupling limit of the Fröhlich model [6].

While Pekar's model is semiclassical, i.e. the lattice properties are incorporated into a classical macroscopic polarization [22], Fröhlich *et al.* [23, 6] introduced the first microscopic model of a polaron. In this model, the lattice dynamics or lattice polarization is treated quantum mechanically. The famous Fröhlich Hamiltonian in 3D has the form

$$\hat{H} = \hat{H}_{el} + \hat{H}_{ions} + \hat{H}_{inter}, \tag{2.1}$$

where

$$\hat{H}_{el} = \frac{\hat{\mathbf{p}}_{el}^2}{2m^*} \tag{2.2}$$

represents the kinetic energy of the electron plus its potential energy in the static, periodic potential field of the lattice,

$$\hat{H}_{ions} = \hbar\omega \sum_{\mathbf{w}} \left(\hat{b}_{\mathbf{w}}^\dagger \hat{b}_{\mathbf{w}} + \frac{1}{2} \right) \tag{2.3}$$

stands for the kinetic and potential energy of the lattice and

$$\hat{H}_{inter} = \sum_{\mathbf{w}} 4\pi i \left(\frac{\hbar e^2}{2\gamma\omega V_3} \right)^{\frac{1}{2}} \frac{1}{w} \left(\hat{b}_{\mathbf{w}}^\dagger e^{-i\mathbf{w}\cdot\hat{\mathbf{r}}_{el}} - \hat{b}_{\mathbf{w}} e^{i\mathbf{w}\cdot\hat{\mathbf{r}}_{el}} \right) \tag{2.4}$$

describes the interaction between the electron and the dynamic lattice (longitudinal optical phonon field). In the above equations, ω is the constant frequency of a longitudinal optical phonon and γ can be interpreted as the vibrating mass of the polarization field (see Sec. 2.3).

The Fröhlich Hamiltonian has been of great interest to various branches of solid-state physics ever since its introduction to the physics community. Besides its physical importance, i.e. properties of electrons in polar materials and ionic crystals, it is also often used as a pure mathematical problem. The Fröhlich Hamiltonian is one of the simplest quantum field theoretical models in solid-state

physics. In a general form, it describes a particle coupled to its environment. For this thesis, the particle will be an electron and its environment will be a longitudinal optical phonon field. A detailed derivation of the Fröhlich Hamiltonian will be given in Sec. 2.3.

2.2 General remarks

This section gives some general remarks on polarons. As mentioned before, in a real lattice the ions are not fixed but oscillate around their equilibrium position. These ionic displacements can be described in terms of phonons (Eq. 1.16) which interact with electrons. In the literature, this is usually called electron-phonon coupling or electron-phonon interaction (EPI). The strength of the interaction is referred to as electron-phonon coupling strength. EPI has two different effects [17]:

- scattering of the electron, leading to electrical resistance and
- changing the properties of the electron.

In an ionic crystal, an electron deforms the lattice in its neighbourhood due to Coulomb forces. This induces vibrations of the crystal lattice leading to a cloud of virtual phonons surrounding the electron. When the electron moves through the lattice, the cloud moves with it. As already mentioned, the complex entity consisting of the electron and the phonon cloud is called a polaron which has an increased effective mass and a lower energy than the Bloch electron. Electron-phonon coupling is of course material dependent. Whether we are considering ionic polar crystals, metals or a covalent materials, the form of the electron-phonon interaction, the strength of the EPI and especially the relevant phonon modes, which couple to the electron, changes. This thesis will exclusively focus on ionic polar crystals. In later chapters, it will be seen that the dimensionality D of the system plays also a major role in determining the properties of the polaron [17, 24].

Polarons can be classified according to the coupling strength between the electron and the phonon field. The stronger the coupling the more phonons will be in the cloud surrounding the electron. If the average number $\bar{N}$ of phonons in the cloud (see Sec. 6.1.3) is $\bar{N} \ll 1$, it is called a weak-coupling polaron. If on the other hand $\bar{N} \gg 1$, the polaron will be regarded as a strong-coupling polaron [17]. The size r_p of the polaron is also important. It is measured by the extension of the lattice distortion induced by the excess electron [25]. A small polaron has a size of order of the lattice constant $r_p \approx a$. In this case, the atomic structure of the lattice has to be taken into account when deriving a suitable Hamilton operator, e.g. Holstein Hamiltonian [26, 27]. Large polarons have $r_p \gg a$, so that the discreteness of the lattice can be ignored and the continuum approximation becomes valid, e.g. Fröhlich Hamiltonian [6].

2.3 The Fröhlich Hamiltonian

In this section, a detailed derivation of the Fröhlich Hamiltonian will be given. It is closely based on Fröhlich's original paper "Electrons in lattice fields" [6] and his lecture in "Polarons and Excitons" [28] but also considers ideas from Haken [1] and Mitra *et al.* [29].

The Fröhlich Hamiltonian describes a free (no interaction with other electrons) conduction electron in an isotropic, ionic crystal. The main idea in deriving this model is to keep the description of the motion of the electron and of the ion lattice as simple as possible. Therefore it is assumed that the electron is slowly moving and low-lying in the conduction band and behaves like a Bloch electron if the lattice dynamics are neglected, i.e. if the lattice ions produce a static, strictly periodic potential field. Then the energy dispersion of the electron is given by a single valued (one energy band), quadratic function of its momentum $\hbar\mathbf{k}$

$$\epsilon_n(\mathbf{k}) = \epsilon(\mathbf{k}) = \frac{\hbar^2 k^2}{2m^*}. \tag{2.5}$$

In real crystals, the electron experiences also other forces resulting from deviations of the strictly periodic potential due to ionic deformations and displacements from their equilibrium positions. Neglecting the deformations, the displacements of the lattice ions can be described by attaching displacement vectors $\mathbf{z}_i$ to each lattice point i. This leads to individual dipole moments $e^*\mathbf{z}_i$ with an effective charge e^*. Since the electron lies at the lower edge of the conduction band (small k value), its De Broglie wavelength is large compared to the interionic spacing which means that the electron's wave function changes only little over one lattice constant. If it is further assumed that the important phonon modes have a similarly long wavelength, the atomicity of the lattice can be ignored and the continuum approximation may be used. The individual displacement vectors then become a continuous function of position and the dipole moments get replaced by a dipole density or an electric polarization field $e^*\mathbf{z}_i \to \mathbf{P}(\mathbf{r})$. Lattice dynamcis are therefore described in terms of $\mathbf{P}(\mathbf{r})$. Our derivation of the Fröhich Hamiltonian follows a standard quantization procedure:

- derive equations of motions for the coupled system (electron + polarization field)
- introduce Lagrange function
- introduce Hamilton function with conjugate momenta and coordinates
- quantization.

The model is largely based on macroscopic dielectric theory. In a polar crystal, the dielectric constant $\epsilon(\omega)$ has low- and high-frequency resonances in the infrared

frequency range at ω_{ir} and in the optical or ultraviolet frequency range at ω_{op}. The first one corresponds approximately to the displacement polarization of the ionic lattice when a positive and negative ion oscillate in antiphase and the second one corresponds to the polarization due to the deformation of the electronic cloud of the ions. Therefore the total polarization $\mathbf{P}_{tot}$ may be written as a linear superposition of

$$\mathbf{P}_{tot} = \mathbf{P}_{ir} + \mathbf{P}_{op}. \tag{2.6}$$

From classical electrodynamics, the general relations between the electric displacement field $\mathbf{D}$, the electric field $\mathbf{E}$ and the electric polarization field $\mathbf{P}$

$$\mathbf{D} = \mathbf{E} + 4\pi\mathbf{P}, \quad \mathbf{D} = \epsilon(\omega)\mathbf{E}, \quad \mathbf{P} = \frac{1}{4\pi}\left(1 - \frac{1}{\epsilon(\omega)}\right)\mathbf{D} \tag{2.7}$$

are known. In the static field limit, both polarizations $\mathbf{P}_{ir}$ and $\mathbf{P}_{op}$ have time to fully develop and from the relations in Eq. 2.7 it follows

$$\mathbf{P}_{tot} = \frac{1}{4\pi}\left(1 - \frac{1}{\epsilon_0}\right)\mathbf{D}, \tag{2.8}$$

where ϵ_0 is the static dielectric constant. In the high-frequency field limit, corresponding to the frequency ω_∞, where $\omega_{op} \ll \omega_\infty \ll \omega_{ir}$, only $\mathbf{P}_{op}$ contributes to the polarization because the electrons giving rise to ionic deformations have a much smaller inertia than the heavy ions. Thus

$$\mathbf{P}_{op} = \frac{1}{4\pi}\left(1 - \frac{1}{\epsilon_\infty}\right)\mathbf{D}, \tag{2.9}$$

with ϵ_∞ as the high frequency dielectric constant. Combining the static and high-frequency case, the polarization due to the displacements of ions can be expressed in terms of an effective dielectric constant $\bar{\epsilon}$:

$$\mathbf{P}_{ir} = \frac{1}{4\pi}\left(\frac{1}{\epsilon_\infty} - \frac{1}{\epsilon_0}\right)\mathbf{D} = \frac{1}{4\pi\bar{\epsilon}}\mathbf{D}. \tag{2.10}$$

The reason for the above calculations is that we are only interested in the interaction between $\mathbf{P}_{ir}$ and the electron. Since the electronic clouds, which contribute to $\mathbf{P}_{op}$, can follow a slow electron adiabatically, the optical polarization will always be excited independent of the electron's velocity. When deriving the Hamiltonian, terms that contain $\mathbf{P}_{op}$ can be considered as constant and so they are going to be omitted in the following (see [6, 28] for a more rigorous justification). The important part of the polarization $\mathbf{P}_{ir}$ and ω_{ir} will be denoted simply as $\mathbf{P}$ and ω from now on.

Before deriving the equations of motion for the electron and the polarization field, it pays off to think about which vibrational modes of the lattice actually interact with the electron. As is well known, in a 3 dimensional crystal lattice with n_I ions

in a unit cell, there are $3n_I$ different branches of vibration for each wave vector $\mathbf{w}$. Let's assume that there are two different ions in a unit cell and therefore 6 different branches. For 3 of these branches, their dispersion $\omega(\mathbf{w}) \rightarrow 0$ for $\mathbf{w} \rightarrow \mathbf{0}$ corresponding to rigid translations of the whole crystal. They are called acoustic phonons/branches and do not contribute to the electric polarization $\mathbf{P}(\mathbf{r})$, thus they will be ignored. The other 3 branches are called optical branches and their dispersion does not go to zero when $\mathbf{w}$ does. They correspond to vibrations where neighbouring ions are moving out-of-phase and therefore produce dipole moments. These are the interesting modes for the Fröhlich polaron. Optical phonons can be further classified as longitudinal and transversal. Longitudinal optical branches are to a good approximation parallel to $\mathbf{w}$ while transversal optical branches are perpendicular to $\mathbf{w}$. Since the transversal branches do not create any polarization along the wave vector, their effect will also be neglected. Fröhlich further assumes that the phonons are dispersionless $\omega(\mathbf{w}) = \omega$ for all $\mathbf{w}$. So the only phonons that will be considered from now on are longitudinal optical phonons with a constant dispersion ω independent of the wave vector [30].

To derive an equation of motion for the electric polarization field under the influence of an electron, let's assume that each dipole moment can be described as a free harmonic oscillator if no external field, in our case an electron, is present. The total energy of all N_I dipole moments is then given by

$$\sum_i \frac{m_i}{2}(\dot{\mathbf{z}}_i^2 + \omega^2 \mathbf{z}_i^2), \tag{2.11}$$

with m_i being its vibrating mass, $\mathbf{z}_i$ its displacement vector and ω its characteristic frequency. Upon changing from a discrete ionic lattice to a dielectric continuum, the mass density $\rho_m(\mathbf{r})$ is introduced

$$m_i = \rho_m(\mathbf{r})d\mathbf{r} \tag{2.12}$$

and a new parameter γ is defined as

$$\frac{m_i}{(e^*)^2} = \frac{\rho_m(\mathbf{r})}{(e^*)^2}d\mathbf{r} = \gamma d\mathbf{r}. \tag{2.13}$$

The total energy (kinetic + potential energy) of the free polarization field can then be written as

$$T_{pol} + V_{pol} = \int \frac{\gamma}{2}\dot{\mathbf{P}}^2(\mathbf{r})d\mathbf{r} + \int \frac{\gamma}{2}\omega^2\mathbf{P}^2(\mathbf{r})d\mathbf{r} \tag{2.14}$$

and the equation of motion for the free polarization field is a simple harmonic oscillator equation

$$\ddot{\mathbf{P}}(\mathbf{r}) + \omega^2\mathbf{P}^2(\mathbf{r}) = 0. \tag{2.15}$$

If the effect of an electron on the motion of $\mathbf{P}(\mathbf{r})$ should be incorporated into Eq. 2.15, one can start with the interaction energy between an electron with charge $-e$ at position $\mathbf{r}_{el}$ and a dipole moment $\mathbf{p}_d$ at position $\mathbf{r}$:

$$-e\frac{(\mathbf{r}-\mathbf{r}_{el})}{|\mathbf{r}-\mathbf{r}_{el}|^3}\mathbf{p}_d. \tag{2.16}$$

Again, when we are interested in the total energy and use the continuum approximation, the dipole moment gets replaced with a polarization field $\mathbf{P}(\mathbf{r})$ and the interaction energy is integrated to obtain

$$H_{inter} = -\int e\frac{(\mathbf{r}-\mathbf{r}_{el})}{|\mathbf{r}-\mathbf{r}_{el}|^3}\mathbf{P}(\mathbf{r})d\mathbf{r}. \tag{2.17}$$

Putting this all together into a Lagrange function yields

$$L' = T_{pol} - V_{pol} - H_{inter} = \int \frac{\gamma}{2}\dot{\mathbf{P}}^2(\mathbf{r})d\mathbf{r} - \int \frac{\gamma}{2}\omega^2\mathbf{P}^2(\mathbf{r})d\mathbf{r} + \int e\frac{(\mathbf{r}-\mathbf{r}_{el})}{|\mathbf{r}-\mathbf{r}_{el}|^3}\mathbf{P}(\mathbf{r})d\mathbf{r}. \tag{2.18}$$

The equation of motion for the polarization field in the presence of an electron is handed to us with help of the Euler-Lagrange equations

$$\frac{d}{dt}\frac{\delta L'\left(\mathbf{P}(\mathbf{r}),\dot{\mathbf{P}}(\mathbf{r})\right)}{\delta\dot{\mathbf{P}}_i(\mathbf{r}')} - \frac{\delta L'\left(\mathbf{P}(\mathbf{r}),\dot{\mathbf{P}}(\mathbf{r})\right)}{\delta\mathbf{P}_i(\mathbf{r}')} = 0, \tag{2.19}$$

where $i = x, y, z$. After performing the functional derivatives, one arrives at

$$\ddot{\mathbf{P}}(\mathbf{r}') + \omega^2\mathbf{P}(\mathbf{r}') = e\frac{(\mathbf{r}'-\mathbf{r}_{el})}{|\mathbf{r}'-\mathbf{r}_{el}|^3}\frac{1}{\gamma} = -\nabla_{\mathbf{r}'}\frac{e}{|\mathbf{r}'-\mathbf{r}_{el}|}\frac{1}{\gamma} = \mathbf{D}(\mathbf{r}',\mathbf{r}_{el})\frac{1}{\gamma}. \tag{2.20}$$

$\mathbf{D}(\mathbf{r}',\mathbf{r}_{el})$ is the electric displacement field whose source is the electronic point charge at $\mathbf{r}_{el}$. So the interaction term in the Lagrangian becomes

$$-\int \mathbf{D}(\mathbf{r},\mathbf{r}_{el})\cdot\mathbf{P}(\mathbf{r})d\mathbf{r}. \tag{2.21}$$

If no electron is present, the equation of motion in Eq. 2.20 reduces to Eq. 2.15.

Now it is time to find the parameter γ. For this purpose, let us consider the static case of Eq. 2.20, i.e. $\dot{\mathbf{P}}(\mathbf{r}) = 0$:

$$\gamma\omega^2\mathbf{P}(\mathbf{r}) = \mathbf{D}(\mathbf{r},\mathbf{r}_{el}). \tag{2.22}$$

If this equation is compared with Eq. 2.10, it immediately gives

$$\gamma = \frac{4\pi}{\omega^2}\bar{\epsilon} = \frac{4\pi}{\omega^2}\left(\frac{1}{\epsilon_\infty} - \frac{1}{\epsilon_0}\right)^{-1}. \tag{2.23}$$

This completes the derivation of the equation of motion for the polarization field.

It is still necessary to obtain an equation for the electron's motion. The electronic coordinates $\mathbf{r}_{el}$ already appear in the interaction term in the Lagrangian in Eq. 2.18 as a variable of $\mathbf{D}(\mathbf{r}, \mathbf{r}_{el})$. The electric displacement field for an electron at position $\mathbf{r_{el}}$ obeys

$$\nabla \times \mathbf{D}(\mathbf{r}, \mathbf{r}_{el}) = 0, \quad \nabla \cdot \mathbf{D}(\mathbf{r}, \mathbf{r}_{el}) = 4\pi\rho(\mathbf{r}) = 4\pi\delta(\mathbf{r} - \mathbf{r}_{el}). \tag{2.24}$$

By assuming that the interaction of $\mathbf{P}(\mathbf{r})$ with the magnetic field of the slow moving electron is negligible compared to the electrostatic interaction, the rotational part of $\mathbf{P}(\mathbf{r})$ becomes unimportant and it is permissible to write

$$\nabla \times \mathbf{P}(\mathbf{r}) = 0, \tag{2.25}$$

which allows us to define a polarization potential

$$4\pi\mathbf{P}(\mathbf{r}) = \nabla_{\mathbf{r}}\Phi(\mathbf{r}). \tag{2.26}$$

If the terms for $\mathbf{D}(\mathbf{r}, \mathbf{r}_{el})$ and for $\mathbf{P}(\mathbf{r})$ from Eq. 2.20 and 2.26 are put into the interaction term in Eq. 2.21, if it is integrated by parts and if the relation from Eq. 2.24 is used, one gets

$$\begin{aligned} -\int \mathbf{D}(\mathbf{r}, \mathbf{r}_{el}) \cdot \mathbf{P}(\mathbf{r}) d\mathbf{r} &= \frac{e}{4\pi} \int \nabla_{\mathbf{r}} \frac{1}{|\mathbf{r} - \mathbf{r}_{el}|} \nabla_{\mathbf{r}}\Phi(\mathbf{r}) d\mathbf{r} = \\ &= -\frac{e}{4\pi} \int \Phi(\mathbf{r}) \nabla^2_{\mathbf{r}} \frac{1}{|\mathbf{r} - \mathbf{r}_{el}|} d\mathbf{r} = e\Phi(\mathbf{r}_{el}). \end{aligned} \tag{2.27}$$

To be able to derive equations of motion for the electron from a Lagrangian, it is necessary to add the kinetic energy term

$$\frac{m^*}{2}\dot{\mathbf{r}}^2_{el}. \tag{2.28}$$

Now it is possible to write down the full Lagrange function for the coupled electron-polarization field system

$$L = \frac{m^*}{2}\dot{\mathbf{r}}^2_{el} + \int \frac{\gamma}{2}\dot{\mathbf{P}}^2(\mathbf{r}) d\mathbf{r} - \int \frac{\gamma}{2}\omega^2\mathbf{P}^2(\mathbf{r}) d\mathbf{r} + \int \mathbf{D}(\mathbf{r}, \mathbf{r}_{el}) \cdot \mathbf{P}(\mathbf{r}) d\mathbf{r}. \tag{2.29}$$

Using again the Euler-Lagrange equations for the general coordinates $\mathbf{r}_{el}$ and $\mathbf{P}(\mathbf{r})$ and its velocities $\dot{\mathbf{r}}_{el}$ and $\dot{\mathbf{P}}(\mathbf{r})$, the classical equations of motion are

$$\ddot{\mathbf{P}}(\mathbf{r}) + \omega^2\mathbf{P}(\mathbf{r}) = \mathbf{D}(\mathbf{r}, \mathbf{r}_{el})\frac{1}{\gamma} \tag{2.30}$$

and

$$m^*\ddot{\mathbf{r}}_{el} = -e\nabla\Phi(\mathbf{r}_{el}). \tag{2.31}$$

The Hamilton function follows from the Lagrangian by performing a Legendre transformation with respect to the generalized velocities $\dot{q}_i$

$$H = \sum_i \dot{q}_i \frac{\partial L}{\partial \dot{q}_i} - L, \tag{2.32}$$

where the sum is over the generalized coordinates q_i and L is the Lagrange function. The partial derivatives of L with respect to $\dot{q}_i$ are the so called conjugate momenta and they are written generally as

$$p_i = \frac{\partial L}{\partial \dot{q}_i}. \tag{2.33}$$

In our case, the conjugate coordinate-momentum pairs are given by

$$\mathbf{r}_{el} \longleftrightarrow m^* \dot{\mathbf{r}}_{el} = \mathbf{p}_{el} \tag{2.34}$$

and

$$\mathbf{P}(\mathbf{r}) \longleftrightarrow \gamma \dot{\mathbf{P}}(\mathbf{r}) = \mathbf{\Pi}(\mathbf{r}). \tag{2.35}$$

Thus the Hamiltonian can be stated as

$$H = \frac{\mathbf{p}_{el}^2}{2m^*} + \int \left[\frac{1}{2\gamma} \mathbf{\Pi}^2(\mathbf{r}) + \frac{\gamma}{2} \omega^2 \mathbf{P}^2(\mathbf{r}) \right] d\mathbf{r} - \int \mathbf{D}(\mathbf{r}, \mathbf{r}_{el}) \cdot \mathbf{P}(\mathbf{r}) d\mathbf{r}. \tag{2.36}$$

Putting everything into Hamilton's equations of motion

$$\dot{q}_i = \frac{\partial H}{\partial p_i} \quad \text{and} \quad \dot{p}_i = -\frac{\partial H}{\partial q_i}, \tag{2.37}$$

leads to the already stated Eq. 2.30 and 2.31.

After having derived the Hamilton function, we can now turn to the quantization. For this purpose, it is convenient to place the excess electron into a cubic dielectric continuum with volume $V_3 = l^3$ (l being the side length of the cube) and impose periodic boundary conditions on the system. The polarization field can be developed into plane waves

$$\mathbf{P}(\mathbf{r}) = \frac{1}{\sqrt{V_3}} \sum_{\mathbf{w}} \mathbf{P}_{\mathbf{w}} e^{i\mathbf{w}\cdot\mathbf{r}}, \tag{2.38}$$

where the periodic boundary conditions restrict the wave vectors to $\mathbf{w} = 2\pi\mathbf{n}/l$ with $\mathbf{n} = (n_1, n_2, n_3)$ and n_i being integers. Since $\mathbf{P}(\mathbf{r})$ is supposed to be real, the coefficients $\mathbf{P}_{\mathbf{w}}$ are not independent but obey

$$\mathbf{P}_{\mathbf{w}}^\dagger = \mathbf{P}_{-\mathbf{w}}, \tag{2.39}$$

where $\mathbf{P}_{\mathbf{w}}^{\dagger}$ is the complex conjugate of $\mathbf{P}_{\mathbf{w}}$. Therefore let us introduce the complex fields $\mathbf{B}(\mathbf{r})$ and $\mathbf{B}^{\dagger}(\mathbf{r})$:

$$\mathbf{B}(\mathbf{r}) = \left(\frac{\gamma\omega}{2\hbar}\right)^{\frac{1}{2}} \left(\mathbf{P}(\mathbf{r}) + \frac{i}{\omega}\dot{\mathbf{P}}(\mathbf{r})\right), \tag{2.40}$$

$$\mathbf{B}^{\dagger}(\mathbf{r}) = \left(\frac{\gamma\omega}{2\hbar}\right)^{\frac{1}{2}} \left(\mathbf{P}(\mathbf{r}) - \frac{i}{\omega}\dot{\mathbf{P}}(\mathbf{r})\right). \tag{2.41}$$

So that $\mathbf{P}(\mathbf{r})$ and $\dot{\mathbf{P}}(\mathbf{r})$ are then given by

$$\mathbf{P}(\mathbf{r}) = \left(\frac{\hbar}{2\gamma\omega}\right)^{\frac{1}{2}} \left(\mathbf{B}^{\dagger}(\mathbf{r}) + \mathbf{B}(\mathbf{r})\right), \tag{2.42}$$

$$\dot{\mathbf{P}}(\mathbf{r}) = \left(\frac{\hbar\omega}{2\gamma}\right)^{\frac{1}{2}} i\left(\mathbf{B}^{\dagger}(\mathbf{r}) - \mathbf{B}(\mathbf{r})\right). \tag{2.43}$$

Putting this into the Hamilton function in Eq. 2.36, while always maintaining the correct order in $\mathbf{B}(\mathbf{r})$ and $\mathbf{B}^{\dagger}(\mathbf{r})$ (important for the quantization later), one obtains

$$\begin{aligned} H = \frac{\mathbf{p}_{el}^2}{2m^*} + \hbar\omega \int \frac{1}{2}\left[\mathbf{B}^{\dagger}(\mathbf{r})\mathbf{B}(\mathbf{r}) + \mathbf{B}(\mathbf{r})\mathbf{B}^{\dagger}(\mathbf{r})\right] d\mathbf{r} - \\ - \frac{\hbar}{2\gamma\omega} \int \mathbf{D}(\mathbf{r}, \mathbf{r}_{el}) \cdot \left(\mathbf{B}^{\dagger}(\mathbf{r}) + \mathbf{B}(\mathbf{r})\right) d\mathbf{r}. \end{aligned} \tag{2.44}$$

If $\mathbf{B}(\mathbf{r})$ and $\mathbf{B}^{\dagger}(\mathbf{r})$ are expanded in terms of plane waves and the condition from Eq. 2.25 is used, we can write

$$\mathbf{B}(\mathbf{r}) = \frac{1}{\sqrt{V_3}} \sum_{\mathbf{w}} \frac{\mathbf{w}}{w} b_{\mathbf{w}} e^{i\mathbf{w}\cdot\mathbf{r}}, \tag{2.45}$$

$$\mathbf{B}^{\dagger}(\mathbf{r}) = \frac{1}{\sqrt{V_3}} \sum_{\mathbf{w}} \frac{\mathbf{w}}{w} b_{\mathbf{w}}^{\dagger} e^{-i\mathbf{w}\cdot\mathbf{r}}, \tag{2.46}$$

which yields

$$\mathbf{P}(\mathbf{r}) = \left(\frac{\hbar}{2\gamma\omega V_3}\right)^{\frac{1}{2}} \sum_{\mathbf{w}} \frac{\mathbf{w}}{w} \left(b_{\mathbf{w}}^{\dagger} e^{-i\mathbf{w}\cdot\mathbf{r}} + b_{\mathbf{w}} e^{i\mathbf{w}\cdot\mathbf{r}}\right). \tag{2.47}$$

Because from Eq. 2.26 follows that $4\pi\mathbf{P}(\mathbf{r}) = \nabla_{\mathbf{r}}\Phi(\mathbf{r})$, the potential clearly is given by

$$\Phi(\mathbf{r}) = 4\pi \left(\frac{\hbar}{2\gamma\omega V_3}\right)^{\frac{1}{2}} \sum_{\mathbf{w}} \frac{i}{w} \left(b_{\mathbf{w}}^{\dagger} e^{-i\mathbf{w}\cdot\mathbf{r}} - b_{\mathbf{w}} e^{i\mathbf{w}\cdot\mathbf{r}}\right). \tag{2.48}$$

The Hamiltonian in terms of $b_{\mathbf{w}}^{\dagger}$ and $b_{\mathbf{w}}$, as well as using $e\Phi(\mathbf{r}_{el})$ for the interaction term, is then

$$H = \frac{\mathbf{p}_{el}^2}{2m^*} + \frac{1}{2}\hbar\omega \sum_{\mathbf{w}} \left[b_{\mathbf{w}}^{\dagger} b_{\mathbf{w}} + b_{\mathbf{w}} b_{\mathbf{w}}^{\dagger}\right] + 4\pi i \left(\frac{\hbar e^2}{2\gamma\omega V_3}\right)^{\frac{1}{2}} \sum_{\mathbf{w}} \frac{1}{w} \left(b_{\mathbf{w}}^{\dagger} e^{-i\mathbf{w}\cdot\mathbf{r}_{el}} - b_{\mathbf{w}} e^{i\mathbf{w}\cdot\mathbf{r}_{el}}\right). \tag{2.49}$$

Up to now everything considered was of classical nature. To go over to quantum mechanics, it is common to impose the usual commutation relations on the conjugate variables $\mathbf{r}_{el}$, $\mathbf{p}_{el}$ and $\mathbf{P}(\mathbf{r})$, $\mathbf{\Pi}(\mathbf{r})$ and to let them become quantum mechanical operators. This means that the commutators between the components of $\hat{\mathbf{r}}_{el}$ and $\hat{\mathbf{p}}_{el}$ are

$$\left[\hat{p}_{el_i}, \hat{r}_{el_j}\right] = -i\hbar\delta_{ij} \tag{2.50}$$

and the commutators between components of $\hat{\mathbf{P}}(\mathbf{r})$ and $\hat{\mathbf{\Pi}}(\mathbf{r})$ are

$$\left[\hat{P}_i(\mathbf{r}), \hat{\Pi}_j(\mathbf{r}')\right] = i\hbar\delta_{ij}\delta(\mathbf{r}-\mathbf{r}'). \tag{2.51}$$

Here δ_{ij} is the Kronecker delta and $\delta(\mathbf{r}-\mathbf{r}')$ is the Dirac delta function. From Eq. 2.51 it follows that

$$\left[\hat{B}_i(\mathbf{r}), \hat{B}_j^\dagger(\mathbf{r}')\right] = \delta_{ij}\delta(\mathbf{r}-\mathbf{r}'). \tag{2.52}$$

Using Eq. 2.45 and 2.46, we get the well known commutators for the Bose operators $\hat{b}_{\mathbf{w}}$ and $\hat{b}^\dagger_{\mathbf{w}'}$:

$$\left[\hat{b}_{\mathbf{w}}, \hat{b}^\dagger_{\mathbf{w}'}\right] = \delta_{\mathbf{w}\mathbf{w}'}, \quad \left[\hat{b}_{\mathbf{w}}, \hat{b}_{\mathbf{w}'}\right] = \left[\hat{b}^\dagger_{\mathbf{w}}, \hat{b}^\dagger_{\mathbf{w}'}\right] = 0. \tag{2.53}$$

It is now obvious that the oscillations of the electric polarization field can be interpreted as Bose particles. The operator $\hat{b}^\dagger_{\mathbf{w}}$ ($\hat{b}_{\mathbf{w}}$) creates (annihilates) an optical longitudinal phonon with wave vector $\mathbf{w}$. The electrons interact with those 'fictitious' particles and the final Hamilton operator can now be stated as

$$\hat{H} = \frac{\hat{\mathbf{p}}^2_{el}}{2m^*} + \hbar\omega\sum_{\mathbf{w}}\left(\hat{b}^\dagger_{\mathbf{w}}\hat{b}_{\mathbf{w}} + \frac{1}{2}\right) + \sum_{\mathbf{w}} V_{\mathbf{w}}\left(\hat{b}^\dagger_{\mathbf{w}} e^{-i\mathbf{w}\cdot\hat{\mathbf{r}}_{el}} - \hat{b}_{\mathbf{w}} e^{i\mathbf{w}\cdot\hat{\mathbf{r}}_{el}}\right). \tag{2.54}$$

Here $V_{\mathbf{w}}$ is the coupling function and given as

$$V_{\mathbf{w}} = 4\pi i\left(\frac{\hbar e^2}{2\gamma\omega V_3}\right)^{\frac{1}{2}}\frac{1}{w}. \tag{2.55}$$

Fröhlich further introduces dimensionless quantities

$$\mathbf{x}_{el} = \mathbf{r}_{el}u, \;\; \mathbf{v} = \mathbf{w}\frac{1}{u}, \;\; S_3 = Vu^3, \tag{2.56}$$

where u is defined as an inverse length with the property

$$\frac{\hbar^2u^2}{2m^*} = \hbar\omega. \tag{2.57}$$

Then the Hamilton operator in units of $\hbar\omega$ (ignoring constant factors like the ground state energy of the polarization field) can be written as

$$\hat{H}' = \frac{\hat{H}}{\hbar\omega} = -\nabla^2_{\mathbf{x}_{el}} + \sum_{\mathbf{v}}\hat{b}^\dagger_{\mathbf{v}}\hat{b}_{\mathbf{v}} + \sum_{\mathbf{v}} V_{\mathbf{v}}\left(\hat{b}^\dagger_{\mathbf{v}} e^{-i\mathbf{v}\cdot\hat{\mathbf{x}}_{el}} - \hat{b}_{\mathbf{v}} e^{i\mathbf{v}\cdot\hat{\mathbf{x}}_{el}}\right), \tag{2.58}$$

with

$$V_{\mathbf{v}} = i \left(\frac{4\pi\alpha}{S_3} \right)^{\frac{1}{2}} \frac{1}{v}. \tag{2.59}$$

The parameter α is the so called coupling constant that determines the strength of the interaction between the electron and phonons. It is a dimensionless quantity given in terms of physical constants and material dependent parameters ω, m^*, ϵ_∞ and ϵ_0 and is primarily responsible for the polaron's properties:

$$\alpha = \frac{2\pi e^2}{\hbar\gamma\omega^3}\sqrt{\frac{2m^*\omega}{\hbar}} = \frac{1}{2}\left(\frac{1}{\epsilon_\infty} - \frac{1}{\epsilon_0}\right)\frac{e^2}{\hbar\omega}\sqrt{\frac{2m^*\omega}{\hbar}}. \tag{2.60}$$

Fröhlich's choice of u leads to units where $\hbar = \omega = 2m^* = 1$. For the rest of this thesis, u is defined a little bit different:

$$\frac{\hbar^2 u^2}{m^*} = \hbar\omega, \tag{2.61}$$

leading to units in which $\hbar = \omega = m^* = 1$. The Hamilton operator is then given by

$$\hat{H}' = \frac{\hat{H}}{\hbar\omega} = -\frac{1}{2}\nabla^2_{\mathbf{x}_{el}} + \sum_{\mathbf{v}} \hat{b}^\dagger_{\mathbf{v}}\hat{b}_{\mathbf{v}} + \sum_{\mathbf{v}} V_{\mathbf{v}} \left(\hat{b}^\dagger_{\mathbf{v}} e^{-i\mathbf{v}\cdot\hat{\mathbf{x}}_{el}} - \hat{b}_{\mathbf{v}} e^{i\mathbf{v}\cdot\hat{\mathbf{x}}_{el}} \right), \tag{2.62}$$

and the coupling function in Eq. 2.58 is replaced by

$$V_{\mathbf{v}} = i \left(\frac{2\sqrt{2}\pi\alpha}{S_3} \right)^{\frac{1}{2}} \frac{1}{v}. \tag{2.63}$$

We will refer to the Hamiltonian as $\hat{H}$, phonon wave vectors as $\mathbf{w}$, electron coordinates as $\mathbf{r}_{el}$ and the volume as V_D, independent of the chosen units.

2.3.1 Alternative form

At last we want to give an alternative form of the Fröhlich Hamiltonian which will be used later for the Diagrammatic Quantum Monte Carlo method. For a detailed derivation see Haken [1]. It is derived by using the same assumptions as before and also by treating the polarization field in the same way. The only difference is that instead of considering the electronic position and its equation of motion (Eq. 2.31), one considers the electronic Schrödinger wave field $\Psi(\mathbf{r}, t)$, its complex conjugate $\Psi^\dagger(\mathbf{r}, t)$ and the time dependent Schrödinger equation. Usually in first quantization, one starts with the particle and after quantization ends up with a wave field. In second quantization, the wave field and its complex conjugate are assumed to be a classical objects and independent and their equations of motion are given by the time dependent Schrödinger equations. Quantization is achieved by imposing commutation relations on the wave fields that then turn into field operators. After expanding the field operators in eigenfunctions of a certain Hamilton operator, it takes the familiar form of second quantization.

In the case of the Fröhlich polaron, we will use an interaction energy term similar to Eq. 2.17 but replace the electron charge with the charge density $\rho_c(\mathbf{r}') = -e\Psi^\dagger(\mathbf{r}')\Psi(\mathbf{r}')$ and integrate over $\mathbf{r}'$. This gives after a partial integration over $\mathbf{r}$

$$H_{inter} = \iint \Psi^\dagger(\mathbf{r}')\Psi(\mathbf{r}')\frac{e}{|\mathbf{r}-\mathbf{r}'|}\left(-\nabla_{\mathbf{r}}\cdot\mathbf{P}(\mathbf{r})\right)d\mathbf{r}d\mathbf{r}'. \tag{2.64}$$

The electronic energy part is given by

$$H_{el} = \int \Psi^\dagger(\mathbf{r})\left(-\frac{\hbar^2}{2m^*}\nabla^2_{\mathbf{r}}\right)\Psi(\mathbf{r})d\mathbf{r}. \tag{2.65}$$

With the energy from the polarization field, this gives us the Hamilton function which can be seen as the total energy of a classic polarization field coupled to a Schrödinger wave field:

$$\begin{aligned} H = \int \Psi^\dagger(\mathbf{r})\left(-\frac{\hbar^2}{2m^*}\nabla^2_{\mathbf{r}}\right)\Psi(\mathbf{r})d\mathbf{r} + \int\left[\frac{1}{2\gamma}\mathbf{\Pi}^2(\mathbf{r}) + \frac{\gamma}{2}\omega^2\mathbf{P}^2(\mathbf{r})\right]d\mathbf{r} + \\ + \iint \Psi^\dagger(\mathbf{r}')\Psi(\mathbf{r}')\frac{e}{|\mathbf{r}-\mathbf{r}'|}\left(-\nabla_{\mathbf{r}}\cdot\mathbf{P}(\mathbf{r})\right)d\mathbf{r}d\mathbf{r}'. \end{aligned} \tag{2.66}$$

Quantization is achieved by introducing commutation relations for the electronic and polarization field operators. It is crucial to not forget that electrons are fermions and therefore their operators have to anticommute, contrary to the Bose operators of the lattice field which do commute. The last step is to expand the operators in plane waves, leading to the final Hamiltonian

$$\hat{H} = \sum_{\mathbf{k}}\frac{\hbar^2k^2}{2m^*}\hat{a}^\dagger_{\mathbf{k}}\hat{a}_{\mathbf{k}} + \sum_{\mathbf{w}}\hbar\omega\hat{b}^\dagger_{\mathbf{w}}\hat{b}_{\mathbf{w}} + \sum_{\mathbf{k},\mathbf{w}} 4\pi i\left(\frac{e^2\hbar}{2V\gamma\omega}\right)^{\frac{1}{2}}\frac{1}{w}\left(\hat{a}^\dagger_{\mathbf{k}-\mathbf{w}}\hat{a}_{\mathbf{k}}\hat{b}^\dagger_{\mathbf{w}} - \hat{a}^\dagger_{\mathbf{k}+\mathbf{w}}\hat{a}_{\mathbf{k}}\hat{b}_{\mathbf{w}}\right). \tag{2.67}$$

The $\hat{a}^\dagger_{\mathbf{k}}$ and $\hat{a}_{\mathbf{k}}$ are creation and annihilation operators of an electron with wave vector $\mathbf{k}$. This is the form of the Fröhlich Hamiltonian which will be used in the Diagrammatic Quantum Monte Carlo.

2.3.2 Fröhlich Hamiltonian in 2 dimensions

Electrons confined to a two dimensional plane can interact with a three dimensional phonon gas. This leads to the concept of the 2D Fröhlich polaron. The overall form of the Fröhlich Hamiltonian stays the same when going from 3D to 2D. The only things that change are the position, velocity and wave vectors, which in 2 dimensions obviously only contain two coordinates instead of three, and the coupling function $V_{\mathbf{w}}$, which in 3D is proportional to $1/w$ but in 2D it is

proportional to $1/\sqrt{w}$. While in 3 dimensions $V_{\mathbf{w}}$ is given by

$$V_{\mathbf{w}}^{3D} = i\left(\frac{2\sqrt{2}\pi\alpha}{V_3}\right)^{\frac{1}{2}}\left(\frac{\hbar^5\omega^3}{m^*}\right)^{\frac{1}{4}}\frac{1}{w}, \tag{2.68}$$

it changes in 2D to [31]

$$V_{\mathbf{w}}^{2D} = i\left(\frac{\sqrt{2}\pi\alpha}{V_2}\right)^{\frac{1}{2}}\left(\frac{\hbar^5\omega^3}{m^*}\right)^{\frac{1}{4}}\frac{1}{\sqrt{w}}, \tag{2.69}$$

where V_2 is the surface area to which the electron is confined. For more detailed information on how to derive the coupling functions for Fröhlich Hamiltonians in D dimensions see Peeters *et al.* [24]. In our units $\hbar = \omega = m* = 1$, the coupling functions are given by

$$V_{\mathbf{w}}^{3D} = i\left(\frac{2\sqrt{2}\pi\alpha}{V_3}\right)^{\frac{1}{2}}\frac{1}{w}, \tag{2.70}$$

$$V_{\mathbf{w}}^{2D} = i\left(\frac{\sqrt{2}\pi\alpha}{V_2}\right)^{\frac{1}{2}}\frac{1}{\sqrt{w}}. \tag{2.71}$$

2.4 Analytic approaches to the Fröhlich Hamiltonian

Although the Fröhlich Hamiltonian does not look very intimidating, there are no exact solutions. One therefore has to resort to approximate analytical and numerical procedures. This section reviews some of the analytical approaches to the Fröhlich Hamiltonian. Those different approaches are usually classified into weak-coupling, intermediate-coupling, strong-coupling and all-coupling theories depending on the strength of the electron-phonon interaction. When we look at the Hamiltonian in Eq. 2.58, we immediately realize that the only parameter determining the coupling strength is α since all other factors are constants. There are no strict borders between the different coupling classes, so we define corresponding α values in Tab. 2.1. They are roughly taken from Refs. [28, 29, 32]. Notice that these values are arbitrary and may differ from values in other literature. They serve only as an approximate guideline.

Coupling theory	α
weak-coupling	$\alpha < 1$
intermediate-coupling	$1 \leq \alpha < 6$
strong-coupling	$6 \leq \alpha$
all-coupling	all

TABLE 2.1: Values of coupling constant α for different coupling theories.

The following approaches are not necessarily the most sophisticated ones. They shall merely give an overview over analytical methods to get a better understanding of the polaron problem. Therefore, the presented results may not be the most accurate available today. Later, when we compare our results to others, we will try to use the best results we can find. (From now on, quantum mechanical operators will no longer be written with a '^' except where confusion is possible.)

2.4.1 Weak-coupling theory

Frölich, Pelzer and Zienau [23] were the first to present a weak-coupling solution to the Fröhlich polaron problem. Since the coupling is assumed to be weak, i.e. $\alpha < 1$, ordinary perturbation theory provides the simplest approach. It treats the electron-phonon interaction as a small perturbation and one can therefore expand the true energies and wave functions of the full Hamiltonian as

$$\begin{aligned} E_n &= E_n^{(0)} + \lambda E_n^{(1)} + \lambda^2 E_n^{(2)} + \dots \\ |n\rangle &= |n^{(0)}\rangle + \lambda\,|n^{(1)}\rangle + \lambda^2\,|n^{(2)}\rangle + \dots \end{aligned} \tag{2.72}$$

E_n and $|n\rangle$ represent an energy eigenvalue and the corresponding eigenstate of the full Hamilton operator, $E_n^{(0)}$ and $|n^{(0)}\rangle$ are eigenvalue and corresponding eigenstate of the unperturbed Hamilton operator H_0 and $E_n^{(m)}$ and $|n^{(m)}\rangle$ are the mth-order corrections to the unperturbed solutions due to the perturbation H_1. The small parameter λ is proportional to $\sqrt{\alpha}$ for the Fröhlich Hamiltonian.

To treat the Hamiltonian from Eq. 2.58 with perturbation theory, it is written as

$$H = H_0 + H_1, \tag{2.73}$$

with

$$H_0 = -\frac{1}{2}\nabla^2_{\mathbf{r}_{el}} + \sum_{\mathbf{w}} b^\dagger_{\mathbf{w}} b_{\mathbf{w}} \tag{2.74}$$

and

$$H_1 = \sum_{\mathbf{w}} V_{\mathbf{w}} \left(b^\dagger_{\mathbf{w}} e^{-i\mathbf{w}\cdot\mathbf{r}_{el}} - b_{\mathbf{w}} e^{i\mathbf{w}\cdot\mathbf{r}_{el}} \right). \tag{2.75}$$

The coupling function $V_{\mathbf{w}}$ is given in Eq. 2.70 for 3D and in Eq. 2.71 for 2D and units are such that $\hbar = \omega = m* = 1$. We want to solve for eigenfunctions $\Psi_\beta(\mathbf{k}, \alpha)$ and eigenvalues $E_\beta(\mathbf{k}, \alpha)$ of the full Hamiltonian:

$$H\Psi_\beta(\mathbf{k}, \alpha) = E_\beta(\mathbf{k}, \alpha)\Psi_\beta(\mathbf{k}, \alpha). \tag{2.76}$$

For a given α and $\mathbf{k}$ value, there exist many different solutions indexed by $\beta = 0, 1, 2, \dots$. In the rest of this thesis, we will only be interested in the solution corresponding to the lowest energy value, i.e. $E_0(\mathbf{k}, \alpha)$ where $E_0(\mathbf{k}, \alpha) \leq E_\beta(\mathbf{k}, \alpha)$.

Eigenfunctions of H_0 are known and given as a product of a free electron wave

function and harmonic oscillator wave functions

$$|\mathbf{k}; n_{\mathbf{w_1}} n_{\mathbf{w_2}} \ldots\rangle = |\phi(\mathbf{k}_1)\rangle\,|\chi\rangle = \frac{1}{\sqrt{V_D}} e^{i\mathbf{k}_1\cdot\mathbf{r}_{el}} \prod_{\mathbf{w}} |n_{\mathbf{w}}\rangle\,, \tag{2.77}$$

where

$$\mathbf{k} = \mathbf{k}_1 + \sum_{\mathbf{w}} \mathbf{w} n_{\mathbf{w}} \tag{2.78}$$

is the total dimensionless wave vector, $|\phi(\mathbf{k}_1)\rangle$ is the free electron's wave function with wave vector $\mathbf{k}_1$, $|\chi\rangle$ is the wave function of a set of uncoupled harmonic oscillators with

$$b^\dagger_{\mathbf{w}} b_{\mathbf{w}}\,|n_{\mathbf{w}}\rangle = n_{\mathbf{w}}\,|n_{\mathbf{w}}\rangle \tag{2.79}$$

and $n_{\mathbf{w}}$ are the number of phonons with wave vector $\mathbf{w}$. The corresponding energy eigenvalues are then (in units of $\hbar\omega$)

$$E_0^{(0)}(\mathbf{k}, \{n_{\mathbf{w}}\}) = \frac{\mathbf{k}_1^2}{2} + \sum_{\mathbf{w}} n_{\mathbf{w}}. \tag{2.80}$$

The interaction term H_1 conserves quasi-momentum, i.e.

$$\left[H_1, -i\nabla_{\mathbf{r}_{el}} + \sum_{\mathbf{w}} \mathbf{w} b^\dagger_{\mathbf{w}} b_{\mathbf{w}}\right] = 0. \tag{2.81}$$

Furthermore, k values are restricted to $k^2/2 < 1$ or equivalently the zeroth-order energy must be smaller than $\hbar\omega$ because for larger values the system becomes degenerate. The perturbation expansion for the energy up to second-order is given by

$$E_0(\mathbf{k},\alpha) = E_0^{(0)}(\mathbf{k}, \{0_{\mathbf{w}}\}) + \langle \mathbf{k}; \{0_{\mathbf{w}}\}|\, H_1\, |\mathbf{k}; \{0_{\mathbf{w}}\}\rangle + \sum_{\mathbf{s}} \frac{|\,\langle \mathbf{k}'; \{n_{\mathbf{w}}\}|\, H_1\, |\mathbf{k}; \{0_{\mathbf{w}}\}\rangle\,|^2}{E_0^{(0)}(\mathbf{k}, \{0_{\mathbf{w}}\}) - E_0^{(0)}(\mathbf{k}', \{n_{\mathbf{w}}\})}. \tag{2.82}$$

The sum over $\mathbf{s}$ in the second-order correction term goes over all eigenstates of the unperturbed system, i.e. over all $\mathbf{k}'$ and over all $n_{\mathbf{w_i}}$, except $|\mathbf{k}; \{0_{\mathbf{w}}\}\rangle$. In case of the Fröhlich Hamiltonian, the perturbation term H_1 (Eq. 2.75) is linear in phonon creation and annihilation operators. This means that it either creates or destroys one phonon when it is applied to a state. Due to the orthogonality of the wave functions in Eq. 2.77, the first order term in Eq. 2.82 vanishes and the second order term reduces to

$$E_0^{(2)}(\mathbf{k}, \{0_{\mathbf{w}}\}) = -\sum_{\mathbf{w}} \frac{|V_{\mathbf{w}}|^2}{\left[\frac{(\mathbf{k}-\mathbf{w})^2}{2} + 1 - \frac{k^2}{2}\right]}. \tag{2.83}$$

In 3D, the perturbation expansion of the energy up to second order in α and up to fourth order in k yields

$$E_0^{3D}(\mathbf{k},\alpha) = \frac{k^2}{2}\left(1 - \frac{\alpha}{6}\right) - \alpha + \mathcal{O}(k^4, \alpha^2) \tag{2.84}$$

and in 2D

$$E_0^{2D}(\mathbf{k},\alpha) = \frac{k^2}{2}\left(1-\frac{\pi}{8}\alpha\right) - \alpha\frac{\pi}{2} + \mathcal{O}(k^4,\alpha^2). \tag{2.85}$$

Thus for an electron at rest ($k = 0$), second-order perturbation theory gives in ordinary units

$$E_0^{3D}(\mathbf{0},\alpha) = -\alpha\hbar\omega + \mathcal{O}(k^4,\alpha^2) \tag{2.86}$$

and

$$E_0^{2D}(\mathbf{0},\alpha) = -\frac{\pi}{2}\alpha\hbar\omega + \mathcal{O}(k^4,\alpha^2). \tag{2.87}$$

This means that the ground state energy of an electron at rest is lowered by its self-energy $\alpha\hbar\omega$ in 3D and by $(\pi/2)\alpha\hbar\omega$ in 2D. By identifying the polaron effective mass in the quadratic term of k

$$E_0(\mathbf{k},\alpha) = E_0(\mathbf{0},\alpha) + \frac{\hbar^2k^2}{2m_{pol}(\alpha)} + \ldots, \tag{2.88}$$

we get as the ratio of the polaron effective mass and the electronic effective mass

$$\frac{m_{pol}^{3D}(\alpha)}{m_{3D}^*} = \frac{1}{1-\alpha/6} \tag{2.89}$$

and

$$\frac{m_{pol}^{2D}(\alpha)}{m_{2D}^*} = \frac{1}{1-\pi\alpha/8}. \tag{2.90}$$

Note that the resulting wave functions from second-order perturbation theory never contain more than one phonon. It seems likely that the wave functions can be improved by allowing more phonons to be in the cloud around the electron. This is done in the intermediate-coupling theory.

2.4.2 Intermediate-coupling theory

Intermediate-coupling theory was developed independently by Gurari [33], Tjablikov [34] and Lee and Pines [35]. Gurari and Lee and Pines used a variational procedure for the 3D Fröhlich polaron with trial wave functions which allow an arbitrary number of phonons to be present. They were able to reproduce the second-order perturbation theory results for the ground state energy from Eq. 2.86. Because of the variational nature of their approach, it is shown that the ground state energy $E_0(\mathbf{0},\alpha)$ obtained from second-order perturbation theory is always greater or equal to the true ground state energy. Also, their results are no longer restricted to $\alpha < 1$. For the effective polaron mass, both methods obtain masses different from perturbation theory:

$$\frac{m_{pol}^{3D}(\alpha)}{m_{3D}^*} = 1 + \frac{\alpha}{6}. \tag{2.91}$$

So that the energy dispersion is given by

$$E_0^{3D}(\mathbf{k},\alpha) = E_0^{3D}(\mathbf{0},\alpha) + \frac{\hbar^2 k^2}{2m_{pol}^{3D}(\alpha)} + \mathcal{O}(k^4). \tag{2.92}$$

Thus for $\mathbf{k} \neq \mathbf{0}$, the energy obtained in the intermediate-coupling is always smaller than second-order perturbation theory. In a subsequent paper, Lee, Low and Pines reproduced the intermediate-coupling results with a canonical transformation and a variational procedure [32]. Using a perturbational method, they were able to estimate the error introduced by the choice of their trial wave function and stated that their results should be valid for $\alpha \leq 6$. Implicit equations for $E_0(\mathbf{k},\alpha)$ in 3D and 2D obtained from the Lee, Low and Pines approach can be found in a paper by Gerlach *et al.* [36].

2.4.3 Strong-coupling theory

Although the criterion for the strong-coupling Fröhlich polaron ($\alpha \geq 6$) is not satisfied for most ionic crystals, it is still of major interest as a pure mathematical problem. The first calculations done on the polaron problem by Pekar and Landau were actually in the strong-coupling limit. They obtained ground state energies proportional to α^2, while in the weak- and intermediate-coupling regime ground state energies depend linearly on α (Eq. 2.86).

The approach we sketch in the following is taken from Devreese's paper [31]. The Fröhlich Hamiltonian used is again given by Eq. 2.58 and the polaron wave function can be written as the product

$$|\Phi\rangle = |\phi\rangle\,|\chi\rangle\,, \tag{2.93}$$

where $|\phi\rangle$ is the electronic part and $|\chi\rangle$ is the field part of the wave function. Both are assumed to be normalized. This is equivalent to the Born-Oppenheimer approximation since the electron adiabatically follows the motion of the ions. We now wish to minimize the expectation value

$$\langle\Phi|\,H\,|\Phi\rangle = \langle\phi|\,\frac{\mathbf{p}_{el}^2}{2}\,|\phi\rangle + \langle\chi|\left[\sum_{\mathbf{w}} b_{\mathbf{w}}^\dagger b_{\mathbf{w}} + \sum_{\mathbf{w}} V_{\mathbf{w}}\left(b_{\mathbf{w}}^\dagger \rho_{\mathbf{w}}^\dagger - b_{\mathbf{w}}\rho_{\mathbf{w}}\right)\right]|\chi\rangle \tag{2.94}$$

with

$$\rho_{\mathbf{w}} = \langle\phi|\,e^{i\mathbf{w}\cdot\mathbf{r}_{el}}\,|\phi\rangle \tag{2.95}$$

and $\rho_{\mathbf{w}}^\dagger$ its complex conjugate. The second term of the expectation value has the form of a displaced harmonic oscillator. As is commonly known, the Hamiltonian of a displaced harmonic oscillator can be diagonalized by using a canonical transformation

$$U = e^{\sum_{\mathbf{w}} V_{\mathbf{w}}(-b_{\mathbf{w}}^\dagger \rho_{\mathbf{w}}^\dagger - b_{\mathbf{w}}\rho_{\mathbf{w}})}. \tag{2.96}$$

Thus the transformed Hamiltonian is given by

$$\langle\Phi|\, U^{-1}HU\,|\Phi\rangle = \langle\phi|\,\frac{\mathbf{p}_{el}^2}{2}\,|\phi\rangle + \langle\chi|\left[\sum_{\mathbf{w}} b_{\mathbf{w}}^\dagger b_{\mathbf{w}} - \sum_{\mathbf{w}} |V_{\mathbf{w}}|^2|\rho_{\mathbf{w}}|^2\right]|\chi\rangle\,. \tag{2.97}$$

It is now obvious that the phonon vacuum state, i.e. the state with no phonons present, minimizes the second term. So the energy expectation value

$$\langle 0|\,\langle\phi|\,H\,|\phi\rangle\,|0\rangle = \langle\phi|\,\frac{\mathbf{p}_{el}^2}{2}\,|\phi\rangle - \sum_{\mathbf{w}} |V_{\mathbf{w}}|^2|\rho_{\mathbf{w}}|^2, \tag{2.98}$$

is still a functional of $|\phi\rangle$. This can be minimized by using a parametrized trial wave function. Since we are in the strong-coupling regime, we expect the electron wave function to be localized and therefore a Gaussian trial wave function comes to mind

$$|\phi\rangle = Ce^{-\frac{\gamma}{2}r_{el}^2}, \tag{2.99}$$

with C being a normalizing factor and γ the variational parameter. After minimizing the energy functional from Eq. 2.98 with respect to γ, one obtains (in units of $\hbar\omega$) in 3D

$$E_0^{3D}(\mathbf{0},\alpha) = -\frac{\alpha^2}{3\pi} = -0.106\alpha^2 + \mathcal{O}(\alpha^0) \tag{2.100}$$

and in 2D [37]

$$E_0^{2D}(\mathbf{0},\alpha) = -\frac{\pi}{8}\alpha^2 = -0.3927\alpha^2 + \mathcal{O}(\alpha^0). \tag{2.101}$$

The polaron effective mass can also be computed using the approximation from Eq. 2.93. This has been done, e.g. by Evrard [38], and is given in 3D by

$$\frac{m_{pol}^{3D}(\alpha)}{m_{3D}^*} = 0.0200\alpha^4. \tag{2.102}$$

Since the ground state energy for strong-coupling as well as for weak- and intermediate-coupling has been obtained with a variational procedure, it constitutes an upper bound for the true ground state energy of the polaron. This means that the result, which gives the lower energy value for a given α, is the better approximation to the true value. By comparing Eq. 2.86 and Eq. 2.100, Fröhlich found that the strong-coupling result is more accurate only for $\alpha \geq 10$. A more detailed review on the strong-coupling theory can be found in Allcock's lecture in [28] and his paper in [39].

2.4.4 All-coupling theory

The most successful theory was introduced by Feynman [7]. He used his path integral formalism and a variational principle to obtain ground state energies and polaron effective masses for arbitrary values of α, therefore it is called an all-coupling theory. Feynman's approach to the Fröhlich polaron problem is based

on the fact that the ground state energy E can be expressed as

$$E = \lim_{\tau\to\infty}\left\{-\frac{1}{\tau}\ln(\mathrm{tr}[e^{-\hat{H}\tau}])\right\}, \tag{2.103}$$

where $\tau = it$, t is imaginary time and $\mathrm{tr}[\hat{\mathrm{A}}]$ is the trace of operator $\hat{A}$. The trace in Eq. 2.103 for the Fröhlich Hamiltonian can be represented by a path integral

$$\mathrm{tr}[e^{-\hat{H}\tau}] = \int_{\substack{\mathcal{C}\{\mathbf{x}(0)=\mathbf{x}(\tau)\}\\ \mathcal{C}\{\mathbf{y_w}(0)=\mathbf{y_w}(\tau)\}}} e^{-S}\mathcal{D}\left(\mathbf{x}(u)\right)\prod_{\mathbf{w}}\mathcal{D}\left(\mathbf{y_w}(u)\right), \tag{2.104}$$

where $\mathbf{x}$ is the electron coordinate, $\mathbf{y_w}$ are the phonon coordinates and S is the action functional. After performing the path integral over phonon coordinates, the action for the polaron problem is given by ($\tau \to \infty$)

$$S = \frac{1}{2}\int_0^\tau \dot{\mathbf{x}}^2(u)du - \frac{\alpha}{\sqrt{8}}\iint_0^\tau \frac{e^{-|u-s|}}{|\mathbf{x}(u)-\mathbf{x}(s)|}duds. \tag{2.105}$$

The first term corresponds to the kinetic energy of the electron and the second term to a retarded potential that depends on the past with weight $e^{-|u-s|}$. The resulting path integral can not be evaluated exactly, so Feynman relied on a variational method. First, the path integral is rewritten as

$$\begin{aligned}\int e^{-S}\mathcal{D}\left(\mathbf{x}(u)\right) = \frac{\int e^{-(S-S_1)}e^{-S_1}\mathcal{D}\left(\mathbf{x}(u)\right)}{\int e^{-S_1}\mathcal{D}\left(\mathbf{x}(u)\right)}\int e^{-S_1}\mathcal{D}\left(\mathbf{x}(u)\right) \equiv \\ \equiv \left\langle e^{-(S-S_1)}\right\rangle_{S_1}\int e^{-S_1}\mathcal{D}\left(\mathbf{x}(u)\right).\end{aligned} \tag{2.106}$$

Here S_1 is a trial action that can be chosen freely and $\langle\,\rangle_{S_1}$ is interpreted as an average with respect to e^{-S_1}. The variational upper bound is established by using the inequality

$$\left\langle e^{-(S-S_1)}\right\rangle_{S_1} \leq e^{-\langle S-S_1\rangle_{S_1}}. \tag{2.107}$$

With these results and Eq. 2.103, the true ground state energy E can be approximated by (in the limit $\tau \to \infty$)

$$E \leq E_1 + \frac{1}{\tau}\langle S - S_1\rangle_{S_1}, \tag{2.108}$$

where

$$E_1 = \lim_{\tau\to\infty}\left\{-\frac{1}{\tau}\ln\int e^{-S_1}\mathcal{D}(\mathbf{x}(u))\right\}. \tag{2.109}$$

Depending on the choice of the trial action, one can obtain upper bounds for the ground state energy for different α values. For example, a trial action according to

$$S_1 = \frac{1}{2}\int_0^\tau \dot{\mathbf{x}}^2(u)du \tag{2.110}$$

reproduces the second-order perturbation theory results in the weak-coupling regime. The same trial action with an additional term describing a harmonic

potential yields the strong-coupling results. To obtain a procedure that works well for all coupling strengths, Feynman chose a trial action that describes an electron coupled via a spring to a "fictitious" particle with finite mass M_F. The action takes the form

$$S_1 = \frac{1}{2}\int_0^\tau \dot{\mathbf{x}}^2(u)du + \frac{C}{2}\iint_0^\tau e^{-W|u-s|}|\mathbf{x}(u)-\mathbf{x}(s)|duds, \tag{2.111}$$

with C and W being variational parameters. The final inequality reads for 3D

$$\begin{aligned} E_0^{3D}(\mathbf{0},\alpha) &\leq E_1^{3D} + \frac{1}{\tau}\left\langle S^{3D} - S_1^{3D}\right\rangle_{S_1^{3D}} \\ &\xrightarrow{\tau\to\infty} \frac{3}{4V}(V-W)^2 - \frac{\alpha V}{\sqrt{\pi}}\int_0^\infty \frac{e^{-u}du}{\left[W^2u - \left((V^2-W^2)/V\right)\left(1-e^{-uV}\right)\right]^{1/2}} \end{aligned} \tag{2.112}$$

and for 2D [37]

$$\begin{aligned} E_0^{2D}(\mathbf{0},\alpha) &\leq E_1^{2D} + \frac{1}{\tau}\left\langle S^{2D} - S_1^{2D}\right\rangle_{S_1^{2D}} \\ &\xrightarrow{\tau\to\infty} \frac{1}{2V}(V-W)^2 - \frac{\alpha}{2}\sqrt{\frac{\pi}{2}}\int_0^\infty \frac{e^{-u}du}{\left[\frac{W^2}{2V^2}u - \left(\frac{V^2-W^2}{2V^3}\right)\left(1-e^{-uV}\right)\right]^{1/2}}. \end{aligned} \tag{2.113}$$

One should now vary V and W to get the lowest upper bounds for the energy. Furthermore, Feynman was able to estimate the effective polaron mass with only slight changes in his approach [7, 29, 28, 30]. One finds as $\alpha \to 0$ [31, 37]:

$$E_0^{3D}(\mathbf{0},\alpha) = -\alpha - 0.0123\alpha^2 + \mathcal{O}(\alpha^3), \tag{2.114}$$

$$\frac{m_{pol}^{3D}(\alpha)}{m_{3D}^*} = 1 + \frac{\alpha}{6} + 0.025\alpha^2 + \mathcal{O}(\alpha^3), \tag{2.115}$$

$$E_0^{2D}(\mathbf{0},\alpha) = -\frac{\pi}{2}\alpha - \frac{\pi^2}{216}\alpha^2 + \mathcal{O}(\alpha^3), \tag{2.116}$$

$$\frac{m_{pol}^{2D}(\alpha)}{m_{2D}^*} = \frac{\pi}{8}\alpha + 0.1272348\alpha^2 + \mathcal{O}(\alpha^3), \tag{2.117}$$

and as $\alpha \to \infty$ [31, 37]:

$$E_0^{3D}(\mathbf{0},\alpha) = -0.106\alpha^2 - 2.83 + \mathcal{O}(\alpha^{-2}), \tag{2.118}$$

$$\frac{m_{pol}^{3D}(\alpha)}{m_{3D}^*} = 0.0202\alpha^4 + \mathcal{O}(\alpha^2), \tag{2.119}$$

$$E_0^{2D}(\mathbf{0},\alpha) = -\frac{\pi}{8}\alpha^2 + \mathcal{O}(\alpha^0), \tag{2.120}$$

$$\frac{m_{pol}^{2D}(\alpha)}{m_{2D}^*} = 0.733\alpha^4 + \mathcal{O}(\alpha^2). \tag{2.121}$$

There are no analytic expressions for the intermediate-coupling regime but one can find values for the energy and effective mass through numerical calculation that

interpolate smoothly between the weak- and strong-coupling results.

2.4.5 Scaling relations

Peeters and Devreese [40] presented very useful scaling relations which allows one to obtain the ground state energy and effective polaron mass in 2D from known results in 3D. These relations are valid for the Feynman polaron model and given by

$$E_0^{2D}(\mathbf{0},\alpha) = \frac{2}{3} E_0^{3D}\left(\mathbf{0}, \frac{3\pi}{4}\alpha\right), \tag{2.122}$$

$$\frac{m_{pol}^{2D}(\alpha)}{m_{2D}^*} = \frac{m_{pol}^{3D}\left(\frac{3\pi}{4}\alpha\right)}{m_{3D}^*}. \tag{2.123}$$

2.4.6 Other analytic properties

In [36] Gerlach *et al.* discuss some interesting features of the ground state energy $E_0(\mathbf{0},\alpha)$ and the energy dispersion $E_0(\mathbf{k},\alpha)$, i.e. the lowest energies for a fixed α as a function of k. Note that the energy $E_0(\mathbf{k},\alpha)$ depends only on the modulus k of the wave vector $\mathbf{k}$ and not the direction.

- *Dispersion*: The polaron dispersion is strictly increasing as a function of k below the continuum edge. The continuum edge $E_c(\alpha)$ is defined as the energy value

$$E_c(\alpha) = E_0(\mathbf{0},\alpha) + \hbar\omega, \tag{2.124}$$

  i.e. it is one optical phonon energy above the ground state (see [41]). We can further define $k_c(\alpha)$ as the wave vector length at which $E_0(k_c,\alpha) = E_c(\alpha)$. In 2D, the continuum edge is approximated asymptotically by $E_0(k,\alpha)$ which means that $k_c(\alpha) = \infty$, whereas in 3D, the polaron energy dispersion intersects $E_c(\alpha)$ at a finite value $k = k_c(\alpha)$. Furthermore, below the continuum edge the dispersion satisfies

$$E_0(\mathbf{k},\alpha) \leq \min\left(E_0(\mathbf{0},\alpha) + k^2, E_0(\mathbf{0},\alpha) + \hbar\omega\right). \tag{2.125}$$

- *Ground state energy*: $E_0(\mathbf{0},\alpha)$ is a strictly decreasing, real analytic function of α. Upper bounds to the ground state energies are found in variational calculations presented in the previous sections. The exact perturbation expansion up to second order for small α values is known and given by

$$E_0(\mathbf{0},\alpha) = -q_1\alpha - q_2\alpha^2 + \mathcal{O}(\alpha^3), \tag{2.126}$$

  where the 2D and 3D coefficients are

$$\begin{aligned} q_1^{2D} &= \frac{\pi}{2}, \quad q_2^{2D} = 0.06397\ldots \\ q_1^{3D} &= 1, \quad q_2^{3D} = 0.01591\ldots \quad . \end{aligned} \tag{2.127}$$

In the strong-coupling limit, there exists the relation

$$\lim_{\alpha\to\infty} \frac{E_0(\mathbf{0},\alpha)}{\alpha^2} = -\eta, \tag{2.128}$$

with the exact coefficients in two and three dimensions

$$\begin{aligned} \eta^{2D} &= 0.4047\ldots \\ \eta^{3D} &= 0.1085\ldots. \end{aligned} \tag{2.129}$$

In Ch. 6, we will use these relations to test the accuracy of our implementation.

Chapter 3

Many-body physics and Feynman diagrams

The description of real quantum systems consisting of many particles interacting with each other requires the knowledge of the many-body wave function. This has to be calculated from the corresponding Schrödinger equation and is usually impossible. Even for model systems like the Fröhlich Hamiltonian, which already represents a simplified description of the real world, is the direct solution of the Schrödinger equation impractical. It is therefore necessary to resort to other methods to retrieve information from a many-body system. One possibility is the use of Green's functions. They contain most of the interesting physical quantities like the ground state energy, lifetime and energies of quasi-particles and others. To obtain a Green's function, one can either solve a specific equation of motion (differential equation) or use a perturbation expansion. The exact Green's functions are as hard to determine as the many-body wave function, so that we will rely on perturbation theory. The perturbation expansion can be put into a one-to-one correspondence with an infinite sum over Feynman diagrams, i.e. each term in the expansion corresponds to one or more Feynman diagrams [2, 42, 43].

Since the Diagrammatic Quantum Monte Carlo method (at least in our case) is mainly based on imaginary time Green's functions and Feynman diagrams, this chapter is used to introduce general aspects of this approach. In Sec. 3.3 this method is applied to the Fröhlich polaron to obtain a diagrammatic expansion for its Green's function. All diagrams in this thesis have been drawn with the TikZ-Feynman package [44].

3.1 Green's functions

Green's functions are usually known from mathematics as a method to solve inhomogeneous differential equations. The Green's functions used in many-body physics and quantum field theory are loosely related to them and in the literature often referred to as propagators and correlation functions. They appear in many different shapes and forms: causal, retarded, advanced, single-particle,

two-particle, and many more. We will not bother about most of them but simply give the mathematical definition of the one which will be used throughout this thesis.

The single-particle causal Green's function in real time for arbitrary temperature T is given by

$$G^T(\nu_2, t_2, \nu_1, t_1) = -i \left\langle \hat{T}\big[c_{\nu_2}(t_2)c^\dagger_{\nu_1}(t_1)\big] \right\rangle = -i\frac{1}{Z}\mathrm{tr}\big(\hat{T}\big[c_{\nu_2}(t_2)c^\dagger_{\nu_1}(t_1)\big]\rho\big). \tag{3.1}$$

Here the $\langle \dots \rangle$ is an average over a grand canonical ensemble, $\hat{T}$ is the Wick time-ordering operator defined as

$$\hat{T}\big[c_{\nu_2}(t_2)c^\dagger_{\nu_1}(t_1)\big] = \begin{cases} c_{\nu_2}(t_2)c^\dagger_{\nu_1}(t_1) & \text{if } t_2 > t_1 \\ \epsilon c^\dagger_{\nu_1}(t_1)c_{\nu_2}(t_2) & \text{if } t_2 \leq t_1 \end{cases}, \tag{3.2}$$

where $\epsilon = +1$ for bosons and $\epsilon = -1$ for fermions, that orders operators from left to right in decreasing time and introduces a factor of -1 every time two fermion operators are interchanged (for equal times, creation operators are on the left of annihilation operators [43]) and $c_{\nu_2}(t_2)$ ($c^\dagger_{\nu_1}(t_1)$) are annihilation (creation) operators in the Heisenberg picture that annihilate (create) a particle in state ν_2 (ν_1):

$$\begin{aligned} c_{\nu_2}(t_2) &= e^{+\frac{i}{\hbar}\mathcal{H}t_2}c_{\nu_2}e^{-\frac{i}{\hbar}\mathcal{H}t_2} \\ c^\dagger_{\nu_1}(t_1) &= e^{+\frac{i}{\hbar}\mathcal{H}t_1}c^\dagger_{\nu_1}e^{-\frac{i}{\hbar}\mathcal{H}t_1}, \end{aligned} \tag{3.3}$$

where $\mathcal{H} = H - \mu N$ with H as the full Hamiltonian, μ as the chemical potential and N as the number operator. The expectation value is then written with the help of the density matrix $\rho = e^{-\beta\mathcal{H}}$ and the partition function $Z = \mathrm{tr}e^{-\beta\mathcal{H}}$ in which $\beta = 1/(k_B T)$ is the usual inverse of the Boltzmann constant times the temperature.

The above definition is valid for all temperatures. We are only interested in the case $T = 0$, i.e. the Green's function at zero temperature, and $t_2 > t_1$. This simplifies the expression for the single-particle Green's function to an expectation value with respect to the true ground state:

$$G(\nu_2, t_2, \nu_1, t_1) = -i\frac{\langle\Psi_0|\, c_{\nu_2}(t_2)c^\dagger_{\nu_1}(t_1)\,|\Psi_0\rangle}{\langle\Psi_0|\Psi_0\rangle}. \tag{3.4}$$

$|\Psi_0\rangle$ is the ground state of the full Hamilton operator H and the Heisenberg operators $c_{\nu_2}(t_2)$ and $c^\dagger_{\nu_1}(t_1)$ are now given as in Eq. 3.3 but with $\mathcal{H}$ replaced by H. In this form, the Green's function is just the probability amplitude that if a particle in state ν_1 is added to the ground state of the interacting system at time t_1, the system will be in the ground state with an added particle in ν_2 at time t_2 [43]. This

can be seen immediately when we write $G(\nu_2, t_2, \nu_1, t_1)$ as

$$G(\nu_2, t_2, \nu_1, t_1) = -i \frac{\langle \Psi_0 | \, e^{+\frac{i}{\hbar}Ht_2} c_{\nu_2} e^{-\frac{i}{\hbar}H(t_2-t_1)} c^\dagger_{\nu_1} e^{-\frac{i}{\hbar}Ht_1} \, | \Psi_0 \rangle}{\langle \Psi_0 | \Psi_0 \rangle} \tag{3.5}$$

and identify the operator $\exp(-\frac{i}{\hbar}Ht)$ as the time evolution operator $U_S(t,0)$ in the Schrödinger picture (assuming H has no explicit time dependence) with the property

$$|\psi(t)\rangle = U_S(t,0) \, |\psi(0)\rangle \, . \tag{3.6}$$

For later use, let us also define an N-body Green's function as

$$G(\nu_{2N}, t_{2N}, \ldots, \nu_1, t_1) = -i \frac{\langle \Psi_0 | \, c_{\nu_{2N}}(t_{2N}) \ldots c_{\nu_{N+1}}(t_{N+1}) c^\dagger_{\nu_N}(t_N) \ldots c^\dagger_{\nu_1}(t_1) \, | \Psi_0 \rangle}{\langle \Psi_0 | \Psi_0 \rangle}, \tag{3.7}$$

which gives the probability amplitude that if a particle in state ν_1 is added to the ground state at time t_1, another particle in state ν_2 is added at time t_2 and so on, then at time t_{N+1} a particle will be observed in state ν_{N+1}, at time t_{N+2} another particle will be observed in state ν_{N+2} and so forth [43]. To make the notation easier, it is assumed that $t_1 < \cdots < t_N < \cdots < t_{2N}$ and that the particles are all of the same kind.

The real time Green's functions are not practical for the Diagrammatic Quantum Monte Carlo method. Their diagrammatic expansions consist of complex-valued terms and a Monte Carlo sampling over those diagrams introduces a sign problem [45]. It is therefore convenient to use Green's functions in the imaginary time formalism. Let us introduce the real variable $\tau = it$. Since we assume τ to be real, t has to be a pure imaginary quantity, thus imaginary time formalism.

The imaginary time single-particle Green's function is defined for $\tau_2 > \tau_1$ as (cf. Eq. 3.4)

$$G(\nu_2, \tau_2, \nu_1, \tau_1) = -\frac{\langle \Psi_0 | \, c_{\nu_2}(\tau_2) c^\dagger_{\nu_1}(\tau_1) \, | \Psi_0 \rangle}{\langle \Psi_0 | \Psi_0 \rangle} \tag{3.8}$$

and the imaginary time many-particle Green's function for $\tau_{2N} > \cdots > \tau_{N+1} > \tau_N > \cdots > \tau_1$ as (cf. Eq. 3.7)

$$G(\nu_{2N}, \tau_{2N}, \ldots, \nu_1, \tau_1) = -\frac{\langle \Psi_0 | \, c_{\nu_{2N}}(\tau_{2N}) \ldots c_{\nu_{N+1}}(\tau_{N+1}) c^\dagger_{\nu_N}(\tau_N) \ldots c^\dagger_{\nu_1}(\tau_1) \, | \Psi_0 \rangle}{\langle \Psi_0 | \Psi_0 \rangle}. \tag{3.9}$$

The Heisenberg operators depend on τ and are given by

$$\begin{aligned} c_{\nu_2}(\tau_2) &= e^{+\frac{1}{\hbar}H\tau_2} c_{\nu_2} e^{-\frac{1}{\hbar}H\tau_2}, \\ c^\dagger_{\nu_1}(\tau_1) &= e^{+\frac{1}{\hbar}H\tau_1} c^\dagger_{\nu_1} e^{-\frac{1}{\hbar}H\tau_1}. \end{aligned} \tag{3.10}$$

Also the imaginary time evolution operator in the Schrödinger picture can now be written as

$$U_S(\tau, 0) = e^{-H\tau}. \tag{3.11}$$

In the rest of this thesis, we will only deal with imaginary time Green's functions.

3.2 Perturbation expansion for the Green's function

For many Hamiltonians, the Green's functions as they are defined in Eq. 3.8 and 3.9 cannot be calculated directly. Fortunately, it is possible to expand them in a perturbation series which can be further mapped onto a sum over Feynman diagrams. Each diagram can be translated into an algebraic equation corresponding to a certain term in the series. The goal is to derive rules on how to write down all Feynman diagrams in a systematic way for an arbitrary order in the series.

To use perturbation theory, the full Hamilton operator is split into a non-interacting H_0 and an interacting H_1 part

$$H = H_0 + H_1. \tag{3.12}$$

We assume that the non-interacting Hamiltonian H_0 is diagonalizable. The expansion of $G(\nu_2, \tau_2, \nu_1, \tau_1)$ in a series is actually based on an expansion of the imaginary time evolution operator $U_I(\tau_2, \tau_1)$ in the Interaction picture. The transformation of an arbitrary operator A_S ($A_H(\tau)$) and an arbitrary state $|\psi_S(\tau)\rangle$ ($|\psi_H\rangle$) from the Schrödinger (Heisenberg) picture to the Interaction picture is given by [42, 43]

$$A_I(\tau) = U_0(0,\tau) A_S U_0(\tau, 0) = e^{\frac{1}{\hbar}H_0\tau} A_S e^{-\frac{1}{\hbar}H_0\tau}, \tag{3.13}$$

$$A_I(\tau) = U_I(\tau, 0) A_H(\tau) U_I(0, \tau) \tag{3.14}$$

and

$$|\psi_I(\tau)\rangle = U_0(0,\tau)\,|\psi_S(\tau)\rangle = e^{\frac{1}{\hbar}H_0\tau}\,|\psi_S(\tau)\rangle\,, \tag{3.15}$$

$$|\psi_I(\tau)\rangle = U_I(\tau, 0)\,|\psi_H\rangle\,. \tag{3.16}$$

The time dependence of $|\psi_I(\tau)\rangle$ is obtained by differentiating Eq. 3.15 with respect to τ and the use of the Schrödinger equation $\partial/\partial\tau\,|\psi_S(\tau)\rangle = -1/\hbar H\,|\psi_S(\tau)\rangle$:

$$\begin{aligned}
\frac{\partial}{\partial\tau}|\psi_I(\tau)\rangle &= \frac{\partial}{\partial\tau}U_0(0,\tau)\,|\psi_S(\tau)\rangle + U_0(0,\tau)\frac{\partial}{\partial\tau}|\psi_S(\tau)\rangle = \\
&= \frac{1}{\hbar}\big(U_0(0,\tau)H_0 - U_0(0,\tau)H\big)\,|\psi_S(\tau)\rangle = \\
&= \frac{1}{\hbar}U_0(0,\tau)(-H_1)U_0(\tau,0)\,|\psi_I(\tau)\rangle = \\
&= -\frac{1}{\hbar}H_1^I\,|\psi_I(\tau)\rangle\,.
\end{aligned} \tag{3.17}$$

Using the fact that $|\psi_I(\tau)\rangle = U_I(\tau,\tau_0)\,|\psi_I(\tau_0)\rangle$ and that $|\psi_I(\tau)\rangle$ is an arbitrary state, we get a differential equation for the time evolution operator $U_I(\tau,\tau_0)$ in the

Interaction picture:

$$\frac{\partial}{\partial\tau}U_I(\tau,\tau_0) = -\frac{1}{\hbar}H_1^I U_I(\tau,\tau_0). \tag{3.18}$$

This equation can be integrated formally from τ_0 to τ giving

$$U_I(\tau,\tau_0) = 1 - \frac{1}{\hbar}\int_{\tau_0}^{\tau} d\tau_1 H_1^I(\tau_1)U_I(\tau_1,\tau_0), \tag{3.19}$$

where $U_I(\tau_0,\tau_0) = 1$ is used. The imaginary time evolution operator appears again under the integral and so by iteration one obtains a series expansion

$$\begin{aligned} U_I(\tau,\tau_0) &= 1 - \frac{1}{\hbar}\int_{\tau_0}^{\tau} d\tau_1 H_1^I(\tau_1) + \left(-\frac{1}{\hbar}\right)^2 \int_{\tau_0}^{\tau} d\tau_1 \int_{\tau_0}^{\tau_1} d\tau_2 H_1^I(\tau_1)H_1^I(\tau_2) + \cdots = \\ &= \sum_{n=0}^{\infty}\left(-\frac{1}{\hbar}\right)^n \int_{\tau_0}^{\tau} d\tau_1 \cdots \int_{\tau_0}^{\tau_{n-1}} d\tau_n H_1^I(\tau_1)\ldots H_1^I(\tau_n), \end{aligned} \tag{3.20}$$

while always keeping the $H_1^I(\tau)$ in the correct time order. With the imaginary time-ordering operator $\hat{T}_\tau$, which is defined for two operators as (the extension to more operators is straightforward)

$$\hat{T}_\tau\left[H_1^I(\tau_1)H_1^I(\tau_2)\right] = H_1^I(\tau_1)H_1^I(\tau_2)\Theta(\tau_1-\tau_2) + H_1^I(\tau_2)H_1^I(\tau_1)\Theta(\tau_2-\tau_1), \tag{3.21}$$

where $\Theta(\tau)$ is the step function, the expansion of the time evolution operator finally becomes [2, 43]

$$\begin{aligned} U_I(\tau,\tau_0) &= \sum_{n=0}^{\infty}\frac{1}{n!}\left(-\frac{1}{\hbar}\right)^n \int_{\tau_0}^{\tau} d\tau_1 \cdots \int_{\tau_0}^{\tau} d\tau_n \hat{T}_\tau\left[H_1^I(\tau_1)\ldots H_1^I(\tau_n)\right] = \\ &= \hat{T}_\tau\left[\exp\left(-\frac{1}{\hbar}\int_{\tau_0}^{\tau} d\tau' H_1^I(\tau')\right)\right]. \end{aligned} \tag{3.22}$$

Since in the definitions of the Green's functions (Eq. 3.8 and 3.9) there appear imaginary time-dependent operators in the Heisenberg picture and the ground state of the full Hamiltonian, which of course is unknown, it is essential that we can relate them somehow to the imaginary time evolution operator in the Interaction picture and the ground state of the non-interacting Hamilton operator H_0. This is achieved via the Gell-Mann and Low theorem, which expresses the ground state of the interacting system in terms of the ground state of the non-interacting system [42]

$$\frac{|\Psi_0\rangle}{\langle\Phi_0|\Psi_0\rangle} = \lim_{\epsilon\to 0}\frac{U_I^\epsilon(0,\pm\infty)\,|\Phi_0\rangle}{\langle\Phi_0|\,U_I^\epsilon(0,\pm\infty)\,|\Phi_0\rangle}. \tag{3.23}$$

Here $|\Phi_0\rangle$ is the ground state of H_0, $\epsilon > 0$ is a positive quantity and $U_I^\epsilon(0,\pm\infty)$ is the imaginary time evolution operator in the Interaction picture corresponding to the Hamiltonian $H = H_0 + e^{-\epsilon|\tau|}H_1$, i.e. as $\epsilon \to 0$ and $\tau \to 0$ the interaction is adiabatically switched on.

It can now be shown that with the Gell-Mann and Low theorem it is possible to rewrite an expectation value of Heisenberg operators with respect to the ground state of the interacting system H as an expectation value of operators in the Interaction picture with respect to the ground state of the non-interacting system H_0:

$$\frac{\langle\Psi_0|\, A_H(\tau')B_H(\tau)\,|\Psi_0\rangle}{\langle\Psi_0|\Psi_0\rangle} = \lim_{\epsilon\to 0}\frac{\langle\Phi_0|\, U_I^\epsilon(\infty,\tau')A_I(\tau')U_I^\epsilon(\tau',\tau)B_I(\tau)U_I^\epsilon(\tau,-\infty)\,|\Phi_0\rangle}{\langle\Phi_0|\, U_I^\epsilon(\infty,0)U_I^\epsilon(0,-\infty)\,|\Phi_0\rangle} =$$
$$= \lim_{\epsilon\to 0}\frac{1}{\langle\Phi_0|\, U_I^\epsilon(\infty,-\infty)\,|\Phi_0\rangle}\sum_{n=0}^{\infty}\frac{1}{n!}\left(-\frac{1}{\hbar}\right)^n\int_{-\infty}^{\infty}d\tau_1\cdots\int_{-\infty}^{\infty}d\tau_n e^{-\epsilon(|\tau_1|+\cdots+|\tau_n|)}$$
$$\times\,\langle\Phi_0|\,\hat{T}\big[H_1^I(\tau_1)\ldots H_1^I(\tau_n)A_I(\tau')B_I(\tau)\big]\,|\Phi_0\rangle \tag{3.24}$$

Here $\hat{T}[\ldots]$ is the Wick time-ordering operator from Eq. 3.2 only for imaginary times. For more details see [2, 42].

Taking the limit $\epsilon \to 0$, it is now possible to write the single-particle Green's function as

$$-G(\nu_2,\tau',\nu_1,\tau) =$$
$$=\sum_{n=0}^{\infty}\frac{1}{n!}\left(-\frac{1}{\hbar}\right)^n\int_{-\infty}^{\infty}d\tau_1\cdots\int_{-\infty}^{\infty}d\tau_n\frac{\langle\Phi_0|\,\hat{T}\big[H_1^I(\tau_1)\ldots H_1^I(\tau_n)c_{\nu_2}^I(\tau')c_{\nu_1}^{I\dagger}(\tau)\big]\,|\Phi_0\rangle}{\langle\Phi_0|\, U_I(\infty,-\infty)\,|\Phi_0\rangle}. \tag{3.25}$$

According to the linked cluster theorem [2, 42, 43], the matrix element in the denominator gets cancelled by so called unconnected diagrams (terms) from the numerator. So we only have to consider connected or linked diagrams. In case of the Fröhlich Hamiltonian, there are no unconnected diagrams and the denominator is equal to 1. Nevertheless, the final perturbation expansion of the single-particle Green's function is written as

$$-G(\nu_2,\tau',\nu_1,\tau) =$$
$$=\sum_{n=0}^{\infty}\frac{1}{n!}\left(-\frac{1}{\hbar}\right)^n\int_{-\infty}^{\infty}d\tau_1\cdots\int_{-\infty}^{\infty}d\tau_n\,\langle\Phi_0|\,\hat{T}\big[H_1^I(\tau_1)\ldots H_1^I(\tau_n)c_{\nu_2}^I(\tau')c_{\nu_1}^{I\dagger}(\tau)\big]\,|\Phi_0\rangle_{conn}\,. \tag{3.26}$$

The expression for the N-body Green's function is similar. To obtain Feynman diagrams, we have to evaluate the matrix elements

$$\langle\Phi_0|\,\hat{T}\big[H_1^I(\tau_1)\ldots H_1^I(\tau_n)c_{\nu_2}^I(\tau')c_{\nu_1}^{I\dagger}(\tau)\big]\,|\Phi_0\rangle_{conn}\,, \tag{3.27}$$

where the "*conn*" refers to connected diagrams. This can be done with the help of Wick's theorem and will be demonstrated for the Fröhlich polaron in the next section.

3.3 Feynman diagrams for the Fröhlich polaron

From now on, we will use the Fröhlich Hamiltonian from Eq. 2.67, i.e.

$$H_0 = \sum_{\mathbf{k}} \epsilon(\mathbf{k}) a^\dagger_{\mathbf{k}} a_{\mathbf{k}} + \sum_{\mathbf{w}} \hbar\omega b^\dagger_{\mathbf{w}} b_{\mathbf{w}}, \tag{3.28}$$

$$H_1 = \sum_{\mathbf{k},\mathbf{w}} \left(V_{\mathbf{w}} b^\dagger_{\mathbf{w}} a^\dagger_{\mathbf{k}-\mathbf{w}} a_{\mathbf{k}} + V^*_{\mathbf{w}} b_{\mathbf{w}} a^\dagger_{\mathbf{k}+\mathbf{w}} a_{\mathbf{k}} \right). \tag{3.29}$$

The ground state of the non-interacting Hamiltonian H_0 is a state with no phonon and no electron present, i.e. the electron-phonon vacuum state $|\Phi_0\rangle = |0\rangle$.

Our main focus in the following will be on the one-electron Green's function and the one-electron-N-phonon Green's function. In the perturbation series in Eq. 3.26, the time values are set to $\tau = 0$ and $\tau' = \tau$ with $\tau > 0$. Let $a^\dagger_{\mathbf{k}}$, $a_{\mathbf{k}}$ and $b^\dagger_{\mathbf{w}}$, $b_{\mathbf{w}}$ be the electron and phonon creation, annihilation operators respectively. Then the one-electron Green's function is given as

$$G(\mathbf{k}_2, \tau, \mathbf{k}_1, 0) = -\langle \Psi_0 | \, a_{\mathbf{k}_2}(\tau) a^\dagger_{\mathbf{k}_1}(0) \, | \Psi_0 \rangle \tag{3.30}$$

and the one-electron-N-phonon Green's function as

$$\begin{aligned} G(\mathbf{k}_2, \tau, \mathbf{k_1}, 0; \mathbf{q}_{2N}, \tau, \ldots, \mathbf{q}_{N+1}, \tau, \mathbf{q}_N, 0, \ldots, \mathbf{q}_1, 0) = \\ - \langle \Psi_0 | \, b_{\mathbf{q}_{2N}}(\tau) \ldots b_{\mathbf{q}_{N+1}}(\tau) a_{\mathbf{k}_2}(\tau) a^\dagger_{\mathbf{k}_1}(0) b^\dagger_{\mathbf{q}_1}(0) \ldots b^\dagger_{\mathbf{q}_N}(0) \, | \Psi_0 \rangle \, , \end{aligned} \tag{3.31}$$

where the $\mathbf{q}_i$ are wave vector of so called external phonons (see e.g. Fig. 3.3, 3.4 or 3.5). The one-electron Green's function is clearly a special case of the one-electron-N-phonon Green's function. Let us also define the one-phonon Green's function as

$$D(\mathbf{w}_2, \tau, \mathbf{w}_1, 0) = -\langle \Psi_0 | \, b_{\mathbf{w}_2}(\tau) b^\dagger_{\mathbf{w}_1}(0) \, | \Psi_0 \rangle \, . \tag{3.32}$$

Before the Feynman diagrams for the Fröhlich polaron can be derived, it is instructive to think what the electron and phonon operators look like in the Interaction picture. Therefore we need the commutators of those operators with H_0. They are caluculated as follows:

$$\begin{aligned} [H_0, a_{\mathbf{k}}] &= \sum_{\mathbf{k}'} \epsilon(\mathbf{k}') [a^\dagger_{\mathbf{k}'} a_{\mathbf{k}'}, a_{\mathbf{k}}] + \sum_{\mathbf{w}} \hbar\omega [b^\dagger_{\mathbf{w}} b_{\mathbf{w}}, a_{\mathbf{k}}] = \\ &= \sum_{\mathbf{k}'} \epsilon(\mathbf{k}') \left(a^\dagger_{\mathbf{k}'} a_{\mathbf{k}'} a_{\mathbf{k}} - a_{\mathbf{k}} a^\dagger_{\mathbf{k}'} a_{\mathbf{k}'} \right) = \\ &= \sum_{\mathbf{k}'} \epsilon(\mathbf{k}') \left(\{ -\delta_{\mathbf{k}',\mathbf{k}} + a_{\mathbf{k}} a^\dagger_{\mathbf{k}'} \} a_{\mathbf{k}'} - a_{\mathbf{k}} a^\dagger_{\mathbf{k}'} a_{\mathbf{k}'} \right) = \\ &= \sum_{\mathbf{k}'} -\epsilon(\mathbf{k}') \delta_{\mathbf{k}',\mathbf{k}} a_{\mathbf{k}'} = -\epsilon(\mathbf{k}) a_{\mathbf{k}}, \end{aligned} \tag{3.33}$$

$$[H_0, a^\dagger_{\mathbf{k}}] = \epsilon(\mathbf{k}) a^\dagger_{\mathbf{k}}, \tag{3.34}$$

$$[H_0, b_{\mathbf{w}}] = -\hbar\omega b_{\mathbf{w}}, \tag{3.35}$$

$$[H_0, b^\dagger_{\mathbf{w}}] = \hbar\omega b^\dagger_{\mathbf{w}}. \tag{3.36}$$

According to Eq. 3.13 and based on the above commutators, the operators in the Interaction picture are expressed as

$$\begin{aligned} a^I_{\mathbf{k}}(\tau) = e^{\frac{1}{\hbar}H_0\tau} a_{\mathbf{k}} e^{-\frac{1}{\hbar}H_0\tau} = a_{\mathbf{k}} + \frac{1}{\hbar}[H_0, a_{\mathbf{k}}]\tau + \frac{1}{\hbar^2 2!}[H_0,[H_0,a_{\mathbf{k}}]]\tau^2 + \cdots = \\ = a_{\mathbf{k}} - \frac{1}{\hbar}\epsilon(\mathbf{k})a_{\mathbf{k}}\tau + \frac{1}{\hbar^2 2!}\epsilon(\mathbf{k})^2\tau^2 a_{\mathbf{k}} + \cdots = a_{\mathbf{k}} e^{-\frac{1}{\hbar}\epsilon(\mathbf{k})\tau}, \end{aligned} \tag{3.37}$$

$$a^{I\dagger}_{\mathbf{k}}(\tau) = a^\dagger_{\mathbf{k}} e^{\frac{1}{\hbar}\epsilon(\mathbf{k})\tau}, \tag{3.38}$$

$$b^I_{\mathbf{w}}(\tau) = b_{\mathbf{w}} e^{-\frac{1}{\hbar}\hbar\omega\tau} = b_{\mathbf{w}} e^{-\omega\tau}, \tag{3.39}$$

$$b^{I\dagger}_{\mathbf{w}}(\tau) = b^\dagger_{\mathbf{w}} e^{\frac{1}{\hbar}\hbar\omega\tau} = b^\dagger_{\mathbf{w}} e^{\omega\tau}. \tag{3.40}$$

Let us further define the so called free electron Green's function as

$$\begin{aligned} G^0(\mathbf{k}_2,\tau,\mathbf{k}_1,0) = -\langle 0|\, a^I_{\mathbf{k}_2}(\tau) a^{I\dagger}_{\mathbf{k}_1}(0)\,|0\rangle = -\langle 0|\, e^{-\frac{1}{\hbar}\epsilon(\mathbf{k}_2)\tau} a_{\mathbf{k}_2} a^\dagger_{\mathbf{k}_1}\,|0\rangle = \\ = -e^{-\frac{1}{\hbar}\epsilon(\mathbf{k}_2)\tau}\langle 0|\,\delta_{\mathbf{k}_2,\mathbf{k}_1} - a^\dagger_{\mathbf{k}_1} a_{\mathbf{k}_2}\,|0\rangle = -e^{-\frac{1}{\hbar}\epsilon(\mathbf{k}_1)\tau}\delta_{\mathbf{k}_2,\mathbf{k}_1}, \end{aligned} \tag{3.41}$$

where the fact was used that an annihilation operator applied to the vacuum state gives zero. The Kronecker-δ ensures that if no interaction is present, the electron can not be scattered out of its initial state $\mathbf{k}_1$. This allows us to write the free electron propagator as $G^0(\mathbf{k},\tau)$. The same goes for the free phonon Green's function

$$D^0(\mathbf{w}_2,\tau,\mathbf{w}_1,0) = -\langle 0|\, b^I_{\mathbf{w}_2}(\tau) b^{I\dagger}_{\mathbf{w}_1}(0)\,|0\rangle = -e^{-\omega\tau}\delta_{\mathbf{w}_2,\mathbf{w}_1} = D^0(\mathbf{w},\tau). \tag{3.42}$$

There are different ways to calculate the matrix elements in the perturbation expansion. The straightforward way would be to use the commutation relations between the operators, just like it was done above for the free electron and phonon Green's functions. This becomes quite tedious for higher order terms in the series. Instead we make use of Wick's theorem.

3.3.1 Wick's theorem

The normal order of operators is defined such that all creation operators are to the left of all annihilation operators. Let $\hat{N}[\dots]$ be the operator which brings a product of operators into normal order, i.e.

$$\hat{N}[ab^\dagger c^\dagger d e^\dagger g\dots] = (-1)^P b^\dagger c^\dagger e^\dagger \dots adg\dots, \tag{3.43}$$

where P is the number of permutations of fermion operators needed to get the operators into normal order. A normal ordered product is convenient because its expectation value with respect to the non-interacting ground state $|0\rangle$ always yields zero.

A contraction of operators is defined as the difference between the Wick imaginary time-ordered and the normal ordered product of two operators [43]:

$$\overbrace{AB} = \hat{T}[AB] - \hat{N}[AB]. \tag{3.44}$$

So for our problem the contraction of one electron annihilation and one electron creation operator in the Interaction picture yields ($\tau_2 > \tau_1$)

$$\begin{aligned}\overbrace{a^I_{\mathbf{k}_2}(\tau_2)a^{I\dagger}_{\mathbf{k}_1}(\tau_1)} &= a^I_{\mathbf{k}_2}(\tau_2)a^{I\dagger}_{\mathbf{k}_1}(\tau_1) - (-1)a^{I\dagger}_{\mathbf{k}_1}(\tau_1)a^I_{\mathbf{k}_2}(\tau_2) = \\ &= (a_{\mathbf{k}_2}a^\dagger_{\mathbf{k}_1} + a^\dagger_{\mathbf{k}_1}a_{\mathbf{k}_2})e^{-\frac{1}{\hbar}\left(\epsilon(\mathbf{k}_2)\tau_2 - \epsilon(\mathbf{k}_1)\tau_1\right)} = \delta_{\mathbf{k}_2,\mathbf{k}_1}e^{-\frac{1}{\hbar}\epsilon(\mathbf{k}_2)(\tau_2-\tau_1)}.\end{aligned} \tag{3.45}$$

If the creation and annihilation operators are interchanged, then the contraction above gives the same result with an additional minus sign. This follows from the definition of the time-ordering and normal-ordering operator. In the same fashion, the contractions between phonon operators and electron and phonon operators can be calculated:

$$\begin{aligned}&\overbrace{a^I_{\mathbf{k}_2}(\tau_2)a^{I\dagger}_{\mathbf{k}_1}(\tau_1)} = 0, \qquad \tau_2 \leq \tau_1, \\ &\overbrace{b^I_{\mathbf{w}_2}(\tau_2)b^{I\dagger}_{\mathbf{w}_1}(\tau_1)} = \delta_{\mathbf{w}_2,\mathbf{w}_1}e^{-\omega(\tau_2-\tau_1)}, \qquad \tau_2 > \tau_1, \\ &\overbrace{b^I_{\mathbf{w}_2}(\tau_2)b^{I\dagger}_{\mathbf{w}_1}(\tau_1)} = 0, \qquad \tau_2 \leq \tau_1, \\ &\overbrace{a^I_{\mathbf{k}_2}(\tau_2)a^I_{\mathbf{k}_1}(\tau_1)} = \overbrace{a^{I\dagger}_{\mathbf{k}_2}(\tau_2)a^{I\dagger}_{\mathbf{k}_1}(\tau_1)} = \\ &= \overbrace{b^I_{\mathbf{w}_2}(\tau_2)b^I_{\mathbf{w}_1}(\tau_1)} = \overbrace{b^{I\dagger}_{\mathbf{w}_2}(\tau_2)b^{I\dagger}_{\mathbf{w}_1}(\tau_1)} = \cdots = 0.\end{aligned} \tag{3.46}$$

For Wick's theorem, it is also necessary to calculate normal products of operators and contractions. As can be seen in Eq. 3.46, the contraction between two operators is a c-number and not an operator. One can therefore put contractions in front of the normal product. It is common to only contract adjacent operators and so care has to be taken when the contraction is between fermion operators. Each time two fermion operators are permuted a factor of (-1) is introduced. For example, assume that all operators are fermionic:

$$\begin{aligned}\hat{N}[\overbrace{ABCDE}\,F\ldots] &= (-1)\hat{N}[\overbrace{ABCE}\,DF\ldots] = (-1)^2\hat{N}[\overbrace{ABE}\,CDF\ldots] = \\ &= (-1)^3\hat{N}[\overbrace{AE}\,BCDF\ldots] = -\overbrace{AE}\,\hat{N}[BCDF\ldots].\end{aligned} \tag{3.47}$$

Wick's theorem finally states that a (imaginary) time-ordered product can be written as a sum over the normal product, the normal products with one contraction, the normal products with two contractions,..., the fully contracted normal products [43]. When the expectation value of an imaginary time ordered product is taken with respect to ground states of the non-interacting Hamiltonian, like they appear in the perturbation expansion, then all the normal products in the

sum become zero (since they all have electron or phonon annihilation operators operating on the electron and phonon vacuum state). Left is a sum over fully contracted operators, i.e. where each operator belongs to one and only one contraction. So to calculate the matrix element of the n^{th}-order term in the perturbation series, we have to sum over all possible ways the operators can be fully contracted. Those fully contracted operator products, which yield a non-zero value, can then be drawn as nth-order Feynman diagrams.

With all the considerations in this section, we are now able to tackle the perturbation expansion of the Green's function for the Fröhlich polaron. From Eq. 3.45 and 3.46, it can be seen that the only contractions that give non-zero values are the ones between an electron annihilation and an electron creation operator and the ones between a phonon annihilation and a phonon creation operator as long as the creation occurs before the annihilation. If their values are compared to the free electron and free phonon Green's function, it is obvious that they are the same (except for a minus sign):

$$\overbrace{a^I_{\mathbf{k}_2}(\tau)a^{I\dagger}_{\mathbf{k}_1}(0)} = -G^0(\mathbf{k}_1,\tau) \qquad \tau > 0, \tag{3.48}$$

$$\overbrace{b^I_{\mathbf{w}_2}(\tau)b^{I\dagger}_{\mathbf{w}_1}(0)} = -D^0(\mathbf{w}_1,\tau) \qquad \tau > 0. \tag{3.49}$$

The only non-zero terms in the diagrammatic expansion will consist of products of free electron and free phonon propagators.

Our interest is primarily in the imaginary time one-electron Green's function (cf. Eq. 3.26):

$$\begin{aligned} G(\mathbf{k},\tau,\mathbf{k},0) = G(\mathbf{k},\tau) &= -\left\langle \Psi_0 \right| a_{\mathbf{k}}(\tau)a^\dagger_{\mathbf{k}}(0)\left|\Psi_0\right\rangle = \\ &= -\sum_{n=0}^{\infty}\frac{1}{n!}\left(-\frac{1}{\hbar}\right)^n \int_{-\infty}^{\infty} d\tau_1 \cdots \int_{-\infty}^{\infty} d\tau_n \left\langle 0\right| \hat{T}\left[H^I_1(\tau_1)\ldots H^I_1(\tau_n)a^I_{\mathbf{k}}(\tau)a^{I\dagger}_{\mathbf{k}}(0)\right]\left|0\right\rangle_{conn} = \\ &= -\sum_{n=0}^{\infty}\frac{1}{n!}\left(-\frac{1}{\hbar}\right)^n \mathcal{F}_n(\mathbf{k},\tau), \end{aligned} \tag{3.50}$$

where $\mathcal{F}_n(\mathbf{k},\tau)$ denotes the contribution of the nth-order term and τ is assumed to be greater than zero.

Let's start with the zeroth-order term. It is given by

$$\mathcal{F}_0(\mathbf{k},\tau) = \left\langle 0\right| \hat{T}\left[a^I_{\mathbf{k}}(\tau)a^{I\dagger}_{\mathbf{k}}(0)\right]\left|0\right\rangle = e^{-\frac{1}{\hbar}\epsilon(\mathbf{k})\tau} = -G^0(\mathbf{k},\tau). \tag{3.51}$$

This has already been evaluated in Eq. 3.41 and is just the free electron propagator.

In the first order term, the interaction Hamiltonian H_1 occurs once. This means that in each expectation value (see Eq. 3.52) there will only be a single phonon

operator. States with a different number of phonons are orthogonal and so the expectation values will evaluate to zero. The same goes for all other terms with an uneven number of phonon operators, i.e. where n is uneven. For the sake of completeness, let us write down the first order term anyway:

$$\begin{aligned}\mathcal{F}_1(\mathbf{k},\tau) &= \int_{-\infty}^{\infty} d\tau_1 \langle 0|\hat{T}\big[H_1^I(\tau_1)a_{\mathbf{k}}^I(\tau)a_{\mathbf{k}}^{I\dagger}(0)\big]|0\rangle = \\ &= \int_{-\infty}^{\infty} d\tau_1 \sum_{\mathbf{k}',\mathbf{w}'} \Big\{ \langle 0|\hat{T}\big[V_{\mathbf{w}'}b_{\mathbf{w}'}^{I\dagger}(\tau_1)a_{\mathbf{k}'-\mathbf{w}'}^{I\dagger}(\tau_1)a_{\mathbf{k}'}^I(\tau_1)a_{\mathbf{k}}^I(\tau)a_{\mathbf{k}}^{I\dagger}(0)\big]|0\rangle + \\ &+ \langle 0|\hat{T}\big[V_{\mathbf{w}'}^*b_{\mathbf{w}'}^I(\tau_1)a_{\mathbf{k}'+\mathbf{w}'}^{I\dagger}(\tau_1)a_{\mathbf{k}'}^I(\tau_1)\big)a_{\mathbf{k}}^I(\tau)a_{\mathbf{k}}^{I\dagger}(0)\big]|0\rangle \Big\} = 0.\end{aligned} \tag{3.52}$$

The first interesting contribution is the second order term. It can be written as

$$\begin{aligned}\mathcal{F}_2(\mathbf{k},\tau) &= \int_{-\infty}^{\infty} d\tau_1 \int_{-\infty}^{\infty} d\tau_2 \langle 0|\hat{T}\big[H_1^I(\tau_1)H_1^I(\tau_2)a_{\mathbf{k}}^I(\tau)a_{\mathbf{k}}^{I\dagger}(0)\big]|0\rangle = \\ &= \int_{-\infty}^{\infty} d\tau_1 \int_{-\infty}^{\infty} d\tau_2 \sum_{\mathbf{k}',\mathbf{w}'}\sum_{\mathbf{k}'',\mathbf{w}''} \mathcal{D}_1 + \mathcal{D}_2 + \mathcal{D}_3 + \mathcal{D}_4,\end{aligned} \tag{3.53}$$

where the sums from H_1 have been put in front of the time-ordered product and the rest has been expanded into four different expectation values $\mathcal{D}_i$. $\mathcal{D}_1$ and $\mathcal{D}_2$ are

$$\mathcal{D}_1 = \langle 0|\hat{T}\big[V_{\mathbf{w}'}b_{\mathbf{w}'}^{I\dagger}(\tau_1)a_{\mathbf{k}'-\mathbf{w}'}^{I\dagger}(\tau_1)a_{\mathbf{k}'}^I(\tau_1)V_{\mathbf{w}''}^*b_{\mathbf{w}''}^{I\dagger}(\tau_2)a_{\mathbf{k}''-\mathbf{w}''}^{I\dagger}(\tau_2)a_{\mathbf{k}''}^I(\tau_2)a_{\mathbf{k}}^I(\tau)a_{\mathbf{k}}^{I\dagger}(0)\big]|0\rangle \tag{3.54}$$

and

$$\mathcal{D}_2 = \langle 0|\hat{T}\big[V_{\mathbf{w}'}b_{\mathbf{w}'}^I(\tau_1)a_{\mathbf{k}'+\mathbf{w}'}^{I\dagger}(\tau_1)a_{\mathbf{k}'}^I(\tau_1)V_{\mathbf{w}''}^*b_{\mathbf{w}''}^I(\tau_2)a_{\mathbf{k}''+\mathbf{w}''}^{I\dagger}(\tau_2)a_{\mathbf{k}''}^I(\tau_2)a_{\mathbf{k}}^I(\tau)a_{\mathbf{k}}^{I\dagger}(0)\big]|0\rangle\,. \tag{3.55}$$

From Eq. 3.45 and 3.46, the possible contractions are known. In both terms we see that there is no way to contract the phonon operators so that they yield a non-zero value. Therefore $\mathcal{D}_1$ and $\mathcal{D}_2$ can be set to zero. The remaining two terms are

$$\mathcal{D}_3 = \langle 0|\hat{T}\big[V_{\mathbf{w}'}b_{\mathbf{w}'}^{I\dagger}(\tau_1)a_{\mathbf{k}'-\mathbf{w}'}^{I\dagger}(\tau_1)a_{\mathbf{k}'}^I(\tau_1)V_{\mathbf{w}''}^*b_{\mathbf{w}''}^I(\tau_2)a_{\mathbf{k}''+\mathbf{w}''}^{I\dagger}(\tau_2)a_{\mathbf{k}''}^I(\tau_2)a_{\mathbf{k}}^I(\tau)a_{\mathbf{k}}^{I\dagger}(0)\big]|0\rangle \tag{3.56}$$

and

$$\mathcal{D}_4 = \langle 0|\hat{T}\big[V_{\mathbf{w}'}b_{\mathbf{w}'}^I(\tau_1)a_{\mathbf{k}'+\mathbf{w}'}^{I\dagger}(\tau_1)a_{\mathbf{k}'}^I(\tau_1)V_{\mathbf{w}''}^*b_{\mathbf{w}''}^{I\dagger}(\tau_2)a_{\mathbf{k}''-\mathbf{w}''}^{I\dagger}(\tau_2)a_{\mathbf{k}''}^I(\tau_2)a_{\mathbf{k}}^I(\tau)a_{\mathbf{k}}^{I\dagger}(0)\big]|0\rangle\,. \tag{3.57}$$

Let's focus on $\mathcal{D}_3$. One way to evaluate this expectation value would be to try out all possible combinations of contractions and see which yield a non-zero result. This is not very efficient. It pays off to think about some rules before rushing into it. A very important observation is that every time two operators are contracted it gives a restriction on the time order. For example, the contraction between the phonon operators gives

$$\overbrace{b_{\mathbf{w}''}^I(\tau_2)b_{\mathbf{w}'}^{I\dagger}(\tau_1)} = e^{-\omega\tau}\delta_{\mathbf{w}'',\mathbf{w}'}\Theta(\tau_2-\tau_1), \tag{3.58}$$

where the step function is defined as

$$\Theta(\tau) = \begin{cases} 1 & \text{if } \tau > 0 \\ 0 & \text{if } \tau \leq 0 \end{cases}. \tag{3.59}$$

It takes care of the fact that the contraction is equal to zero if the creation operator comes after the annihilation operator, i.e. if $\tau_1 > \tau_2$. In the same way it is found that the operators are contracted in a concrete time order $0 < \cdots < \tau_i < \cdots < \tau$ to yield a non-zero value. In our case, the time order is $0 < \tau_1 < \tau_2 < \tau$. It is instructive to bring the electron operators in that order. Remember that for every interchange of fermion operators a factor of -1 is introduced. Luckily, the electron operators always appear in pairs for a certain time τ_i and so to bring them in any arbitrary order will always require an even number of permutations. If this is done for $\mathcal{D}_3$, we get

$$\begin{aligned}\mathcal{D}_3 &= V_{\mathbf{w}'} V^*_{\mathbf{w}''} \overbrace{b^I_{\mathbf{w}''}(\tau_2) b^{I\dagger}_{\mathbf{w}'}(\tau_1)}\, \overbrace{a^I_{\mathbf{k}}(\tau) a^{I\dagger}_{\mathbf{k}''+\mathbf{w}''}(\tau_2)}\, \overbrace{a^I_{\mathbf{k}''}(\tau_2) a^{I\dagger}_{\mathbf{k}'-\mathbf{w}'}(\tau_1)}\, \overbrace{a^I_{\mathbf{k}'}(\tau_1) a^{I\dagger}_{\mathbf{k}}(0)} = \\ &= V_{\mathbf{w}'} V^*_{\mathbf{w}''} e^{-\omega\tau} \delta_{\mathbf{w}'',\mathbf{w}'} \Theta(\tau_2 - \tau_1) \delta_{\mathbf{k},\mathbf{k}''+\mathbf{w}''} e^{-\frac{1}{\hbar}\epsilon(\mathbf{k}''+\mathbf{w}'')(\tau-\tau_2)} \Theta(\tau - \tau_2) \times \\ &\times \delta_{\mathbf{k}'',\mathbf{k}'-\mathbf{w}'} e^{-\frac{1}{\hbar}\epsilon(\mathbf{k}'-\mathbf{w}')(\tau_2-\tau_1)} \Theta(\tau_2 - \tau_1) \delta_{\mathbf{k}',\mathbf{k}} e^{-\frac{1}{\hbar}\epsilon(\mathbf{k})\tau_1} \Theta(\tau_1).\end{aligned} \tag{3.60}$$

That is the only non-zero contribution from $\mathcal{D}_3$. Including the sums and the integrals gives

$$\begin{aligned}&\int_0^\tau d\tau_2 \int_0^{\tau_2} d\tau_1 \sum_{\mathbf{w}'} |V_{\mathbf{w}'}|^2 e^{-\omega\tau} e^{-\frac{1}{\hbar}\epsilon(\mathbf{k})(\tau-\tau_2)} e^{-\frac{1}{\hbar}\epsilon(\mathbf{k}-\mathbf{w}')(\tau_2-\tau_1)} e^{-\frac{1}{\hbar}\epsilon(\mathbf{k})\tau_1} = \\ &\int_0^\tau d\tau_2 \int_0^{\tau_2} d\tau_1 \int d\mathbf{w} \frac{V_D}{(2\pi)^D} G^0(\mathbf{k},\tau_1) |V_{\mathbf{w}}|^2 G^0(\mathbf{k}-\mathbf{w},\tau_2-\tau_1) D^0(\mathbf{w},\tau_2-\tau_1) \times \\ &\times G^0(\mathbf{k},\tau-\tau_2),\end{aligned} \tag{3.61}$$

where the summations over $\mathbf{k}', \mathbf{k}''$ and $\mathbf{w}''$ have been done, the effect of the Θ-functions has been incorporated in the integration limits and the last sum over $\mathbf{w}'$ has been renamed and transformed into an integral over $\mathbf{w}$.

If we now look at $\mathcal{D}_4$, it is seen that it has a similar form as $\mathcal{D}_3$ except that the dummy variables τ_1 and τ_2 have been switched. It therefore contributes with

$$\int_0^\tau d\tau_1 \int_0^{\tau_1} d\tau_2 \int d\mathbf{w} \frac{V_D}{(2\pi)^D} G^0(\mathbf{k},\tau_2) |V_{\mathbf{w}}|^2 G^0(\mathbf{k}-\mathbf{w},\tau_1-\tau_2) D^0(\mathbf{w},\tau_1-\tau_2) G^0(\mathbf{k},\tau-\tau_1) \tag{3.62}$$

to the perturbation expansion which is exactly the same as $\mathcal{D}_3$. So finally, the second order contribution can be written as:

$$\mathcal{F}_2(\mathbf{k},\tau) = \int_0^\tau d\tau_2 \int_0^{\tau_2} d\tau_1 \int d\mathbf{w} \frac{V_D}{(2\pi)^D} 2 \times \mathcal{D}_3. \tag{3.63}$$

The factor of 2 cancels with the factor $1/2!$ from the perturbation expansion of the Green's function $G(\mathbf{k}, \tau)$. This happens for all other higher order terms in the series since any of the $n!$ permutations of the dummy variables τ_i gives the same contribution.

One would go on now to the next non-zero term, the 4^{th}-order term, and proceed in the same way as before. This gets quite lengthy. Instead, it is more efficient to state a general procedure on how to get all contributions for the nth-order perturbation term:

- Start by choosing an arbitrary order for the internal times τ_i, for example $0 < \tau_1 < \cdots < \tau_i < \tau_{i+1} < \cdots < \tau_n < \tau$. The order doesn't matter because the τ_i are just dummy variables and contributions from a different order will get cancelled by the factor $1/n!$.
- Arrange the electron operators in that order and contract them:

$$\overbrace{a^I_{\mathbf{k}}(\tau) a^{I\dagger}_{\mathbf{k}_n - \mathbf{w}_n}(\tau_n)} \ldots \overbrace{a^I_{\mathbf{k}_2}(\tau_2) a^{I\dagger}_{\mathbf{k}_1 - \mathbf{w}_1}(\tau_1)} \overbrace{a^I_{\mathbf{k}_1}(\tau_1) a^{I\dagger}_{\mathbf{k}}(0)} . \tag{3.64}$$

  This establishes the time order with the help of the Θ-functions. In the end each contraction will contribute a free electron propagator $-G^0(\mathbf{k}_l, \tau_i - \tau_j)$. The factors of -1 which are introduced by interchanging two electron operators drop out since it always takes an even number of permutations to bring them in a certain time order.

- Try out all possible combinations of contractions between phonon operators which do no violate the time order, i.e. which do not add a step function that yields zero in combination with the other step functions from the electron contractions. Each contraction between phonon operators will contribute a free phonon propagator $-D^0(\mathbf{w}_l, \tau_i - \tau_j)$. For each phonon propagator add the factor $|V_{\mathbf{w}_l}|^2$.
- Get rid of the Θ-functions and Kronecker-deltas by changing the integration limits and performing all possible sums over wave vectors. Change the remaining sums over phonon wave vectors to integrals by using

$$\sum_{\mathbf{w}} \to \int d\mathbf{w} \frac{V_D}{(2\pi)^D}. \tag{3.65}$$

3.3.2 Feynman diagrams

With the above considerations, it is now possible to define rules on how to translate the non-zero contributions from the perturbation expansion of the Green's function into Feynman diagrams. For this purpose, let us introduce the following notation:

- free electron Green's functions are drawn as solid lines (electron line)

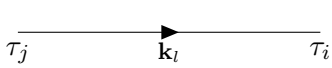

$$= -G^0(\mathbf{k}_l, \tau_i - \tau_j) = e^{-\frac{1}{\hbar}\epsilon(\mathbf{k}_l)(\tau_i - \tau_j)} \tag{3.66}$$

- free phonon Green's functions are drawn as wiggly lines (internal phonon line)

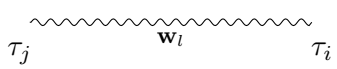

$$= -D^0(\mathbf{w}_l, \tau_i - \tau_j) = e^{-\omega(\tau_i - \tau_j)} \tag{3.67}$$

- coupling functions are drawn as vertices (vertex)

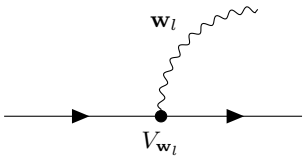

$$= |V_{\mathbf{w}_l}| \tag{3.68}$$

The general procedure to obtain all Feynman diagrams for the nth-order term in the perturbation expansion is as follows (it will be demonstrated here for the 4^{th}-order term): Start by drawing an electron line from 0 to τ, add n vertices and label them.

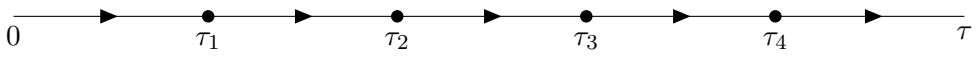

FIGURE 3.1: Electron backbone line of a 4^{th}-order diagram.

This yields the so called electron backbone line consisting of $n + 1$ free electron propagators, shown in Fig. 3.1, and is the result from the contractions of all electron operators in Eq. 3.64. Now add the phonon propagators by always connecting two vertices with a phonon line. This has to be done in all possible ways. So that in the end, each vertex has one incoming electron line, one outgoing electron line and either one incoming or one outgoing phonon line. At last, label the edges with the correct wave vectors. From the interaction Hamiltonian H_1, it is obvious that the total wave vector $\mathbf{k}$ is conserved every time a phonon is created or annihilated. For the 4^{th}-order perturbation term, this yields the diagrams shown in Fig. 3.2.

To obtain the nth-order term of the perturbation expansion from the Feynman diagrams, one can first use the rules defined in Eq. 3.66, 3.67 and 3.68 to translate them back into an algebraic form and take their sum. Then one integrates over all internal phonon wave vectors and over all internal times τ_i, while paying attention to use the correct integration limits according to the time order. Finally, a factor of $1/\hbar^n$ is multiplied.

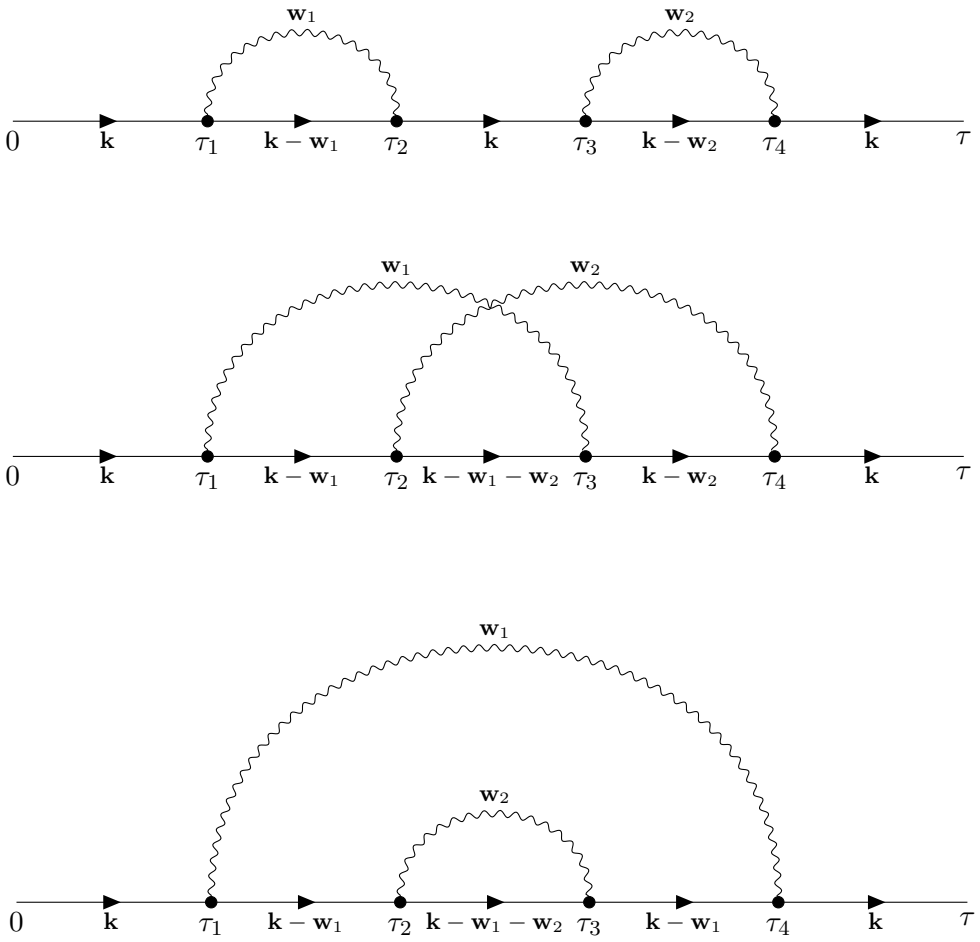

FIGURE 3.2: 4^{th}-order diagrams of the one-electron Green's function $G(\mathbf{k}, \tau)$.

In the DQMC method, which is introduced later, also the one-electron-N-phonon Green's function are needed:

$$\begin{aligned} G_N(\mathbf{k}, \tau; \mathbf{q}_1, \ldots, \mathbf{q}_N) &= -\left\langle \Psi_0 \right| b_{\mathbf{q}_N}(\tau) \ldots b_{\mathbf{q}_1}(\tau) a_{\mathbf{k}_1}(\tau) a^\dagger_{\mathbf{k}_1}(0) b^\dagger_{\mathbf{q}_1}(0) \ldots b^\dagger_{\mathbf{q}_N}(0) \left| \Psi_0 \right\rangle = \\ &= -\sum_{n=0}^{\infty} \frac{1}{n!} \left(-\frac{1}{\hbar} \right)^n \int_{-\infty}^{\infty} d\tau_1 \cdots \int_{-\infty}^{\infty} d\tau_n \left\langle 0 \right| \hat{T} \big[H_1^I(\tau_1) \ldots H_1^I(\tau_n) \times \\ &\times b^I_{\mathbf{q}_N}(\tau) \ldots b^I_{\mathbf{q}_1}(\tau) a^I_{\mathbf{k}_1}(\tau) a^{I\dagger}_{\mathbf{k}_1}(0) b^{I\dagger}_{\mathbf{q}_1}(0) \ldots b^{I\dagger}_{\mathbf{q}_N}(0) \big] \left| 0 \right\rangle , \end{aligned} \tag{3.69}$$

where $\mathbf{k} = \mathbf{k}_1 + \sum_N \mathbf{q}_N$. Its diagrammatic expansion can be obtained in exactly the same way as above. Therefore the diagrams will not be derived. Instead a few examples of the Feynman diagrams for the one-electron-two-phonon Green's function are shown below.

The zeroth-order term is depicted in Fig. 3.3. The second-order term of the perturbation series consists already of five different types of diagrams. One of them

is shown in Fig. 3.4. Figure 3.5 contains a 10^{th}-order diagram. The electron wave vectors have been omitted but keep in mind that the total wave vector is always conserved.

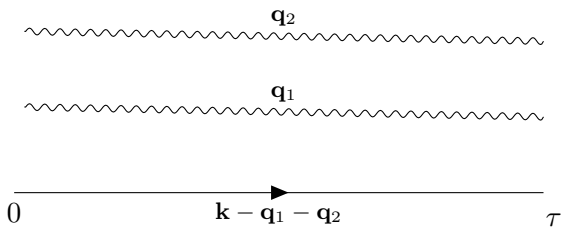

FIGURE 3.3: 0^{th}-order diagram of the one-electron-2-phonon Green's function $G(\mathbf{k},\tau;\mathbf{q}_1,\mathbf{q}_2)$.

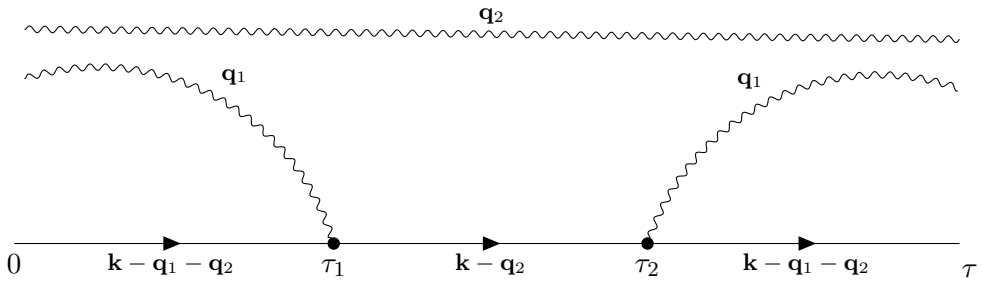

FIGURE 3.4: 2^{nd}-order diagram of the one-electron-2-phonon Green's function $G(\mathbf{k},\tau;\mathbf{q}_1,\mathbf{q}_2)$.

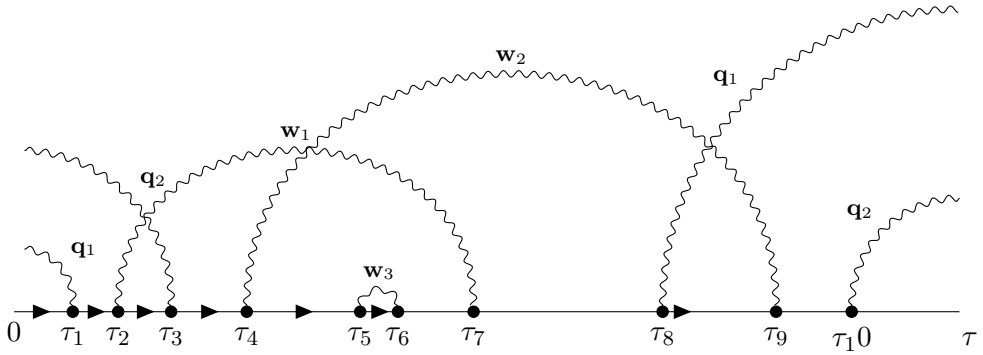

FIGURE 3.5: 10^{th}-order diagram of the one-electron-2-phonon Green's function $G(\mathbf{k},\tau;\mathbf{q}_1,\mathbf{q}_2)$.

Note that we are distinguishing between two different phonon lines. So called external phonon propagators are attached to the diagram ends and labeled as $\mathbf{q}_i$. They appear in the definition of the one-electron-N-phonon Green's function, e.g. Eq. 3.69. The others are called internal phonon propagators. They are only attached to the electron backbone line and labeled as $\mathbf{w}_i$. This is of course just a notational convenience.

3.4 Usefulness of Green's functions

In the last section, it was shown in detail how to obtain a perturbation expansion of the Green's function in terms of Feynman diagrams but it is still not clear what physical information is contained in the Green's functions. To show this, let us insert a complete set of eigenstates $H|\beta_{\mathbf{k}}\rangle = E_\beta(\mathbf{k})|\beta_{\mathbf{k}}\rangle$ of the full Hamilton operator into the definition of the one-electron Green's function in Eq. 3.50:

$$\begin{aligned} G(\mathbf{k},\tau) &= -\langle\Psi_0| a_{\mathbf{k}}(\tau)a^\dagger_{\mathbf{k}}(0)|\Psi_0\rangle = -\sum_\beta \langle\Psi_0| e^{+\frac{1}{\hbar}H\tau}a_{\mathbf{k}}e^{-\frac{1}{\hbar}H\tau}|\beta_{\mathbf{k}}\rangle\langle\beta_{\mathbf{k}}| a^\dagger_{\mathbf{k}}|\Psi_0\rangle = \\ &= -\sum_\beta e^{\frac{1}{\hbar}E_{vac}\tau}e^{-\frac{1}{\hbar}E_\beta(\mathbf{k})\tau}\langle\Psi_0| a_{\mathbf{k}}|\beta_{\mathbf{k}}\rangle\langle\beta_{\mathbf{k}}| a^\dagger_{\mathbf{k}}|\Psi_0\rangle = \\ &= -\sum_\beta |\langle\beta_{\mathbf{k}}| a^\dagger_{\mathbf{k}}|\Psi_0\rangle|^2 e^{-\frac{1}{\hbar}E_\beta(\mathbf{k})\tau}, \end{aligned} \tag{3.70}$$

where $H|\Psi_0\rangle = E_{vac}|\Psi_0\rangle$ is used and the fact that the Fröhlich polaron describes a single electron problem so that there must not be any particle present in $|\Psi_0\rangle$, i.e. it is the vacuum state with eigenvalue $E_{vac} = 0$ [28]. The factor

$$Z^{(0)}_\beta(\mathbf{k}) = |\langle\beta_{\mathbf{k}}| a^\dagger_{\mathbf{k}}|\Psi_0\rangle|^2 \tag{3.71}$$

is a number between 0 and 1 and measures the overlap between the free electron state $a^\dagger_{\mathbf{k}}|\Psi_0\rangle$ and an eigenstate of the polaron $|\beta_{\mathbf{k}}\rangle$. The superscript $^{(0)}$ indicates that we are dealing with the one-electron-0-phonon Green's function.

The Green's function from Eq. 3.70 consists of terms which all decay exponentially with τ. Terms with large $E_\beta(\mathbf{k})$ will decay faster and so as $\tau \to \infty$, the term with the lowest energy $E_0(\mathbf{k})$ ($\beta = 0$) will be projected out:

$$G(\mathbf{k},\tau\to\infty) \to -Z^{(0)}_0(\mathbf{k})e^{-\frac{1}{\hbar}E_0(\mathbf{k})\tau}. \tag{3.72}$$

$E_0(\mathbf{k})$ is the lowest energy of the polaron for a given $\mathbf{k}$ value and the corresponding Z-factor $Z^{(0)}_0(\mathbf{k})$ is called the quasiparticle weight. We will usually write $E_0(\mathbf{k}) = E_0(\mathbf{k},\alpha)$ to emphasize the dependence on the coupling constant α.

The same approach applies to the one-electron-N-phonon Green's function:

$$\begin{aligned} G_N(\mathbf{k},\tau;\mathbf{q}_1,\ldots,\mathbf{q}_N) &= -\sum_\beta |\langle\beta_{\mathbf{k}}| a^\dagger_{\mathbf{k}_1}b^\dagger_{\mathbf{q}_1}\ldots b^\dagger_{\mathbf{q}_N}|\Psi_0\rangle|^2 e^{-\frac{1}{\hbar}E_\beta(\mathbf{k})\tau} = \\ &= -\sum_\beta Z^{(N)}_\beta(\mathbf{k};\mathbf{q}_1,\ldots,\mathbf{q}_N)e^{-\frac{1}{\hbar}E_\beta(\mathbf{k})\tau}, \end{aligned} \tag{3.73}$$

where the Z-factor measures the overlap between a true eigenstate of the polaron and a state with a free electron with wave vector $\mathbf{k}_1$ and N free phonons with wave vectors $\mathbf{q}_1,\ldots,\mathbf{q}_N$. Remember that $\mathbf{k} = \mathbf{k}_1 + \sum_i \mathbf{q}_i$. Again, in the long imaginary

time limit the term with the lowest energy gets projected out

$$G_N(\mathbf{k}, \tau \to \infty; \mathbf{q}_1, \ldots, \mathbf{q}_N) \to Z_0^{(N)}(\mathbf{k}; \mathbf{q}_1, \ldots, \mathbf{q}_N) e^{-\frac{1}{\hbar} E_0(\mathbf{k})\tau}. \tag{3.74}$$

So the Green's functions contain information on the ground state and excited energies as well as the quasiparticle weights. In Ch. 5, the DQMC method is used to retrieve quantities like the effective mass, average number of phonons in the cloud and others with the help of Green's functions.

Chapter 4

Diagrammatic Quantum Monte Carlo

The Monte Carlo (MC) method does not refer to a single specific procedure but to a huge class of stochastic numerical algorithms. The word "stochastic" describes the deliberate use of random numbers which is inherent to all Monte Carlo methods. MC techniques have made their way to a lot of different fields ranging from statistics, mathematics and physics to economics and finance. They are mainly used for numerical integrations of high-dimensional integrals, simulating complex processes and generating random samples from probability distributions.

A Quantum Monte Carlo (QMC) method is also not some specific algorithm but simply a MC procedure applied to a quantum mechanical problem [46]. Examples are the Variational Monte Carlo, the Diffusion Monte Carlo, the Path Integral Monte Carlo (PIMC) or the Diagrammatic Quantum Monte Carlo (DQMC). Interesting for the Fröhlich polaron problem is especially the PIMC and DQMC method. In [47] Titantah *et al.* used a PIMC technique to obtain free energies of the Fröhlich polaron for different coupling strengths and temperatures and in [9] Prokfev *et al.* and in [10] Mishchenko *et al.* calculated Green's functions for the Fröhlich Hamiltonian with the DQMC.

This chapter reviews general aspects of MC methods and introduces the Diagrammatic Quantum Monte Carlo. It begins by stating basic principles and notations that will be used later in this chapter. This is followed by a short overview of MC integration and Markov Chain Monte Carlo (MCMC) techniques with special focus on the Metropolis-Hastings algorithm. The last section is devoted to the DQMC method.

4.1 Basic principles

For the following discussion, notation and ideas from [45, 46] are employed. In most cases, Monte Carlo methods are used to calculate the ratio of two N-dimensional integrals or sums. A famous example from statistical mechanics is the average of an

observable O over an ensemble. This can be written as

$$\langle O \rangle = \frac{\sum_{i_1,\ldots,i_N} O_{i_1,\ldots,i_N} e^{-1/(k_B T) E_{i_1,\ldots,i_N}}}{\sum_{i_1,\ldots,i_N} e^{-1/(k_B T) E_{i_1,\ldots,i_N}}} = \frac{\sum_i O_i w_i}{\sum_i w_i}, \tag{4.1}$$

where the sum over $i = \{i_i, \ldots, i_N\}$ is over the whole configuration space for N degrees of freedom, w_i is the weight and O_i is the observable evaluated for configuration i. Note that the sum over i is not one simple sum but actually are N sums over each degree of freedom. If the degree of freedom i_j is continuous, then the sum becomes an integral:

$$\sum_{i_j} \to \int di_j. \tag{4.2}$$

In statistical mechanics, the weight function is given by the Boltzmann factor $e^{-1/(k_B T) E_i}$ and the denominator is called the partition function Z. Both together can be interpreted as the probability that the system will have the configuration i

$$P_i = \frac{w_i}{Z} = \frac{e^{-1/(k_B T) E_i}}{\sum_i e^{-1/(k_B T) E_i}}. \tag{4.3}$$

The average of O then becomes the expectation value of the random variable O_i with respect to the probability distribution P_i

$$\langle O \rangle = E_{P_i}[O_i] = \sum_i O_i P_i. \tag{4.4}$$

Since the sum has to be performed over all possible configurations, which is in most situations not doable, one can estimate $\langle O \rangle$ by drawing a set of M configurations $\{i^{(k)} : k = 1, \ldots, M\}$ according to the probability distribution P_i, calculate $O_{i^{(k)}}$ for each $i^{(k)}$ and take their arithmetic mean

$$\langle O \rangle = E_{P_i}[O_i] \approx \frac{1}{M} \sum_{k=1}^{M} O_{i^{(k)}}. \tag{4.5}$$

This is what is usually done in Monte Carlo methods. The difficulty lies in sampling the distribution function. For this purpose, one can use Markov Chain Monte Carlo techniques as will be shown in Sec. 4.3.

The above considerations can be formulated in a more general notation. Let X be a continuous random variable (in the discrete case, substitute integrals by sums) that can take the values $x \in \mathcal{B}$ and let $p_X(x)$ be its distribution function. Then the expectation value and variance of a function $h(X)$ of the random variable X are defined as

$$E[h(X)] = \langle h(X) \rangle = \int_{\mathcal{B}} h(x) p_X(x) dx \tag{4.6}$$

and

$$Var[h(X)] = \sigma^2_{h(X)} = \int_{\mathcal{B}} \big(h(x) - E[h(X)]\big)^2 p_X(x)dx = \langle h^2(X)\rangle - \langle h(X)\rangle^2 . \quad (4.7)$$

If the function $h(X)$ is the identity function that maps $x \mapsto x$, then the above definitions give the expectation value and variance of the random variable X.

The expectation value can be approximated by drawing M samples $x_1, \ldots, x_M$ from p_X, calculating the value $h(x_i) = h_i$ for each sample and taking the arithmetic mean

$$E[h(X)] \approx \bar{h}(X) = \frac{1}{M}\sum_{i=1}^{M} h_i. \quad (4.8)$$

This is called the sample mean. Its expectation value is

$$E[\bar{h}(X)] = \langle \bar{h}(X)\rangle = \frac{1}{M}\sum_{i=1}^{M}\langle h_i\rangle = \frac{1}{M}\sum_{i=0}^{M}\langle h\rangle = \langle h(X)\rangle \quad (4.9)$$

and its variance is

$$\begin{aligned}\sigma^2_{\bar{h}(X)} &= \langle \bar{h}^2(X)\rangle - \langle \bar{h}(X)\rangle^2 = \frac{1}{M^2}\left\langle \sum_{i,j=1}^{M} h_i h_j \right\rangle - \langle h(X)\rangle^2 = \\ &= \frac{1}{M^2}\left\langle \sum_{i=1}^{M} h_i^2 + \sum_{i\neq j}^{M} h_i h_j \right\rangle - \langle h(X)\rangle^2 = \\ &= \frac{1}{M}\left(\left\langle \frac{1}{M}\sum_{i=1}^{M} h_i^2 \right\rangle - \langle h(X)\rangle^2\right) = \frac{\sigma^2_{h(X)}}{M}.\end{aligned} \quad (4.10)$$

It is assumed that there is no correlation between the samples, i.e. $\langle h_i h_j\rangle = \langle h_i\rangle\langle h_j\rangle = \langle h(X)\rangle^2$. Equation 4.10 shows that the variance of the sample mean can be reduced by making M larger, thus by using more samples. From the central limit theorem, it is known that as $M \to \infty$ the distribution of $\bar{h}(X)$ approaches a normal distribution with mean $\langle \bar{h}(X)\rangle = \langle h(X)\rangle$ and variance $\sigma^2_{\bar{h}(X)}$. This allows us to introduce the usual confidence intervals on our estimation $\bar{h}(X)$ of the true expectation value $E[h(X)]$ by using the standard error $\sqrt{\sigma^2_{\bar{h}(X)}} = \sigma_{\bar{h}(X)} = \sigma_{h(X)}/\sqrt{M}$.

Unfortunately, $\sigma^2_{h(X)}$ is unknown but it can be approximated by the sample variance defined as

$$s^2_{h(X)} = \frac{1}{M-1}\sum_{i=1}^{M}(h_i - \bar{h}(X))^2. \quad (4.11)$$

Putting this approximation into Eq. 4.10 and taking the square root gives us the so called sample standard error $s_{\bar{h}(X)}$ which can be used as an error bar for the

estimated expectation value:

$$s_{\bar{h}(X)} = \frac{s_{h(X)}}{\sqrt{M}} = \sqrt{\frac{\sum_{i=1}^{M}\left(h_i - \bar{h}(X)\right)^2}{M(M-1)}} = \sqrt{\frac{\sum_{i=1}^{M}\left(h_i^2 - \bar{h}^2(X)\right)}{M(M-1)}}. \tag{4.12}$$

So the probability that the true expectation value $\langle h(X)\rangle$ is found within a certain confidence interval $[\bar{h}(X) - ks_{\bar{h}(X)}, \bar{h}(X) + ks_{\bar{h}(X)}]$ of the approximated one $\bar{h}(X)$ may be written as [46]

$$\begin{aligned} P\big(\bar{h}(X) - s_{\bar{h}(X)} \leq \langle h(X)\rangle \leq \bar{h}(X) + s_{\bar{h}(X)}\big) &\approx 0.68 \\ P\big(\bar{h}(X) - 2s_{\bar{h}(X)} \leq \langle h(X)\rangle \leq \bar{h}(X) + 2s_{\bar{h}(X)}\big) &\approx 0.95 \\ P\big(\bar{h}(X) - 3s_{\bar{h}(X)} \leq \langle h(X)\rangle \leq \bar{h}(X) + 3s_{\bar{h}(X)}\big) &\approx 0.99. \end{aligned} \tag{4.13}$$

In the above considerations, it is assumed that samples x_i are uncorrelated. This is not the case for most problems. Especially when using Markov Chain Monte Carlo techniques with local updates, as will be done later, autocorrelations are commonplace. Equation 4.12 underestimates the error if the samples are correlated. Thus it is necessary to think of a more sophisticated error estimation (the approximation of the expectation value is not influenced by correlations and Eq. 4.8 is still valid).

It is possible to show that if correlations between samples are present, the variance of $\bar{h}(X)$ can be expressed as

$$\sigma^2_{\bar{h}(X)} = \frac{\sigma^2_{h(X)}}{M}\big(1 + 2\tau_X\big), \tag{4.14}$$

where $\tau_X \geq 0$ is the autocorrelation time which is only zero if the samples are uncorrelated. If we compare this result to Eq. 4.10, we immediately see that the effective size of the sample has been reduced from M to $M/(1 + 2\tau_X)$ and that the use of Eq. 4.10 instead of Eq. 4.14 underestimates the variance and thus the error. One way to obtain a reliable error bar would be to estimate τ_X. Another way is the so called blocking method.

4.1.1 Blocking method

The blocking method actually uses the naive error estimator from Eq. 4.12. To get rid of the correlation, it puts the data into B blocks of block size $b = M/B$ and calculates the mean $\bar{h}_j^b$ for each block j. If the block size is large enough, the block averages $\bar{h}_j^b$ become independent and the naive error estimation can be used. This will be shown in a little bit more detail in the following. We can rewrite the variance of the sample

mean as

$$Var\big[\bar{h}(X)\big] = Var\left[\frac{1}{M}\sum_{i=1}^{M} h_i\right] = Var\left[\frac{1}{B}\sum_{j=1}^{B}\left(\frac{1}{b}\sum_{i=(j-1)b+1}^{jb} h_i\right)\right] = \\ = Var\left[\frac{1}{B}\sum_{j=1}^{B}\bar{h}_j^b\right]. \tag{4.15}$$

By using the identities $Var[aX] = a^2 Var[X]$ and $Var[X+Y] = Var[X] + Var[Y]$ for two independent random variables X and Y and a constant a, Eq. 4.15 may be simplified to

$$Var\big[\bar{h}(X)\big] = \frac{1}{B^2}\sum_{j=1}^{B} Var\big[\bar{h}_j^b\big]. \tag{4.16}$$

This is only valid if the block size is large enough and the block means $\bar{h}_j^b$ are no longer correlated. If we further assume that the $\bar{h}_j^b$ have a common variance, $Var[\bar{h}_j^b] = Var[\bar{h}_{block}]$ for each j, we arrive at the result

$$\sigma^2_{\bar{h}(X)} = Var\big[\bar{h}(X)\big] = \frac{1}{B}Var[\bar{h}_{block}] \approx \frac{1}{B}s^2_{\bar{h}_{block}} = \frac{1}{B(B-1)}\sum_{j=1}^{B}\big(\bar{h}_j^b - \bar{h}\big)^2. \tag{4.17}$$

In practice one obtains error estimates for different block sizes using the square root of Eq. 4.17. The error will increase with the block size. As soon as the blocks become statistical independent, i.e. when their size is large enough, the error will stay roughly constant and its value can be used as an estimate. It is therefore advisable to plot the calculated error or variance as a function of the block size. Figure 4.1 shows the sample standard error of an energy estimate as a function of the block size.

4.2 Monte Carlo integration

The estimator of an expectation value from Eq. 4.8 and the error analysis from Sec. 4.1.1 may be used to calculate definite integrals. An integral over a volume $\mathcal{V}$ of the form

$$I = \int_{\mathcal{V}} h(\mathbf{r})d\mathbf{r} = \int_{\mathcal{V}} 1 \times h(\mathbf{r})d\mathbf{r} \tag{4.18}$$

can be interpreted as an expectation value of the constant function $c(\mathbf{r}) = 1$ of the random variable $\mathbf{r}$ with distribution function $h(\mathbf{r})$. Of course the function $h(\mathbf{r})$ would have to fulfill all requirements of a probability distribution and would have to be normalized over $\mathcal{V}$ so that the above integral is known to be unity. As will be seen in the following, there is still a way to map a definite integral onto an expectation value.

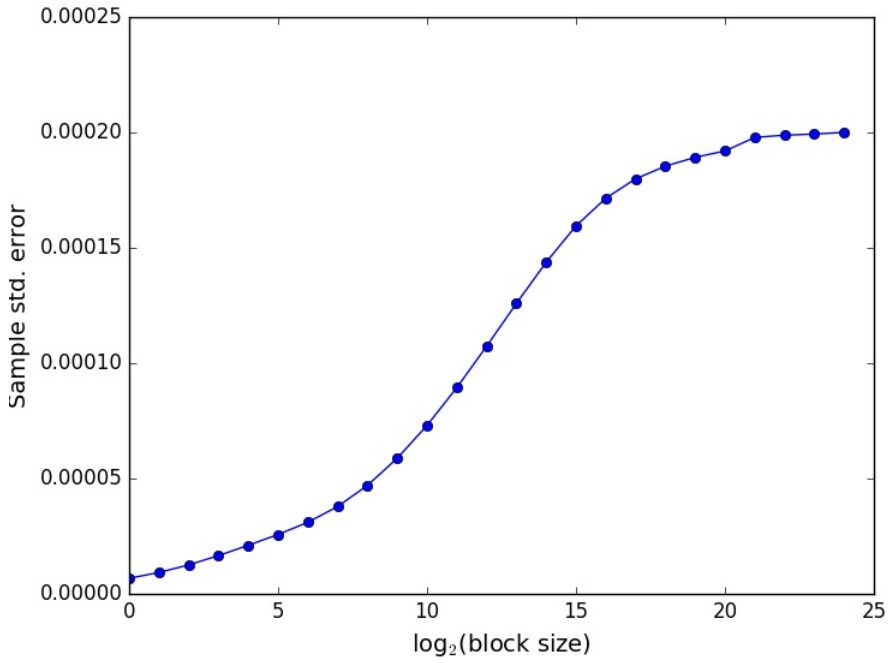

FIGURE 4.1: Error of an energy Monte Carlo estimate as a function of the block size.

Let $f : \mathbb{R}^D \to \mathbb{R}$ be a smooth function over some volume $\Omega \in \mathbb{R}^D$. Standard numerical quadrature methods would approximate the integral of f over Ω by

$$I = \int_\Omega f(\mathbf{r})d\mathbf{r} \approx \frac{V}{M}\sum_{i=1}^{M} w_i f(\mathbf{r}_i), \tag{4.19}$$

where $r \in \mathbb{R}^D$, $\mathbf{r}_i$ are equidistant (e.g. Simpson's rule) or non-equidistant points (Gaussian integration) distributed over Ω, w_i are weights specified by the integration rule and V is the volume of Ω. The error of the approximation depends on the method used, the number of grid points, the dimension and of course on the integrand. For example, for a hypercubic mesh in D-dimensional space with M points the error σ scales as

$$\sigma \propto M^{-k/D}, \tag{4.20}$$

where $k \geq 0$ is dependent on the integration rule [48]. This means that approximating integrals in higher dimensions is very ineffective using standard numerical integration.

In Monte Carlo integration, the weights are all set to 1 and the points are chosen randomly according to some probability distribution $p(\mathbf{r})$ with $\int_\Omega p(\mathbf{r})d\mathbf{r} = 1$,

$p(\mathbf{r}) \geq 0$ and $p(\mathbf{r}) \neq 0$ whenever $f(\mathbf{r}) \neq 0$. The integral can be rewritten as

$$I = \int_\Omega f(\mathbf{r}) d\mathbf{r} = \int_\Omega f(\mathbf{r}) \frac{p(\mathbf{r})}{p(\mathbf{r})} d\mathbf{r} = \int_\Omega \frac{f(\mathbf{r})}{p(\mathbf{r})} p(\mathbf{r}) d\mathbf{r} = E_p \left[\frac{f(\mathbf{r})}{p(\mathbf{r})} \right], \tag{4.21}$$

where $E_p[f(\mathbf{r})/p(\mathbf{r})]$ is the expectation value of the function $g(\mathbf{r}) = f(\mathbf{r})/p(\mathbf{r})$ with respect to p. Approximating the expectation value with a finite sum yields the MC estimation I_{MC} of the integral:

$$I = \int_\Omega f(\mathbf{r}) d\mathbf{r} = E_p[g(\mathbf{r})] = \lim_{M \to \infty} \left(\frac{1}{M} \sum_{i=1}^{M} g(\mathbf{r}_i) \right) \approx \frac{1}{M} \sum_{i=1}^{M} g(\mathbf{r}_i) = I_{MC}, \tag{4.22}$$

where the points $\{\mathbf{r}_i\},\ i = 1, \cdots, M$, are drawn from the probability distribution $p(\mathbf{r})$. According to the last section, the variance of the Monte Carlo estimate $\sigma^2_{I_{MC}}$ is now given as

$$\sigma^2_{I_{MC}} = Var[I_{MC}] = Var \left[\frac{1}{M} \sum_{i=1}^{M} g(\mathbf{r}_i) \right] = \frac{Var[g(\mathbf{r})]}{M} = \frac{\sigma_g^2}{M}, \tag{4.23}$$

i.e. the error made in the MC approximation to the original integral scales as

$$\sigma_{I_{MC}} = \frac{\sigma_g}{\sqrt{M}} \propto M^{-1/2}. \tag{4.24}$$

This means that the accuracy of the MC estimate is only dependent on the function g and the number of sampling points M and not the dimension which makes it more favourable for approximating multi-dimensional integrals than standard numerical integration methods [48].

There are two obvious ways to reduce the error in the MC estimate. One way is to use more sampling points which of course can be done easily but at the expense of performance. The other way is to reduce the variance of the function $g(\mathbf{r})$. This is called "importance sampling". By choosing the probability distribution $p(\mathbf{r})$ such that $g(\mathbf{r}) = f(\mathbf{r})/p(\mathbf{r}) \approx const$, the variance of g will be reduced. It can be achieved using a $p(\mathbf{r})$ that resembles the shape of f. In other words, we want to sample from regions where $|f(\mathbf{r})|$ is large with a higher probability than from regions where $|f(\mathbf{r})|$ is small, i.e. important regions should be sampled more frequently.

In practice the difficulty lies in finding a suitable $p(\mathbf{r})$ and to generate samples from it. The latter can be handled with Markov chain Monte Carlo algorithms.

4.3 Marko Chain Monte Carlo

Markov Chain Monte Carlo (MCMC) techniques are used to sample from complex probability distributions. By generating a Markov chain that has the desired

distribution as its stationary distribution, one is able to draw samples from it. There exist many different MCMC methods but here the focus lies on the Metropolis-Hastings algorithm [49] which is of great importance for the DQMC implementation.

A Markov chain is a stochastic process defined by its state space $X = \{X_i\}$, a transition operator $P(X_j, t+1|X_i, t)$ and an initial distribution $\pi^{(0)}$ at time $t = 0$. At any given time t, the chain is in a certain state X_i and propagates to the next state X_j at time $t+1$ according to the transition probability $P(X_j, t+1|X_i, t)$. Transition probabilities are normalized and obey

$$\sum_j P(X_j, t+1|X_i, t) = 1. \tag{4.25}$$

The Markov property tells us that the transition to the next state is only dependent on the current one and not on any states the chain has visited before, i.e. a Markov chain is memoryless. This dependence is the reason why MCMC methods produce correlated samples but it also allows one to use local updates, i.e. the current state is reused and only changed a little bit instead of producing a completely new random state from scratch. Other important properties required from the Markov chain are time-homogeneity, irreducibility and aperiodicity. This means that the transition operator does not change with time, every state is accessible within a finite number of transitions and that transitions to any state can occur at irregular time intervals. A Markov chain possessing these properties has a unique stationary distribution π which is an eigenvector of P with eigenvalue 1 and satisfies

$$\pi P = \pi \tag{4.26}$$

for all $t \geq T_{eq}$, where T_{eq} is the so called burn-in time. The existence of the unique stationary distribution follows from the fact that P is an ergodic stochastic matrix [46]. The goal of MCMC techniques is to construct transition probabilities such that given an arbitrary initial distribution $\pi^{(0)}$, the Markov chain evolves after T_{eq} steps into its stationary distribution π, which is equal to the target distribution $p(X)$ that we want to sample. After reaching the stationary distribution, the constructed Markov chain generates a sequence of states which represents samples from $p(X)$.

The Metropolis-Hastings algorithm gives us a recipe to construct a Markov chain, especially a transition operator P, that leads an initial distribution to the desired target distribution $p(X)$. Let $p(X, t)$ be the probability that the chain is in state X at time t. We can write down the so called master equation

$$p(X, t) - p(X, t+1) = -\sum_{X'} P(X', X)p(X, t) + \sum_{X'} P(X, X')p(X', t), \tag{4.27}$$

which describes the change of the probability $p(X,t)$ with time. Since we are looking for a stationary distribution, i.e. $p(X,t) = p(X,t+1)$, the master equation turns into

$$\sum_{X'} P(X',X)p(X) = \sum_{X'} P(X,X')p(X'). \tag{4.28}$$

This equation is obviously satisfied if detailed balance is required for all pairs (X,X'):

$$P(X',X)p(X) = P(X,X')p(X'). \tag{4.29}$$

In the Metropolis-Hastings algorithm, one uses detailed balance and splits the transition operator into a proposal probability $w_{XX'}$ and an acceptance probability $A_{XX'}$: $P(X',X) = w_{XX'}A_{XX'}$. While the proposal probability is arbitrary and obeys

$$w_{XX'} \geq 0 \quad \text{and} \quad \sum_{X'} w_{XX'} = 1, \tag{4.30}$$

the acceptance probability is given as

$$A_{XX'} = \begin{cases} 1 & \text{if } \frac{w_{X'X}p(X')}{w_{XX'}p(X)} \geq 1 \\ \frac{w_{X'X}p(X')}{w_{XX'}p(X)} = R & \text{if } \frac{w_{X'X}p(X')}{w_{XX'}p(X)} < 1 \end{cases}. \tag{4.31}$$

The algorithm in Fig. 4.2 depicts the pseudocode of the Metropolis-Hastings algorithm. It works by proposing a new state X' according to $w_{XX'}$ and accepting the new state with probability

$$A_{XX'} = \min\left(1, \frac{w_{X'X}p(X')}{w_{XX'}p(X)} = R\right). \tag{4.32}$$

Samples shouldn't be taken right from the start but after some burn-in time to let the Markov chain reach its stationary distribution. One of the great features of this algorithm is that the target distribution doesn't need to be normalized because the normalization factor cancels when calculating R [45, 48, 49]. If the proposal distribution $w_{X'X}$ is symmetric, i.e. $w_{X'X} = w_{XX'}$, then their factors cancel in the calculation of R and the algorithm is simply called Metropolis algorithm.

4.4 Diagrammatic Quantum Monte Carlo

The Diagrammatic Quantum Monte Carlo method is a numerical algorithm based on a Metropolis-Hastings-like sampling procedure to evaluate certain quantities expressed in a diagrammatic expansion. The diagrammatic expansion of Green's functions has been introduced in Ch. 3. In general, they are a popular tool in many-body physics and mathematically they correspond to a series of integrals where the integration variables increase with the order of the series [50, 9].

Let $Q(\{y\})$ be the quantity of interest depending on a set of external variables $\{y\}$.

Input : initial distribution $\pi^{(0)}$
target distribution $p(X)$
proposal distribution $w_{XX'}$
Output: random samples according to $p(X)$

```
samples[];
start from initial state X ~ π^(0);
perform thermalization steps;
while not enough samples do
    draw a proposal sample X' from w_XX';
    calculate p(X) and p(X');
    if w_X'X p(X') ≥ w_XX' p(X) then
        X ← X';
    else
        calculate R = w_X'X p(X') / w_XX' p(X);
        draw random uniform number r;
        if r ≤ R then
            X ← X';
    end
    samples.add(X);
end
return samples;
```

FIGURE 4.2: Metropolis-Hastings algorithm.

Its diagrammatic expansion is then given as

$$Q(\{y\}) = \sum_{n=0}^{\infty} \sum_{\xi_n} \int dx_1 \cdots \int dx_n \mathcal{D}_n\big(\{y\}; \xi_n, x_1, \ldots, x_n\big), \tag{4.33}$$

where the first sum is over all orders n, the second sum indexes different diagrams of the same order, i.e. diagrams with a different topology (cf. the diagrams in Fig. 3.2), and the integrations are over all internal variables x_i. The functions $\mathcal{D}_n\big(\{y\}; \xi_n, x_1, \ldots, x_n\big)$ can be represented by Feynman diagrams and in our case will be given as products of free electron and phonon propagators as well as coupling functions. Note that usually in analytic approaches, the integrals over x_i are incorporated into the definition of the diagrams. Here the diagrams $\mathcal{D}_n$ and the integrals are separated.

The DQMC method represents an algorithm to calculate quantities like $Q(\{y\})$. The idea behind it is to interpret $Q(\{y\})$ as a probability distribution function for $\{y\}$. This allows one to use a MCMC process, like the Metropolis-Hastings algorithm from Fig. 4.2, to generate diagrams in the parameter space $\big\{\{y\}; \xi_n, x_1, \ldots, x_n\big\}$ according to their weight $\mathcal{D}_n\big(\{y\}; \xi_n, x_1, \ldots, x_n\big)$ and collect statistics for the external variables $\{y\}$, for example by a histogram method. After generating a large

number of diagrams, the statistics of $\{y\}$ reproduce a distribution which converges to the exact $Q(\{y\})$ [50].

This can be clarified a little bit further. First of all, it seems quite confusing that one should be allowed to interpret some arbitrary functions $\mathcal{D}_n$ as probabilities or distribution functions. They are not necessarily real, greater than zero over the whole parameter space and certainly not normalized. The restriction of being real and greater than zero can sometimes be bypassed by using a specific representation. In Ch. 3, the change from the real time to imaginary time representation had exactly the purpose to avoid these kind of problems. The difficulty with the normalization is solved within the Metropolis-Hastings algorithm. Suppose that $\mathcal{D}_n^* = \mathcal{D}_n/N$ is the normalized probability distribution with normalization factor N. Then the acceptance probability from state a to b in the Metropolis algorithm is written as

$$R \propto \frac{\mathcal{D}_n(b)}{\mathcal{D}_n(a)} = \frac{N\mathcal{D}_n^*(b)}{N\mathcal{D}_n^*(a)} = \frac{\mathcal{D}_n^*(b)}{\mathcal{D}_n^*(a)}. \tag{4.34}$$

By accepting new states according to their weight $\mathcal{D}_n$, samples are actually drawn from the correctly normalized distribution $\mathcal{D}_n^*$.

Another point of confusion may be the integrals over the internal variables x_i. As mentioned above, those integrals are not incorporated into the definition of the diagrams nor are they evaluated explicitly. The function $\mathcal{D}_n\big(\{y\};\xi_n,x_1,\ldots,x_n\big)$ is used as the joint probability distribution for external as well as internal variables $\big\{\{y\};\xi_n,x_1,\ldots,x_n\big\}$. The integral of this joint probability distribution over the internal variables gives the marginal probability distribution for the external variables only. According to standard probability theory, we are able to draw samples from the marginal distribution

$$\int dx_1 \cdots \int dx_n \mathcal{D}_n\big(\{y\};\xi_n,x_1,\ldots,x_n\big) \tag{4.35}$$

by simply sampling the joint distribution and ignoring the values over which the integrations are performed [51]. And that's what is done in the DQMC procedure.

The main difference to ordinary Monte Carlo algorithms is that the parameter space has a varying dimensionality. So to create a Markov chain that is ergodic, we will have to introduce updates which change the internal variables $\{x_i\}$, the external variables $\{y\}$, the topology ξ_n as well as the order n. It is instructive to divide the updates into two classes [9, 10, 9]:

1. *Class I*: Updates, which do not change the dimension of the parameter space. Those are standard updates known from ordinary MC procedures and are used to change internal variables, external variables and the topology. Suppose we are in state $\mathcal{D}_n\big(\{y\};\xi_n,x_1,\ldots,x_i,\ldots,x_n\big)$ and propose a new

Input : initial configuration $X^{(0)} = \big(\{y\}; \xi_n, x_1, \ldots, x_n\big)$
update procedures $\{U_1, \ldots, U_k\}$
Output: histogram of $Q(\{y\})$

```
histogram[];
start from initial diagram 𝒟 ← X^(0);
while not enough samples do
    choose an update U_i from {U_1, ..., U_k};
    propose a new configuration X' = ({y'}; ξ_n', x_1', ..., x_n') according to U_i;
    calculate acceptance ratio R;
    if R ≥ 1 then
        𝒟 ← X';
    else
        draw random uniform number r;
        if r ≤ R then
            𝒟 ← X';
    end
    histogram[{y}].add(1);
end
return histogram;
```

FIGURE 4.3: Diagrammatic Quantum Monte Carlo algorithm.

state $\mathcal{D}_n\big(\{y\}; \xi_n, x_1, \ldots, x_i', \ldots, x_n\big)$ where the new x_i' is drawn from an arbitrary probability distribution $w(x_i')$. The acceptance probability is according to the Metropolis-Hastings algorithm

$$A_{x_i x_i'} = \min\{1, R\} \tag{4.36}$$

with

$$R = \frac{\mathcal{D}_n\big(\{y\}; \xi_n, x_1, \ldots, x_i', \ldots, x_n\big) w(x_i)}{\mathcal{D}_n\big(\{y\}; \xi_n, x_1, \ldots, x_i, \ldots, x_n\big) w(x_i')}. \tag{4.37}$$

In practice, it is advisable to choose new configurations such that the acceptance probability is high. If the new state could be drawn from the distribution $w(x_i') = \mathcal{D}_n\big(\{y\}; \xi_n, x_1, \ldots, x_i', \ldots, x_n\big)$, the probability of accepting the proposed state/diagram would be unity.

A short remark on how to draw samples x' from a normalized probability distribution $w(x)$: Let r be a uniform random number from the interval $[0, 1]$ and let x_{min} and x_{max} be the minimum and maximum allowed value. A random sample x' is drawn from the distribution $w(x)$ by solving the equation for x':

$$r = \frac{\int_{x_{min}}^{x'} w(x)dx}{\int_{x_{min}}^{x_{max}} w(x)dx}. \tag{4.38}$$

2. *Class II*: Updates, which change the order of diagrams and therefore the dimension of the parameter space. Since detailed balance is assumed (see Sec. 4.3), there is for each update a corresponding inverse update. Let $\mathcal{A}$ be the update that increases the order of the current diagram by m and let $\mathcal{B}$ be its inverse which decreases the order by m. Suppose the current state in the Markov chain is $\mathcal{D}_n\big(\{y\};\xi_n,x_1,\ldots,x_n\big)$ and we propose update $\mathcal{A}$ with probability $p_\mathcal{A}$. That means we also have to propose m new internal variables $x_{n+1},\ldots,x_{n+m}$ from an arbitrary normalized distribution $P(x_1,\ldots,x_m)$. The detailed balance equation is written as

$$\begin{aligned} &p_\mathcal{A}\mathcal{D}_n\big(\{y\};\xi_n,x_1,\ldots,x_n\big)P(x_{n+1},\ldots,x_{n+m})A_{n\to n+m} = \\ &\quad = p_\mathcal{B}\mathcal{D}_{n+m}\big(\{y\};\xi_{n+m},x_1,\ldots,x_n,x_{n+1},\ldots,x_{n+m}\big)A_{n+m\to n}. \end{aligned} \tag{4.39}$$

This leads to the acceptance probability

$$A_{n\to n+m} = \min\{1,R\} \tag{4.40}$$

with

$$R = \frac{p_\mathcal{B}\mathcal{D}_{n+m}\big(\{y\};\xi_{n+m},x_1,\ldots,x_n,x_{n+1},\ldots,x_{n+m}\big)}{p_\mathcal{A}\mathcal{D}_n\big(\{y\};\xi_n,x_1,\ldots,x_n\big)P(x_{n+1},\ldots,x_{n+m})}. \tag{4.41}$$

The distribution $P(x_1,\ldots,x_m)$ can again be chosen to maximize the acceptance ratio. The acceptance probability for update $\mathcal{B}$ is

$$A_{n+m\to n} = \min\left\{1,\frac{1}{R}\right\}. \tag{4.42}$$

Chapter 5

DQMC for the Fröhlich polaron

The last two chapters have introduced all necessary prerequisites to finally apply the Diagrammatic Quantum Monte Carlo method to the Fröhlich polaron. From now on, units will be chosen such that $\hbar = \omega = m^* = 1$. The Fröhlich Hamiltonian is therefore given as

$$\hat{H} = \sum_{\mathbf{k}} \epsilon(\mathbf{k}) \hat{a}^\dagger_{\mathbf{k}} \hat{a}_{\mathbf{k}} + \sum_{\mathbf{w}} \hat{b}^\dagger_{\mathbf{w}} \hat{b}_{\mathbf{w}} + \sum_{\mathbf{k},\mathbf{w}} \left(V_{\mathbf{w}} b^\dagger_{\mathbf{w}} a^\dagger_{\mathbf{k}-\mathbf{w}} a_{\mathbf{k}} + V^*_{\mathbf{w}} b_{\mathbf{w}} a^\dagger_{\mathbf{k}+\mathbf{w}} a_{\mathbf{k}} \right), \tag{5.1}$$

where $\epsilon(\mathbf{k}) = k^2/2$ is the electron dispersion, and $V_{\mathbf{w}}$ is the coupling function which is given in three dimensions as

$$V^{3D}_{\mathbf{w}} = i \left(\frac{2\sqrt{2}\pi\alpha}{V_3} \right)^{\frac{1}{2}} \frac{1}{w} \tag{5.2}$$

and in two dimensions as

$$V^{2D}_{\mathbf{w}} = i \left(\frac{\sqrt{2}\pi\alpha}{V_2} \right)^{\frac{1}{2}} \frac{1}{\sqrt{w}}. \tag{5.3}$$

V_3 and V_2 is the volume of the system under consideration in 3D and 2D, respectively. Our functions of interest will be the one-electron Green's function $G(\mathbf{k}, \tau)$ and the one-electron-N-phonon Green's function $G_N(\mathbf{k}, \tau; \mathbf{q}_1, \ldots, \mathbf{q}_N)$ with $\mathbf{q}_1, \ldots, \mathbf{q}_N$ as the wave vectors of external phonons. Their diagrammatic expansions have the form

$$\begin{aligned} G_N(\mathbf{k}, \tau; \mathbf{q}_1, \ldots, \mathbf{q}_N) &= \langle \Psi_0 | \, b_{\mathbf{q}_N}(\tau) \ldots b_{\mathbf{q}_1}(\tau) a_{\mathbf{k}_1}(\tau) a^\dagger_{\mathbf{k}_1}(0) b^\dagger_{\mathbf{q}_1}(0) \ldots b^\dagger_{\mathbf{q}_N}(0) \, | \Psi_0 \rangle = \\ &= \sum_{n=0,2,4\ldots}^{\infty} \sum_{\xi_n} \int d\tau_1 \ldots d\tau_n \int d\mathbf{w}_1 \frac{V_D}{(2\pi)^D} \ldots d\mathbf{w}_m \frac{V_D}{(2\pi)^D} \times \\ &\times \mathcal{D}_n\big(\mathbf{k}, \tau, \mathbf{q}_1, \ldots, \mathbf{q}_N; \xi_n, \tau_1, \ldots, \tau_n, \mathbf{w}_1, \ldots, \mathbf{w}_m\big), \end{aligned} \tag{5.4}$$

where the function $\mathcal{D}_n\big(\mathbf{k}, \tau, \mathbf{q}_1, \ldots, \mathbf{q}_N; \xi_n, \tau_1, \ldots, \tau_n, \mathbf{w}_1, \ldots, \mathbf{w}_m\big)$ stands for the Feynman diagram of order n with topology ξ_n, $\mathbf{k} = \mathbf{k}_1 + \sum_i \mathbf{q}_i$ is the total wave vector and the integrations are over all internal times τ_i of the vertices and all

internal phonon wave vectors $\mathbf{w}_i$. Note that in the above definition a minus sign has been dropped (cf. Eq. 3.50 and 3.69) since no information content of the Green's function is lost by doing so and because it is more comfortable to work with a positive definite series. Comparing Eq. 5.4 with Eq. 4.33 from the last section, we see that we can make the following identifications

$$\begin{aligned} Q(\{y\}) \quad &\longrightarrow \quad G_N(\mathbf{k},\tau;\mathbf{q}_1,\ldots,\mathbf{q}_N) \\ \{y\} \quad &\longrightarrow \quad \{\mathbf{k},\tau;\mathbf{q}_1,\ldots,\mathbf{q}_N\} \\ n \quad &\longrightarrow \quad \{0,2,4,6,8,\ldots\} \\ \{x_1,\ldots,x_n\} \quad &\longrightarrow \quad \{\tau_1,\ldots,\tau_n,\mathbf{w}_1,\ldots,\mathbf{w}_m\}. \end{aligned} \tag{5.5}$$

Thus the DQMC algorithm may be used to calculate the Green's functions. To satisfy the ergodicity requirement of the Markov chain, it is necessary to implement updates that change the external variables $\mathbf{k}$ and τ, the internal variables τ_i and $\mathbf{w}_i$, the order n and the diagram topology ξ_n (the external phonon wave vectors $\mathbf{q}_i$ are fixed according to the definition of the Green's function). It is advisable to also fix the total wave vector $\mathbf{k}$ before the DQMC simulation, so the histogram will only be collected in the τ-space instead of the $D+1$-dimensional $(\mathbf{k},\tau)$-space. This allows us to drop the $\mathbf{k}$ update.

Another useful tool is the so called guiding function or fictitious potential renormalization [10]. It is used to achieve better sampling by introducing a guiding function that leads the Markov chain to certain regions in parameter space. In our case, each diagram will be multiplied by a factor of $e^{\mu\tau}$, with μ being a free parameter, to renormalize their weights and to ensure that the calculated Green's function will show an exponential decay for large τ values like it has been predicted in Eq. 3.72. A good choice is to set μ just a little bit below the exact ground state energy $E_0(\mathbf{k})$ [9]. The factor $e^{\mu\tau}$ can be put into the free electron propagators:

$$G^0(\mathbf{k},\tau) \longrightarrow G^0(\mathbf{k},\tau,\mu) = e^{-(\epsilon(\mathbf{k})-\mu)\tau}. \tag{5.6}$$

To reverse the effect of the fictitious potential, one can either take care of it during the sampling procedure by multiplying all MC estimators by the inverse of the potential $e^{-\mu\tau}$ or by rescaling the results. In this thesis the latter is used and thus the actually calculated function will be $G(\mathbf{k},\tau)e^{\mu\tau}$, with the long-time behaviour

$$G_N(\mathbf{k},\tau)e^{\mu\tau} \xrightarrow{\tau\to\infty} Z_0^{(N)}(\mathbf{k})e^{-\left(E_0(\mathbf{k})-\mu\right)\tau}. \tag{5.7}$$

Due to finite computer memory and finite computing time ,it is not possible to explore the whole parameter space for τ, i.e. as $\tau\to\infty$. Instead, it is necessary to define some allowed maximum τ_{max}. The same goes for the order n_{max} and the number of external phonon propagators N_{max}.

In this chapter, it will be first shown how to obtain the one-electron Green's

function with the histogram method and a minimum set of updates and how to retrieve the energy and Z-factor of the lowest energy state of the polaron for a given $\mathbf{k}$ value. This will be mainly based on the paper by Prokof'ev *et al.* [9]. After that, the improvements made by Mishchenko *et al.* [10] are considered by expanding the calculations to one-electron-N-phonon Green's functions and using direct MC estimators for various quantities of interest.

5.1 One-electron Green's function - A minimal example

The Feynman diagrams for the one-electron Green's function for the Fröhlich polaron have already been derived in Sec. 3.3. They can be translated into an algebraic form by the rules in Eq. 3.66, 3.67 and 3.68. Note that the free electron propagator has been changed to $e^{-(\epsilon(\mathbf{k})-\mu)\tau}$ due to the fictitious potential $e^{\mu\tau}$ as explained above. For example, the diagram in Fig. 5.1 has the weight

$$\begin{aligned}\mathcal{D}_2\big(\mathbf{k},\tau;\xi_2,\tau_1,\tau_2,\mathbf{w}_1\big) = -G^0(\mathbf{k},\tau_1,\mu)|V_{\mathbf{w}_1}|(-G^0(\mathbf{k}-\mathbf{w}_1,\tau_2-\tau_1,\mu))\times \\ \times\,(-D^0(\mathbf{w}_1,\tau_2-\tau_1))|V_{\mathbf{w}_1}|(-G^0(\mathbf{k},\tau-\tau_1,\mu)).\end{aligned} \tag{5.8}$$

Since we know the expression for the free electron and free phonon Green's function as well as for the coupling function $V_{\mathbf{w}}$, all Feynman diagrams can be evaluated.

5.1.1 Feynman diagrams in computer memory

Before the DQMC procedure is worked out in detail, it pays off to think how to store a diagram in computer memory. Let's consider the second-order diagram given below.

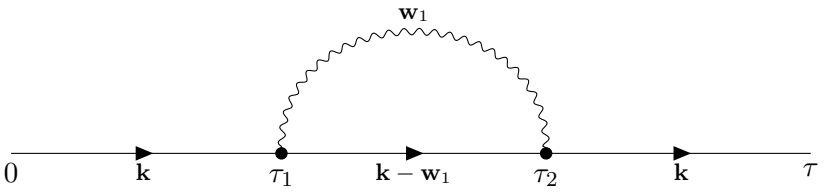

FIGURE 5.1: 2^{nd}-order diagram of the one-electron Green's function $G(\mathbf{k},\tau)$.

One way to store such a diagram would be to just keep the vertices, the total wave vector $\mathbf{k}$ and the length τ of the diagram in memory. A vertex would then consist of an incoming electron wave vector $\mathbf{k}_{in}$, an outgoing electron wave vector $\mathbf{k}_{out}$, an incoming or outgoing phonon wave vector $\mathbf{w}$, a time index τ_i and some kind of pointer, denoted as $conn$, to the vertex to which it is connected via the phonon propagator. By saving all vertices in an ordered list according to their time indices τ_i, it is possible to rebuild the diagram completely. The diagram would then look something like:

- **Diagram**:
  - total wave vector = $\mathbf{k}$
  - current length of the diagram = τ
  - Vertices:
    - Vertex 1:
      - incoming electron wave vector: $\mathbf{k}_{in} = \mathbf{k}$
      - outgoing electron wave vector: $\mathbf{k}_{out} = \mathbf{k} - \mathbf{w}_1$
      - outgoing phonon wave vector: $\mathbf{w} = \mathbf{w}_1$
      - time index: $\tau_i = \tau_1$
      - connection: $conn =$ Vertex 2
    - Vertex 2:
      - incoming electron wave vector: $\mathbf{k}_{in} = \mathbf{k} - \mathbf{w}_1$
      - outgoing electron wave vector: $\mathbf{k}_{out} = \mathbf{k}$
      - incoming phonon wave vector: $\mathbf{w} = \mathbf{w}_1$
      - time index: $\tau_i = \tau_2$
      - connection: $conn =$ Vertex 1

5.1.2 Updates

The next thing that is needed if one wants to use the DQMC algorithm from Fig. 4.3 are updates which allow one to visit the whole space of possible diagrams. To fulfill the ergodicity requirement, we need at least three: one that changes the length τ of the diagram, one that adds phonon lines and one that removes phonon lines. It is easier and probably also more effective to restrict ourselves to only add and remove one phonon propagator at a time. We will also limit the addition and removal update to phonon lines which start and end on the same electron propagator $G^0(\mathbf{k}, \tau, \mu)$ (see Fig. 5.3). This restriction would violate ergodicity. Thus it is necessary to introduce another update which swaps the phonon lines of two neighbouring vertices and therefore changes the topology of the diagram. In detail, these updates can be implemented as follows:

1. **change diagram length-update**: This is an update of *Class I*. Suppose the current diagram has length τ. To change the length of a diagram, we simply select a new τ' between the rightmost vertex at τ_r and τ_{max}. If there are no vertices, then a τ' is chosen between 0 and τ_{max}.

   The acceptance probability has the form of Eq. 4.37. Since it is advisable to have a high acceptance rate, let us first calculate the ratio between the weights of the proposed and current diagram:

$$\frac{\mathcal{D}_n\big(\mathbf{k}, \tau'; \xi_n, \tau_1, \ldots, \mathbf{w}_{n/2}\big)}{\mathcal{D}_n\big(\mathbf{k}, \tau; \xi_n, \tau_1, \ldots, \mathbf{w}_{n/2}\big)} = \frac{e^{-\Delta E \tau'}}{e^{-\Delta E \tau}}, \tag{5.9}$$

where $\Delta E = \epsilon(\mathbf{k}) - \mu$. If we draw the new value τ' from a probability distribution $w(\tau) \propto e^{-\Delta E \tau}$, the acceptance ratio will be unity as long as the proposed length τ' obeys $\tau' \leq \tau_{max}$. This can be achieved by normalizing $w(\tau)$ to unity over the allowed range $[\tau_r, \tau_{max}]$ and solving the following equation for τ' (see Eq. 4.38):

$$r = \frac{\int_{\tau_r}^{\tau'} e^{-\Delta E \tau} d\tau}{\int_{\tau_r}^{\tau_{max}} e^{-\Delta E \tau} d\tau}, \tag{5.10}$$

with r being a uniform random number from the interval $[0, 1]$. Another possibility is to normalize $w(\tau)$ to unity over $[\tau_r, \infty)$ and simply reject the proposed diagram length if $\tau' > \tau_{max}$.

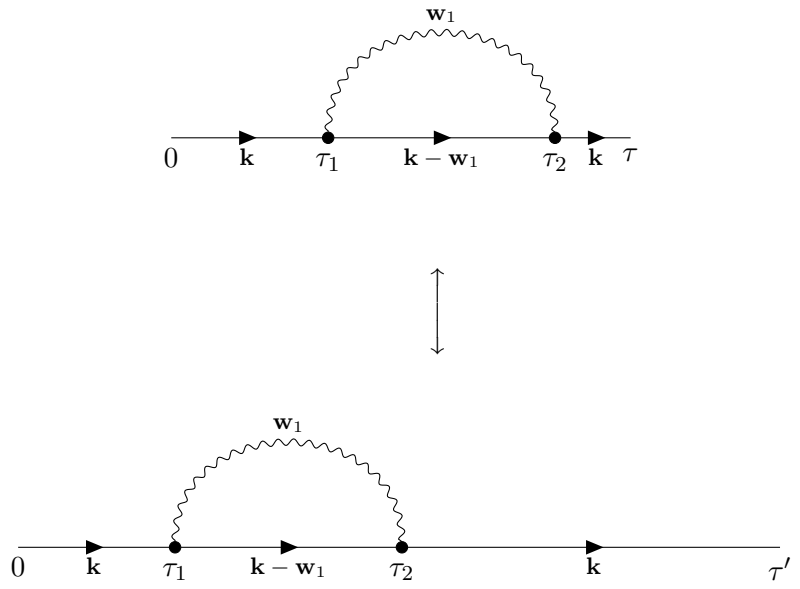

FIGURE 5.2: Update that changes the diagram length τ.

Let's have a look at this update in detail. Suppose that the current diagram is the first diagram from Fig. 5.2. The rightmost vertex is at τ_2. We choose a new diagram length τ' according to

$$\tau' = \tau_2 - \frac{\log(1 - r)}{\Delta E}. \tag{5.11}$$

If τ' is smaller than τ_{max}, then the new diagram length is accepted. If it is larger, it is rejected. Note that the probability distribution used is normalized over $[\tau_2, \infty)$, so we have to check if the proposed length is accepted or not. If the normalization would be over $[\tau_2, \tau_{max}]$, the update would always be accepted.

2. **add phonon propagator-update**: This is an update of *Class II*. It adds a phonon propagator to the diagram and therefore increases the order from n to $n + 2$. We have to propose three new parameters: the left vertex τ', the right vertex

τ'' and a phonon wave vector $\mathbf{w}'$. As mentioned above, this update will be restricted to add the phonon line only to the same electron propagator such that if the electron propagator is enclosed by a vertex at τ_l on the left and a vertex at τ_r on the right, the proposed times have to fulfill $\tau_l < \tau' < \tau'' < \tau_r$. If they violate this restriction or if $n+2 > n_{max}$, the update will be rejected. The ratio of the diagram weights is given by (the chosen electron propagator has the wave vector $\mathbf{k}_1$)

$$\begin{aligned}&\frac{\mathcal{D}_{n+2}\big(\mathbf{k},\tau;\xi_{n+2},\tau_1,\ldots,\mathbf{w}_{n/2},\tau',\tau'',\mathbf{w}'\big)}{\mathcal{D}_n\big(\mathbf{k},\tau;\xi_n,\tau_1,\ldots,\mathbf{w}_{n/2}\big)} = \\ &= \exp\left\{-(\epsilon(\mathbf{k}_1-\mathbf{w}')-\epsilon(\mathbf{k}_1)+1)(\tau''-\tau')\right\}|V_{\mathbf{w}'}|^2\frac{d\mathbf{w}'}{(2\pi)^D}d\tau' d\tau'',\end{aligned} \tag{5.12}$$

where the $+1$ in the exponential comes from the fact that $\omega = 1$. The infinitesimals occur because they do not get cancelled in the ratio. To get rid of them, the three parameters are chosen from a probability distribution $P(\tau_1,\tau_2,\mathbf{w})$ with probability $P(\tau_1,\tau_2,\mathbf{w})d\tau_1 d\tau_2 d\mathbf{w}$. The function P is an arbitrary, normalized distribution which can be chosen to yield fast convergence and a high acceptance rate or to make the sampling from it easy. We focus here on the latter and choose a distribution which factorizes as

$$\begin{aligned}P(\tau_1,\tau_2,\mathbf{w}) &= P_1(\tau_1)P_2(\tau_2|\tau_1)P_3(\mathbf{w}|\tau_1,\tau_2) = \\ &= \underbrace{\frac{1}{n+1}\frac{1}{\tau_r-\tau_l}}_{P_1(\tau_1)}\overbrace{1e^{-1(\tau_2-\tau_1)}}^{P_2(\tau_2|\tau 1)}\underbrace{\left(\frac{\tau_2-\tau_1}{2\pi}\right)^{D/2}e^{-\frac{\mathbf{w}^2}{2}(\tau_2-\tau_1)}}_{P_3(\mathbf{w}|\tau_1,\tau_2)}.\end{aligned} \tag{5.13}$$

To draw a sample $(\tau',\tau'',\mathbf{w}')$ from this distribution, let us first propose the time τ' according to $P(\tau_1)$ by choosing one of the $n+1$ electron propagators with equal probabilities and then choosing τ' uniformly random between τ_l and τ_r, where τ_l is the left and τ_r the right vertex of the electron propagator. Next τ'' is sampled from $P(\tau_2|\tau')$ by calculating

$$\tau'' = \tau' - \frac{\log(1-r)}{1}. \tag{5.14}$$

Finally, the components of the phonon wave vector are chosen from the normal distribution $P(w_i'|\tau',\tau'') = \mathcal{N}\big(0, m/(\tau''-\tau')\big)$ with mean 0 and variance $1/(\tau''-\tau')$. For the acceptance probability in Eq. 4.41, we still need the ratio $p_{\mathcal{B}}/p_{\mathcal{A}}$. The factor $p_{\mathcal{A}}$ is just the probability p_{add} of choosing the "add phonon propagator-update" . The other factor $p_{\mathcal{B}}$ is given as the probability p_{rem} of choosing the "remove phonon propagator-update" (see p.68) times the probability of choosing a phonon propagator randomly, i.e. with the same probability. Since there are $n/2+1$ phonon lines after the add update, the

ratio is

$$\frac{p_{\mathcal{B}}}{p_{\mathcal{A}}} = \frac{p_{rem}}{p_{add}(n/2+1)}. \tag{5.15}$$

The acceptance probability is calculated with

$$R_{add} = \frac{p_{rem}\exp\left\{-(\epsilon(\mathbf{k}_1-\mathbf{w}')-\epsilon(\mathbf{k}_1)+1)(\tau''-\tau')\right\}|V_{\mathbf{w}'}|^2(n+1)(\tau_r-\tau_l)}{p_{add}(n/2+1)(2\pi)^D\exp\left\{-(\tau''-\tau')\right\}\left(\frac{\tau''-\tau'}{2\pi}\right)^{D/2}\exp\left\{-\frac{\mathbf{w}'^2}{2}(\tau''-\tau')\right\}}. \tag{5.16}$$

The overall procedure is demonstrated with an update depicted in Fig. 5.3. We first choose one of the three electron propagators with probability $1/3$. Let's say we pick the one in the middle which goes from the vertex at $\tau_l = \tau_1$ to the vertex at $\tau_r = \tau_2$ with the wave vector $\mathbf{k} - \mathbf{w}_1$. We propose that the left vertex of the new phonon propagator should be at τ' which is taken from the uniform distribution normalized to the interval $[\tau_1, \tau_2]$. The time of the right vertex τ'' is then selected according to Eq. 5.14. Since we again normalized this distribution over the interval $[\tau_1, \infty)$, we have to check if $\tau'' < \tau_2 < \tau_{max}$, else the update is rejected. The components of the phonon wave vector $\mathbf{w}'$ are chosen from the normal distribution $\mathcal{N}\big(0, 1/(\tau''-\tau')\big)$. If the substitution $\mathbf{k}_1 \to \mathbf{k} - \mathbf{w}_1$ is made in Eq. 5.16, it gives us the acceptance probability.

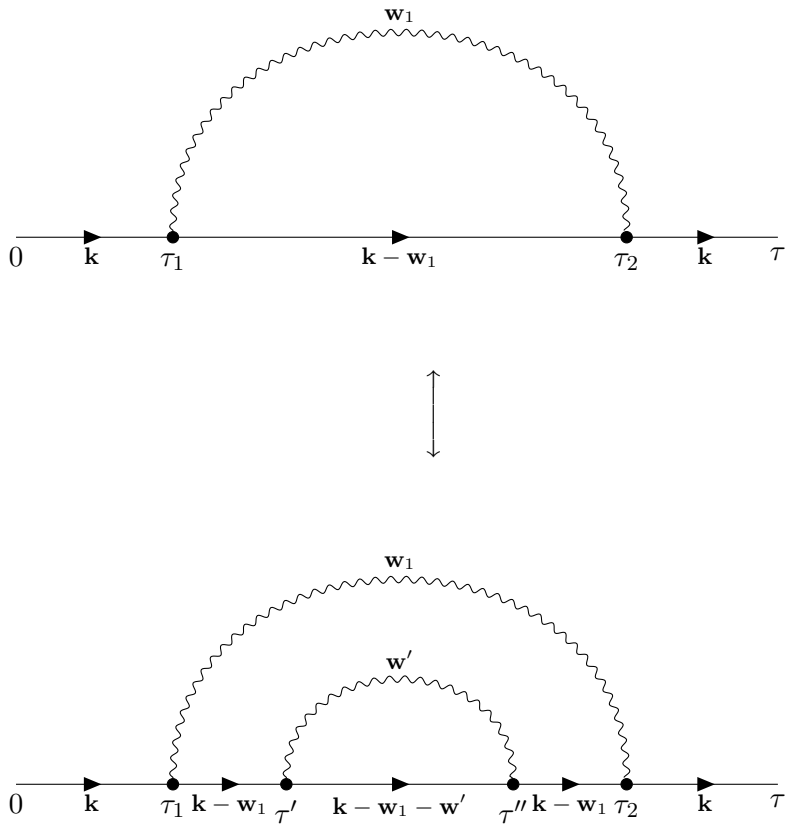

FIGURE 5.3: Update that adds or removes a phonon propagator.

3. **remove phonon propagator-update**: This is also an update of *Class II* and is the inverse of the "add phonon propagator-update" (see p. 65). The acceptance probability is given by $1/R_{add}$ assuming that the update changes the diagram order from $n+2$ to n. Suppose the current diagram is the fourth-order diagram from Fig. 5.3. One of the two phonon propagators is selected with probability $1/2$. If the selected propagator doesn't start and end on the same electron line, like the one with wave vector $\mathbf{w}_1$ going from τ_1 to τ_2, the update is rejected. Otherwise, the corresponding τ values and wave vectors are put into Eq. 5.16 and the acceptance probability is calculated with

$$R_{rem} = \frac{1}{R_{add}}. \tag{5.17}$$

4. **swap-update**: This is an update of *Class I*. It changes the topology of diagrams by swapping the phonon lines of two adjacent vertices and is necessary to fulfill the ergodicity requirement because the add- and remove-updates have been restricted to phonon propagators which start and end on the same electron line. If the two neighbouring vertices are connected via one phonon line or if there are no vertices present, the update is rejected. The acceptance probability for changing the topology from ξ_n to ξ_n' is simply given as the ratio of the corresponding diagrams:

$$\begin{aligned} R_{swap} &= \frac{\mathcal{D}_n\big(\mathbf{k}, \tau; \xi_n, \tau_1, \ldots, \mathbf{w}_{n/2}\big)}{\mathcal{D}_n\big(\mathbf{k}, \tau; \xi_n', \tau_1, \ldots, \mathbf{w}_{n/2}\big)} = \\ &= \exp\left\{-\big(\epsilon(\mathbf{k}_1 + c'\mathbf{w}' - c''\mathbf{w}'') - \epsilon(\mathbf{k}_1) - 1(c' - c'')\big)\big(\tau'' - \tau'\big)\right\}. \end{aligned} \tag{5.18}$$

Here it is assumed that the two adjacent vertices are not connected via a phonon propagator and that the electron propagator between them has a wave vector $\mathbf{k}_1$. The left vertex is at τ' with an incoming/outgoing phonon line with wave vector $\mathbf{w}'$ and the right vertex is at τ'' connected to the phonon line with wave vector $\mathbf{w}''$. The constants c^i are either equal to $+1$ or -1 depending on whether their phonon lines are outgoing ($c^i = +1$), i.e. they are connected via their phonon line to a vertex at τ^* such that $\tau^i < \tau^*$, or incoming ($c^i = -1$), i.e. $\tau^i > \tau^*$.

Figure 5.4 shows an example of the swap-update. A random adjacent vertex pair can be chosen by selecting one of the first $n-1$ vertices with equal probability and then take its right neighbour. If they are connected via a phonon propagator, for example like the vertex pair at τ_1 and τ_2 in the upper diagram in Fig. 5.4, the update is rejected. Suppose the vertex at τ_2 and its right neighbour at τ_3 are chosen. The acceptance probability for proposing the new topology is then

$$R_{swap} = \exp\left\{-\big(\epsilon(\mathbf{k} - \mathbf{w}_1 - \mathbf{w}_2) - \epsilon(\mathbf{k}) - (-2)\big)\big(\tau_3 - \tau_2\big)\right\}. \tag{5.19}$$

The inverse update is proposed in the same way and has the acceptance probability $1/R_{swap}$.

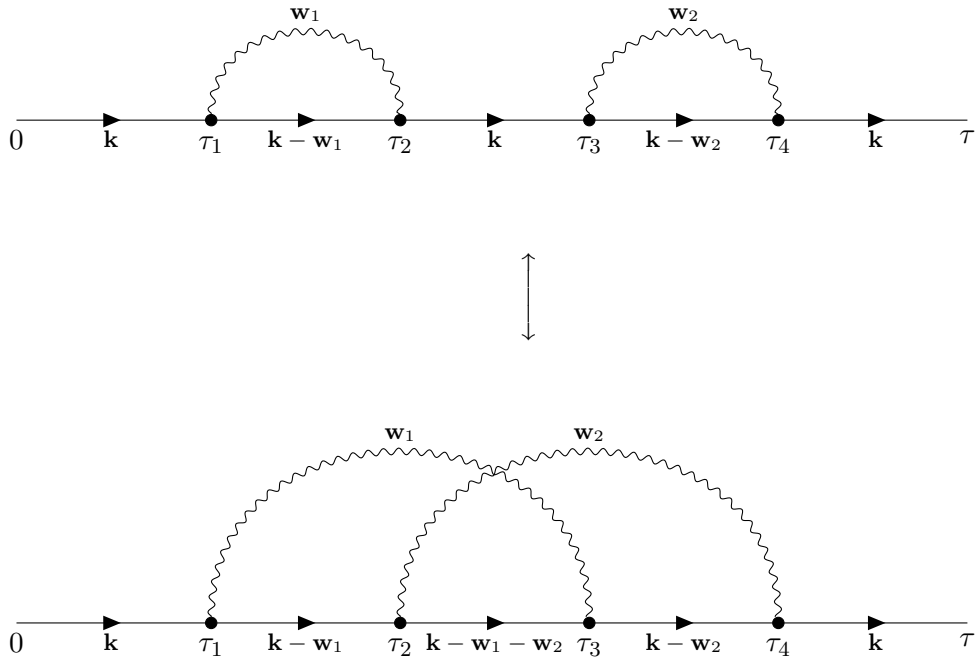

FIGURE 5.4: Update that swaps phonon propagators of two adjacent vertices.

The updates proposed above are neither unique nor the most efficient. They simply allow one to sample the whole space of diagrams and are straightforward to implement.

5.1.3 Statistics and normalization

After every diagram update, accepted or not, statistics are collected in a histogram $G^{(m)}_{MC}(\mathbf{k}, \tau_i)$ for the one-electron Green's function $G(\mathbf{k}, \tau)$, where m is the number of the current MC step and τ_i indexes the bins. Since the $\mathbf{k}$ value is kept fixed for each DQMC run, only statistics for τ are collected. This is done by defining a maximum diagram length τ_{max} and splitting the interval $[0, \tau_{max}]$ into N bins of arbitrary length $\delta\tau_i$ so that $\sum_{i=0}^{N} \delta\tau_i = \tau_{max}$. Suppose that after the mth MC step the current diagram has length τ' which lies in bin τ_j, i.e. $j = \inf\{k : \sum_{i=1}^{k} \delta\tau_i > \tau'\}$. The histogram is updated according to

$$G^{(m)}_{MC}(\mathbf{k}, \tau_j) = G^{(m-1)}_{MC}(\mathbf{k}, \tau_j) + 1. \tag{5.20}$$

That means we are just counting the number of times a diagram falls into bin τ_j. When the simulation is finished, we have to normalize our results. For this purpose, one can use the zeroth-order diagram $\mathcal{D}_0(\mathbf{k}, \tau)$. Let N_0 be the number of times $\mathcal{D}_0(\mathbf{k}, \tau)$ has been created and let M be the total number of MC steps

performed. By integrating $\mathcal{D}_0(\mathbf{k},\tau)$ from 0 to τ_{max}, we get

$$I_0 = \int_0^{\tau_{max}} \mathcal{D}_0(\mathbf{k},\tau)d\tau = \int_0^{\tau_{max}} e^{-(\epsilon(\mathbf{k})-\mu)\tau}d\tau = \frac{1-e^{-(k^2/2-\mu)\tau_{max}}}{k^2/2-\mu}. \tag{5.21}$$

The histogram is now correctly normalized by multiplying $G_{MC}^{(M)}(\mathbf{k},\tau_i)$ with I_0/N_0 and dividing by the length of the bin $\delta\tau_i$:

$$G_{MC}(\mathbf{k},\tau_i) = \frac{G_{MC}^{(M)}(\mathbf{k},\tau_i)I_0}{N_0\delta\tau_i}. \tag{5.22}$$

5.1.4 Energy and Z-factor from histogram

When the DQMC simulation of the Green's function is finished and the histogram has been normalized according to the above equation, one can retrieve the lowest energy for a given $\mathbf{k}$ value of the Fröhlich polaron by using Eq. 5.7. We therefore plot the calculated Green's function $G_{MC}(\mathbf{k},\tau)$ as a function of τ and use an exponential function of the form

$$f(\tau) = Z_0^{(0)MC}(\mathbf{k})e^{-(E_0^{MC}(\mathbf{k})-\mu)\tau} \tag{5.23}$$

to fit it against $G_{MC}(\mathbf{k},\tau)$ for large τ.

Figure 5.5 shows a calculated Green's function $G(\mathbf{0},\tau)$ for $\alpha = 2$ (electron-phonon coupling constant, see Eq. 2.60), $\mathbf{k} = \mathbf{0}$ (total wave vector) and $\mu = -2.2$ (free parameter). The exponential function has been fitted to values for $\tau > 15$ and gives the results $E_0^{MC}(\mathbf{0}) = -2.07629$ and $Z_0^{(0)MC}(\mathbf{0}) = 0.33409$.

5.1.5 Algorithm

Let's summarize the above considerations and put them together into an algorithm. The first thing that is needed is a diagrammatic expansion of the quantity of interest. In our case, it is the one-electron Green's function of the Fröhlich polaron. Its perturbation expansion in Feynman diagrams has been derived in Ch. 3. The next essential part is the implementation of updates which allow us to sample the whole diagram space. It is also necessary to determine the probabilities with which a certain update is addressed. An obvious choice would be to choose equal probabilities for all updates but they can also be tuned to improve the sampling. Then we need to define a maximum diagram length τ_{max}, a maximum diagram order n_{max}, the number of bins for the histogram N_{bins} and their length $\delta\tau_i$. For example, in Fig. 5.5 the values were set to $\tau_{max} = 50$, $n_{max} = 500$, $N_{bins} = 500$ and $\delta\tau_i = 0.1, \forall i = \{1,\ldots,N_{bins}\}$. At last we have to fix the values for α, μ and wave vector $\mathbf{k}$ and start with an initial diagram, for example a zeroth-order diagram with length τ_{init}. The algorithm is summarized in Fig. 5.6.

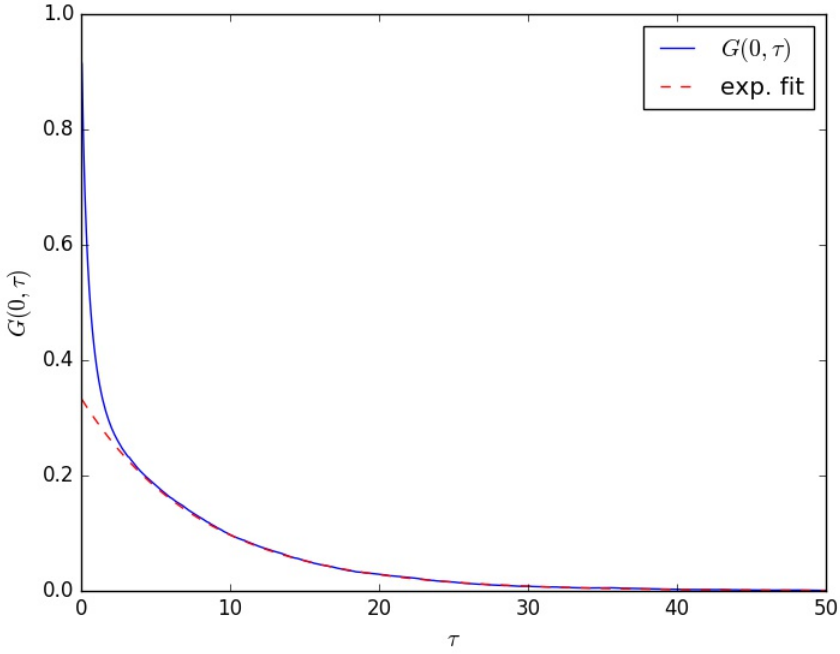

FIGURE 5.5: One-electron Green's function $G(\mathbf{0},\tau)$ and exponential fit for $\alpha = 2$, $\mathbf{k} = \mathbf{0}$ and $\mu = -2.2$.

5.2 One-electron-N-phonon Green's function

In [10] Mishchenko *et al.* improved the above algorithm by considering one-electron-N-phonon Green's functions $G_N(\mathbf{k},\tau;\mathbf{q}_1,\ldots,\mathbf{q}_N)$. This means that the diagrams have one electron line and N phonon lines starting at time 0 and ending at time τ, where τ is the length of the diagram (see Fig. 3.5). Such phonon propagators will be called external phonons. An important realization is that the one-electron Green's function, with which we were concerned in the last section, is actually a special case of the one-electron-N-phonon Green's functions: $G(\mathbf{k},\tau) = G_0(\mathbf{k},\tau)$. Implementing updates which add and remove those external phonon lines connected to the left and right end of the diagrams makes it possible to simulate all $G_N(\mathbf{k},\tau;\mathbf{q}_1,\ldots,\mathbf{q}_N)$ in one single DQMC run. Of course, the external phonon propagators have to be restricted to a maximum N_{max} because computer memory is finite. The introduction of the one-electron-N-phonon Green's functions allows one to obtain information on the phonon cloud around the electron and makes simulations in the strong-coupling regime, i.e. large α values, more efficient [10]. Mishchenko *et al.* further constructed direct MC estimators for the Green's functions, the energy, the effective mass and the Z-factors of Fröhlich polarons. These estimators enable us to use the familiar analysis of Monte Carlo simulations reviewed in Ch. 4.

Input : values for: α, μ, $\mathbf{k}$,
constants: τ_{max}, n_{max}, N_{bins}, $\delta\tau_i$, I_0
initial diagram $\mathcal{D}_{init}(\tau_{init})$
update procedures $\{U_1, \ldots, U_k\}$
updates addressing probabilities $\{p_1, \ldots, p_k\}$
Output: histogram of $G(\mathbf{k}, \tau)$

$G^{(0)}_{MC}[N_{bins}]$;
$N_0 \leftarrow 0$;
$m \leftarrow 0$;
initialize diagram $\mathcal{D}_n(\tau) \leftarrow \mathcal{D}_{init}(\tau_{init})$ and do thermalization steps;
while *not enough samples* **do**
  choose an update U_i from $\{U_1, \ldots, U_k\}$ with probabilities $\{p_1, \ldots, p_k\}$;
  propose a new diagram $\mathcal{D}'_n(\tau')$ according to U_i and set $m \leftarrow m + 1$;
  calculate acceptance ratio R_i;
  if $R \geq 1$ **then**
    $\mathcal{D}_n(\tau) \leftarrow \mathcal{D}'_n(\tau')$;
  else
    if *uniform random number* $r \leq R$ **then**
      $\mathcal{D}_n(\tau) \leftarrow \mathcal{D}'_n(\tau')$;
  end
  $j \leftarrow \inf\{k : \sum_{i=1}^{k} \delta\tau_i > \tau\}$;
  $G^{(m)}_{MC}[j] \leftarrow G^{(m-1)}_{MC}[j] + 1$;
  if $n = 0$ **then**
    $N_0 \leftarrow N_0 + 1$;
end
foreach $j = \{1, \ldots, N_{bins}\}$ **do**
  $G_{MC}[j] \leftarrow \frac{G^{(m)}_{MC}[j] I_0}{N_0 \delta\tau_j}$;
end
return G_{MC};

FIGURE 5.6: DQMC algorithm for the one-electron Green's function of the Fröhlich polaron.

5.2.1 Function of interest

The function of interest in the rest of this chapter is the sum of all one-electron-N-phonon Green's functions and is defined as

$$P(\mathbf{k}, \tau) = G(\mathbf{k}, \tau) + \sum_{N=1}^{\infty} \int \frac{V_D}{(2\pi)^D} d\mathbf{q}_1 \cdots \int \frac{V_D}{(2\pi)^D} d\mathbf{q}_N \tilde{G}_N(\mathbf{k}, \tau; \mathbf{q}_1, \ldots, \mathbf{q}_N). \quad (5.24)$$

Here the first term is the one-electron Green's function from the last section, the integrations are over all external phonon wave vectors $\mathbf{q}_i$ and the $\tilde{G}_N(\mathbf{k}, \tau; \mathbf{q}_1, \ldots, \mathbf{q}_N)$ are one-electron-N-phonon Green's functions with no unattached external phonon lines. For example, the diagrams in Fig. 3.3 and 3.4 have phonon propagators which are not connected to the electron line and are

therefore not included in $\tilde{G}_2(\mathbf{k},\tau;\mathbf{q}_1,\mathbf{q}_2)$. On the other hand, the diagram in Fig. 3.5 is included since both external phonon lines are attached to the electron line. The justification for this is that we are only interested in the long-time behaviour of $P(\mathbf{k},\tau)$ and diagrams with free external phonon propagators are exponentially suppressed due to the factor $e^{-\tau}$ for each disconnected phonon line. Using the completeness relation

$$Z_0^{(0)}(\mathbf{k}) + \sum_{N=1}^{\infty} \int \frac{V_D}{(2\pi)^D} d\mathbf{q}_1 \cdots \int \frac{V_D}{(2\pi)^D} d\mathbf{q}_N Z_0^{(N)}(\mathbf{k};\mathbf{q}_1,\ldots,\mathbf{q}_N) = 1 \tag{5.25}$$

and the long-time behaviour of the Green's functions from Eq. 3.72 and 3.74, one arrives at

$$P(\mathbf{k},\tau\to\infty) \to e^{-E_0(\mathbf{k})\tau}. \tag{5.26}$$

The function $P(\mathbf{k},\tau)$ is simulated in the DQMC procedure by generating diagrams with a variable number of external phonon lines, all of which are connected to electron propagators. The total wave vector $\mathbf{k}$ will again be kept fixed during the DQMC run, i.e. if an external phonon line is added to the diagram, then the wave vectors of electron propagators below that phonon line have to be changed to conserve the total wave vector $\mathbf{k}$ (see Fig. 5.9).

5.2.2 Direct MC estimators

The derivation of direct MC estimators is based on the fact that if the functions $A(\{y\}) = \sum_\nu \mathcal{D}_\nu^A(\{y\})$ and $B(\{y'\}) = \sum_\nu \mathcal{D}_\nu^B(\{y'\})$ are given as diagrammatic expansions and their internal variables ν are defined on the same domain, then their ratio can be approximated with the following Monte Carlo estimator

$$\frac{B(\{y'\})}{A(\{y\})} = \frac{\sum_\nu \mathcal{D}_\nu^B(\{y'\})}{\sum_\nu \mathcal{D}_\nu^A(\{y\})} \approx \frac{1}{M}\sum_{i=1}^{M} \frac{\mathcal{D}_{\nu_i}^B(\{y'\})}{\mathcal{D}_{\nu_i}^A(\{y\}} = \frac{1}{M}\sum_{i=1}^{M} Q, \tag{5.27}$$

where the ν_i are generated according to $\mathcal{D}_\nu^A(\{y\})$. This can be used to estimate the ratio of the function $P(\mathbf{k},\tau)$ with itself but for different external variables.

- *Energy estimator*: The estimator for the polaron energy follows from the observation that

$$\frac{P\big(\mathbf{k},(1+\lambda)\tau\big)}{P(\mathbf{k},\tau)} \xrightarrow{\tau\to\infty} \frac{e^{-E_0(\mathbf{k})(1+\lambda)\tau}}{e^{-E_0(\mathbf{k})\tau}} = e^{-\lambda E_0(\mathbf{k})\tau}. \tag{5.28}$$

  The ratio on the left hand side can be estimated according to Eq. 5.27. Therefore we calculate

$$Q = \frac{\mathcal{D}_n\big(\mathbf{k},(1+\lambda)\tau,\mathbf{q}_1,\ldots,\mathbf{q}_N;\xi_n,\tau_1,\ldots,\tau_n,\mathbf{w}_1,\ldots,\mathbf{w}_m\big)}{\mathcal{D}_n\big(\mathbf{k},\tau,\mathbf{q}_1,\ldots,\mathbf{q}_N;\xi_n,\tau_1,\ldots,\tau_n,\mathbf{w}_1,\ldots,\mathbf{w}_m\big)} =$$
$$= (1+\lambda)^n \prod_i \exp\left(-\lambda\epsilon(\mathbf{k}_i)\Delta\tau_i\right) \prod_j \exp\left(-\lambda\Delta\tau_j\right) \overset{\lambda\to 0}{=}$$

$$\overset{\lambda\to 0}{=} 1 + \lambda \left(n - \sum_i \epsilon(\mathbf{k}_i)\Delta\tau_i - \sum_j \Delta\tau_j \right) + \mathcal{O}(\lambda^2), \tag{5.29}$$

where n is the diagram order or the number of time integrations, i indexes all electron propagators with wave vector $\mathbf{k}_i$ and length $\Delta\tau_i = \tau_r - \tau_l$, where the electron propagator i is between a vertex at time τ_l on the left and one at τ_r on the right, and j goes over all phonon propagators with length $\Delta\tau_j$. By letting $\lambda \to 0$, we can expand Eq. 5.28 in powers of λ like it has already been done in the above equation. The right hand side gives

$$e^{-\lambda E_0(\mathbf{k})\tau} \overset{\lambda\to 0}{=} 1 - \lambda E_0(\mathbf{k})\tau + \mathcal{O}(\lambda^2). \tag{5.30}$$

Comparing both sides with each other, it is clear the lowest energy of the polaron for a given wave vector $\mathbf{k}$ can be estimated with

$$\Big\langle E_0(\mathbf{k},\alpha) \Big\rangle_{MC} = \frac{1}{M}\sum_{k=1}^{M} \frac{1}{\tau_k} \left(-n_k + \sum_i \epsilon(\mathbf{k}_i)\Delta\tau_i + \sum_j \Delta\tau_j \right), \tag{5.31}$$

where τ_k is the length and n_k the order of the current diagram. Remember that we assumed $\tau \to \infty$, so measurements should only be taken when the diagram length τ_k is greater than some minimum threshold τ_{min}.

- *Effective mass estimator*: The effective mass of the polaron can be measured at the bottom of the polaron energy band and is defined as

$$m_{pol}(\alpha) = \left[\frac{d^2 E_0(\mathbf{k},\alpha)}{d\mathbf{k}^2} \right]^{-1}_{\mathbf{k}=0}. \tag{5.32}$$

We can derive an estimator for m_{pol} by realizing that

$$\begin{aligned} &\frac{P(\lambda\hat{\mathbf{e}},\tau)}{P(\mathbf{0},\tau)} \xrightarrow[\lambda\to 0]{\tau\to\infty} \frac{\exp\{-E_0(\lambda\hat{\mathbf{e}})\tau\}}{\exp\{-E_0(\mathbf{0})\tau\}} = \\ &= \exp\big\{-\big(E_0(\lambda\hat{\mathbf{e}}) - E_0(\mathbf{0})\big)\tau\big\} = \exp\left\{-\frac{\lambda^2\tau}{2m_{pol}}\right\} = 1 - \frac{\lambda^2\tau}{2m_{pol}} + \mathcal{O}(\lambda^4), \end{aligned} \tag{5.33}$$

where $\hat{\mathbf{e}}$ is an arbitrary unit vector. The function Q is in this case

$$\begin{aligned} Q &= \frac{\mathcal{D}_n\big(\lambda\hat{\mathbf{e}},\tau,\mathbf{q}_1,\ldots,\mathbf{q}_N;\xi_n,\tau_1,\ldots,\tau_n,\mathbf{w}_1,\ldots,\mathbf{w}_m\big)}{\mathcal{D}_n\big(\mathbf{0},\tau,\mathbf{q}_1,\ldots,\mathbf{q}_N;\xi_n,\tau_1,\ldots,\tau_n,\mathbf{w}_1,\ldots,\mathbf{w}_m\big)} = \\ &= \prod_i \exp\left\{ -\left(\frac{(\mathbf{k}_i + \lambda\hat{\mathbf{e}})^2}{2} - \frac{\mathbf{k}_i^2}{2} \right)\Delta\tau_i \right\} \overset{\lambda\to 0}{=} \\ &\overset{\lambda\to 0}{=} 1 + \lambda(\hat{\mathbf{e}}\bar{\mathbf{k}})\tau - \frac{\lambda^2}{2} + \frac{\lambda^2}{2}(\hat{\mathbf{e}}\bar{\mathbf{k}})^2\tau^2 + \mathcal{O}(\lambda^3), \end{aligned} \tag{5.34}$$

with i running over all electron propagators with length $\Delta\tau_i$ and wave vector $\mathbf{k}_i$ and the average electronic wave vector of a diagram with length τ is

$$\bar{\mathbf{k}} = \frac{1}{\tau}\sum_i \mathbf{k}_i \Delta\tau_i. \tag{5.35}$$

Comparing the coefficients in Eq. 5.33 and 5.34 for the same powers in λ, one arrives at an estimator for the inverse effective mass

$$\left\langle \frac{1}{m_{pol}(\alpha)} \right\rangle_{MC} = \frac{1}{M}\sum_{k=1}^{M}\left(1 - \frac{\tau_k}{D}(\bar{\mathbf{k}}_k)^2\right), \tag{5.36}$$

where D is the dimensionality of the polaron problem under investigation, τ_k the length of the current diagram and $\bar{\mathbf{k}}_k$ its average electronic wave vector. Statistics for the effective mass estimator are only collected if the total wave vector $\mathbf{k} = 0$ and if τ_k is greater than some threshold τ_{min}.

- *Z-factor estimator*: To estimate the integrated Z-factor of the lowest energy state for a given $\mathbf{k}$ and a given number of external phonons N

$$Z_0^{(N)}(\mathbf{k}) = \int \frac{V_D}{(2\pi)^D} d\mathbf{q}_1 \cdots \int \frac{V_D}{(2\pi)^D} d\mathbf{q}_N Z_0^{(N)}(\mathbf{k}; \mathbf{q}_1, \ldots, \mathbf{q}_N), \tag{5.37}$$

the very straightforward MC estimator has been used:

$$\left\langle Z_0^{(N)}(\mathbf{k}) \right\rangle_{MC} = \frac{1}{M}\sum_{k=1}^{M}\delta_{N_k,N}. \tag{5.38}$$

This is just the probability of generating a diagram with N external phonon propagators (cf. the definition of $Z_0^{(N)}(\mathbf{k})$ in Sec. 3.4). With the Z-factors at hand, one can easily estimate the average number of phonons in the cloud around the electron $\hat{N}(\mathbf{k})$:

$$\hat{N}(\mathbf{k}) = \sum_{N=1}^{\infty} Z_0^{(N)}(\mathbf{k}) * N. \tag{5.39}$$

- *Green's function estimator*: Although it is very straightforward to use a histogram method to simulate Green's functions as has been demonstrated in Sec. 5.1, it is always plagued with the trade-off between the systematic and statistical error due to the size of the bins. In [10], an exact estimator for the integrated one-electron-N-phonon Green's functions (see Eq. 5.24) has been introduced. It is given as

$$\begin{aligned} &\left\langle G_N(\mathbf{k}, \tau_0) \right\rangle_{MC} = \\ &= \frac{1}{M}\sum_{k=1}^{M}\frac{1}{\delta\tau_0}\frac{\mathcal{D}_{n_k}\left(\mathbf{k}, \tau_0, \mathbf{q}_1, \ldots, \mathbf{q}_N; \nu_k\right)}{\mathcal{D}_{n_k}\left(\mathbf{k}, \tau_k, \mathbf{q}_1, \ldots, \mathbf{q}_{N_k}; \nu_k\right)}\Theta\left(|\tau_k - \tau_0| - \frac{\delta\tau_0}{2}\right)\delta_{N_k,N}, \end{aligned} \tag{5.40}$$

where ν_k are the internal variables, τ_k is the length, N_k is the number of external phonon propagators and n_k is the order of the current diagram k and Θ is the step function. It is assumed that τ_0 is the center of an arbitrary interval $[\tau_0 - \frac{\delta\tau_0}{2}, \tau_0 + \frac{\delta\tau_0}{2}]$ of length $\delta\tau_0$. The ratio of the diagrams has already been calculated in Eq. 5.29 with the substitution $\lambda = (\tau_0 - \tau_k)/\tau_k$:

$$\begin{aligned}&\frac{\mathcal{D}_{n_k}\big(\mathbf{k}, \tau_0, \mathbf{q}_1, \ldots, \mathbf{q}_N; \nu_k\big)}{\mathcal{D}_{n_k}\big(\mathbf{k}, \tau_k, \mathbf{q}_1, \ldots, \mathbf{q}_{N_k}; \nu_k\big)} = \\ &= \left(1 + \frac{\tau_0 - \tau_k}{\tau_k}\right)^{n_k} \exp\left\{-\frac{\tau_0 - \tau_k}{\tau_k}\left(\sum_i \epsilon(\mathbf{k}_i)\Delta\tau_i + \sum_j \Delta\tau_j\right)\right\}.\end{aligned} \tag{5.41}$$

More estimators and more details can be found in [10]. In the following calculations only the ones presented above were used.

5.2.3 Updates

To be able to sample one-electron-N-phonon Green's functions and ultimately the function $P(\mathbf{k}; \tau)$, it is necessary to upgrade and modify the updates from the last section. The updates are again only restricted by the ergodicity requirement and by the conditions in Eq. 4.37 and 4.41. In our case, we will at least need updates which add and remove internal phonon propagators, which add and remove external phonon propagators and which change the length τ of the diagram. A possible set of updates is presented below.

1. **change diagram length-update**: This is a *Class I* update and basically the same as already introduced in Sec. 5.1.2. The only thing that changes is that the diagrams going to be updated may have phonon lines attached to their ends. We therefore need a different probability distribution from which we choose the new diagram length τ'. The ratio of the diagram weights is given by

$$\frac{\mathcal{D}_n\big(\mathbf{k}, \tau', \mathbf{q}_1, \ldots, \mathbf{q}_N; \xi_n, \tau_1, \ldots, \mathbf{w}_m\big)}{\mathcal{D}_n\big(\mathbf{k}, \tau, \mathbf{q}_1, \ldots, \mathbf{q}_N; \xi_n, \tau_1, \ldots, \mathbf{w}_m\big)} = \frac{e^{-\Delta E\tau'}}{e^{-\Delta E\tau}}, \tag{5.42}$$

with $\Delta E = \epsilon(\mathbf{k}) - \mu + N$. If the new diagram length is chosen according to

$$\tau' = \tau_l - \frac{\log(1-r)}{\Delta E}, \tag{5.43}$$

where τ_l is the right most vertex, then the update will be accepted every time as long as $\tau' < \tau_{max}$. In the example shown in Fig. 5.7, the right most vertex is $\tau_l = \tau_4$ and the new diagram length τ' is determined by calculating

$$\tau' = \tau_4 - \frac{\log(1-r)}{\epsilon(\mathbf{k} - \mathbf{q}_1) - \mu + 1} \tag{5.44}$$

and accepted if $\tau' < \tau_{max}$.

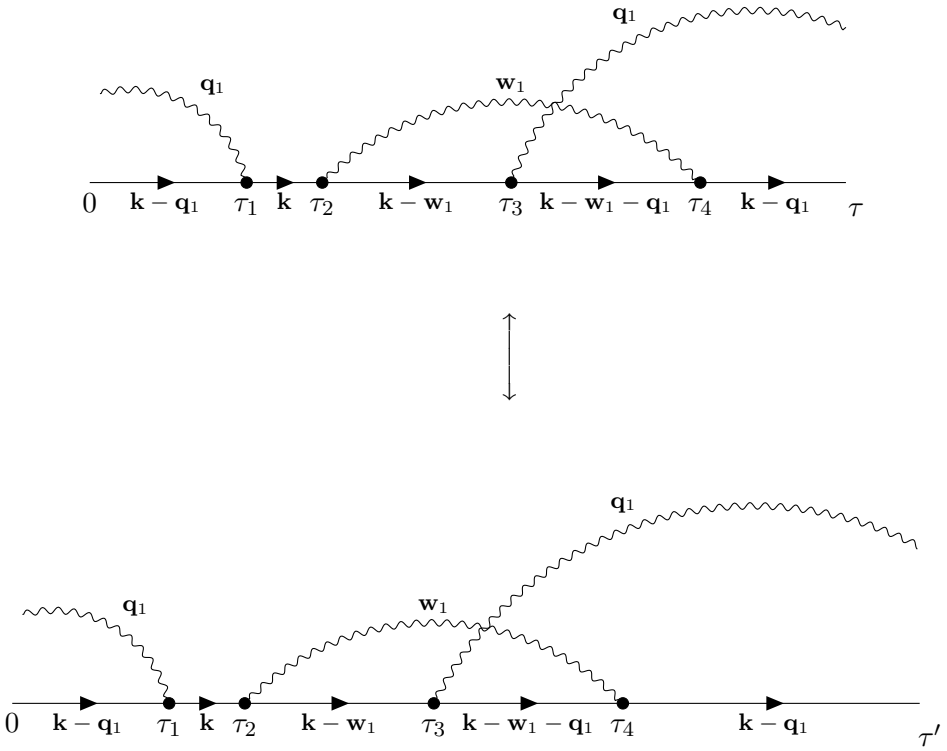

FIGURE 5.7: Update that changes the diagram length τ of a diagram with external phonons.

2. **add internal phonon propagator-update**: A *Class II* update and very similar to the "add phonon propagator-update" (see p. 65). The difference is that we will now remove the restriction that the phonon propagator to be added has to start and end on the same electron line. This only changes the ratio of the diagram weights and therefore the acceptance probability. Apart from that, the new parameters $(\tau', \tau'', \mathbf{w}')$ are drawn from the same probability distribution $P_1(\tau_1)P_2(\tau_2|\tau_1)P_3(\mathbf{w}|\tau_1,\tau_2)$ presented in Eq. 5.13. The ratio of the diagram weights is now

$$\frac{\mathcal{D}_{n+2}\big(\mathbf{k},\tau,\mathbf{q}_1,\ldots,\mathbf{q}_N;\xi_{n+2},\tau_1,\ldots,\mathbf{w}_m,\tau',\tau'',\mathbf{w}'\big)}{\mathcal{D}_n\big(\mathbf{k},\tau,\mathbf{q}_1,\ldots,\mathbf{q}_N;\xi_n,\tau_1,\ldots,\mathbf{w}_m\big)} = \\ = \exp\left\{-\left(\sum_i(\epsilon(\mathbf{k}_i-\mathbf{w}')-\epsilon(\mathbf{k}_i)\Delta\tau_i+(\tau''-\tau')\right)\right\}|V_{\mathbf{w}'}|^2\frac{d\mathbf{w}'}{(2\pi)^D}d\tau' d\tau'', \tag{5.45}$$

where the sum runs over all electron propagators with length $\Delta\tau_i$ between τ' and τ''. We can immediately write down the acceptance probability R^{in}_{add} as

$$\frac{p^{in}_{rem}\exp\left\{-\left(\sum_i(\epsilon(\mathbf{k}_i-\mathbf{w}')-\epsilon(\mathbf{k}_i))\Delta\tau_i+(\tau''-\tau')\right)\right\}|V_{\mathbf{w}'}|^2(n+1)(\tau_r-\tau_l)}{p^{in}_{add}(m+1)(2\pi)^D\exp\left\{-(\tau''-\tau')\right\}\left(\frac{\tau''-\tau'}{2\pi}\right)^{D/2}\exp\left\{-\frac{\mathbf{w}'^2}{2}(\tau''-\tau')\right\}}. \tag{5.46}$$

Here m is the number of internal phonon propagators of the current diagram. If $n+2 > n_{max}$, the update is rejected. An example of the "add internal phonon propagator-update" is shown in Fig. 5.8.

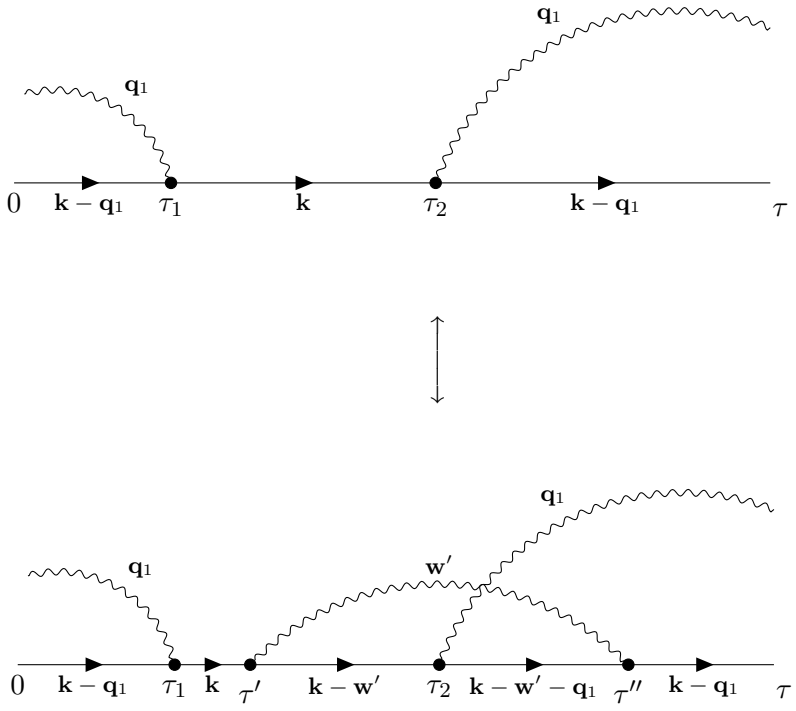

FIGURE 5.8: Update that adds and removes an internal phonon propagator.

3. **remove internal phonon propagator-update**: This is also an update of *Class II* and the inverse of "add internal phonon propagator-update" (see p. 77). Therefore the acceptance probability will be

$$R^{in}_{rem} = \frac{1}{R^{in}_{add}}, \tag{5.47}$$

where R^{in}_{add} is given in Eq. 5.46. For this to be correct, it is assumed that the current diagram is of order $n+2$ and a new diagram of order n is proposed. This update is performed by simply choosing one of the $m+1$ internal phonon propagators with equal probabilities and put the τ values of its left and right vertex as well as its wave vector into the acceptance probability. If accepted, the chosen phonon line is removed. Of course if there are no internal phonon propagators present, we reject the update.

4. **add external phonon propagator-update**: A *Class II* update which increases the order of the current diagram by adding a phonon propagator to the left and right end of the diagram. The overall procedure is very similar to the update which adds an internal phonon line (see p. 77). Let τ' be the proposed

time of the vertex connected to the left end, τ'' the proposed time of the vertex connected to the right end of the diagram and $\mathbf{q}'$ the proposed wave vector of the phonon propagator, e.g. as in the second diagram in Fig 5.9. These parameters are chosen from the following probability distribution:

$$P(\tau_1,\tau_2,\mathbf{q}) = P_1(\tau_1)P_2(\tau_2)P_3(\mathbf{q}|\tau_1,\tau_2) = \\ = \underbrace{1e^{-1(\tau_1)}}_{P_1(\tau_1)}\overbrace{1e^{-1(\tau-\tau_2)}}^{P_2(\tau_2)}\underbrace{\left(\frac{\tau-\tau_2+\tau_1}{2\pi}\right)^{D/2} e^{-\frac{\mathbf{q}^2}{2}(\tau-\tau_2+\tau_1)}}_{P_3(\mathbf{q}|\tau_1,\tau_2)}, \tag{5.48}$$

where τ is the length of the current diagram. $P_1(\tau_1)$ is normalized over $[0,\infty)$ and $P_2(\tau_2)$ is normalized over $(-\infty,\tau]$, so that we have to check if $\tau' < \tau$ and $\tau'' > 0$, else the update is rejected. The components of $\mathbf{q}'$ are drawn from a normal distribution $q_i' \sim \mathcal{N}\big(0, 1/(\tau-\tau''+\tau')\big)$ with mean 0 and variance $1/(\tau-\tau''+\tau')$.

We now have to distinguish between two possibilities. If $\tau' < \tau''$, then we are given a diagram which looks like the second diagram in Fig. 5.9 and the ratio of the diagram weights is given by

$$\frac{\mathcal{D}_{n+2}\big(\mathbf{k},\tau,\mathbf{q}_1,\ldots,\mathbf{q}_{N+1};\xi_{n+2},\tau_1,\ldots,\mathbf{w}_m,\tau',\tau'',\mathbf{q}'\big)}{\mathcal{D}_n\big(\mathbf{k},\tau,\mathbf{q}_1,\ldots,\mathbf{q}_N;\xi_n,\tau_1,\ldots,\mathbf{w}_m\big)} = \\ = \exp\left\{-\left(\sum_i(\epsilon(\mathbf{k}_i-\mathbf{q}')-\epsilon(\mathbf{k}_i))\Delta\tau_i + (\tau'+\tau-\tau'')\right)\right\}|V_{\mathbf{q}'}|^2\frac{d\mathbf{w}'}{(2\pi)^D}d\tau' d\tau'', \tag{5.49}$$

where the sum goes over all electron propagators with length $\Delta\tau_i$ between 0 and τ' and between τ'' and τ. On the other hand, if $\tau' > \tau''$, then the diagram takes the form of the third diagram in Fig. 5.9 and the diagram weight ratio becomes

$$\frac{\mathcal{D}_{n+2}\big(\mathbf{k},\tau,\mathbf{q}_1,\ldots,\mathbf{q}_{N+1};\xi_{n+2},\tau_1,\ldots,\mathbf{w}_m,\tau',\tau'',\mathbf{q}'\big)}{\mathcal{D}_n\big(\mathbf{k},\tau,\mathbf{q}_1,\ldots,\mathbf{q}_N;\xi_n,\tau_1,\ldots,\mathbf{w}_m\big)} = \\ = \exp\left\{-\left(\sum_i(\epsilon(\mathbf{k}_i-\mathbf{q}')-\epsilon(\mathbf{k}_i))\Delta\tau_i + \sum_j(\epsilon(\mathbf{k}_j-2\mathbf{q}')-\epsilon(\mathbf{k}_j))\Delta\tau_j\right)\right\}\times \\ \times\exp\big\{(\tau'+\tau-\tau'')\big\}|V_{\mathbf{q}'}|^2\frac{d\mathbf{q}'}{(2\pi)^D}d\tau' d\tau'', \tag{5.50}$$

where the sum over i goes over all electron propagators between 0 and τ'' and between τ' and τ and the sum over j goes over the other electron propagators between τ'' and τ'. The acceptance probability R_{add}^{ex} is in both cases given by Eq. 4.41 with the probability distribution $P_1(\tau')P_2(\tau'')P_3(\mathbf{q}'|\tau',\tau'')$ from

Eq. 5.48, the corresponding weight ratio and

$$\frac{p_{\mathcal{B}}}{p_{\mathcal{A}}} = \frac{p^{ex}_{rem}}{p^{ex}_{add}(N+1)}. \tag{5.51}$$

If $N + 1 > N_{max}$, the update is automatically rejected.

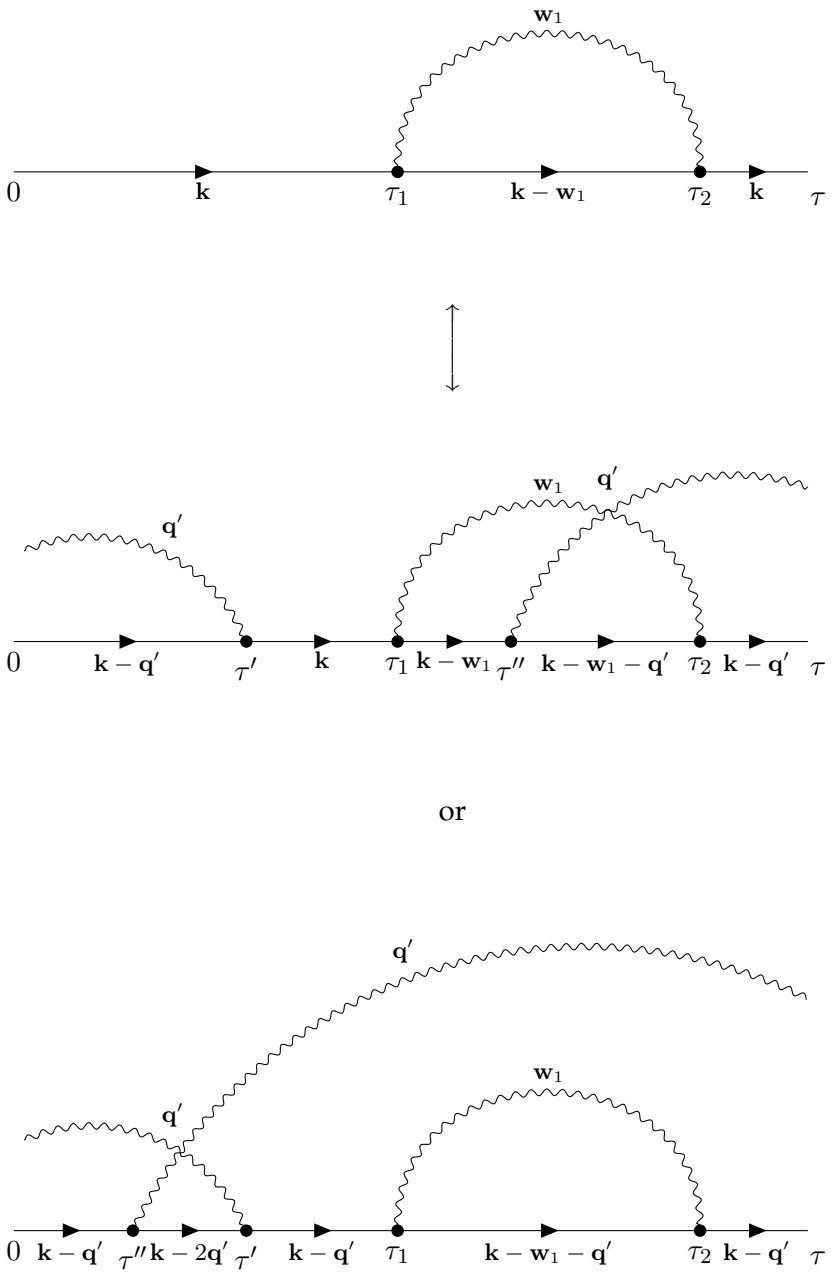

FIGURE 5.9: Update that adds and removes an external phonon propagator.

5. **remove external phonon propagator-update**: This is also a *Class II* update and is the inverse of the "add external phonon propagator-update" (see p. 78). It is performed in exactly the same way as for internal phonon lines. One of

the $N+1$ external phonon propagators is chosen with equal probabilities, the acceptance ratio is calculated

$$R^{ex}_{remove} = \frac{1}{R^{ex}_{add}} \tag{5.52}$$

and the update is either accepted or rejected. If there are no external phonon lines present in the current diagram, we reject the update automatically.

With the updates presented so far, the ergodicity requirement is fulfilled. They are not unique and most of them, if not all, can be further improved. Implementing more updates may also lead to a faster convergence and better sampling of the diagram space. For example, in the calculations done below, three additional updates have been used. These updates were also proposed in [10]:

- **swap-update**: This is the same update which has been introduced for the one-electron Green's function DQMC in Sec. 5.1.2. It swaps internal phonon lines of two neighbouring vertices and its acceptance probability is simply the ratio of the diagram weights. If the vertices are connected via a phonon propagator or if at least one of them is connected to the diagram end, i.e. an external phonon line, then the update is rejected.

- **shift-update**: A *Class I* update which shifts a vertex in time, i.e. it changes its position in the diagram. At first, one vertex is chosen randomly. Suppose this vertex is currently at τ', its left neighbour is at τ_l and its right neighbour at τ_r. Then a new time τ'' is proposed between (τ_l, τ_r) according to

$$\tau'' = \tau_l - \frac{\log\left(1 - r\left(1 - e^{-\Delta E(\tau_r - \tau_l)}\right)\right)}{\Delta E}, \tag{5.53}$$

where $\Delta E = \epsilon(\mathbf{k}_{in}) - \epsilon(\mathbf{k}_{out}) + c'$, $\mathbf{k}_{in}$ is the incoming wave vector, $\mathbf{k}_{out}$ is the outgoing wave vector and $c' = +1$ if the phonon line of the vertex is incoming or $c' = -1$ if it is outgoing (see "swap-update" in Sec. 5.1.2). This update is always accepted unless there are no vertices in the current diagram.

- **stretch length-update**: This is a *Class I* update. It stretches or compresses the whole diagram like a spring. In fact, each electron propagator and the above lying phonon propagators are stretched or compressed one at the time. For the first electron line, a new length is proposed just as it is done in the "change diagram length-update" (see p. 76). As long as the length of the whole diagram is smaller than τ_{max}, the new length of the electron line is accepted. The same is done for all other electron propagators of the diagram.

5.2.4 Statistics and normalization

Using the updates from above, one is able to generate Feynman diagrams for the one-electron-N-phonon Green's functions and therefore also for the function

$P(\mathbf{k},\tau)$ introduced in Sec. 5.2.1. It allows us to use the direct MC estimators for the energy, effective mass, Z-factor and the Green's functions themselves. After every update, the estimators for the current diagram are evaluated and collected. Remember that some of them should only be collected if the length of the diagram or the total wave vector $\mathbf{k}$ are in a certain range. In the end, the estimators for the energy, effective mass and Z-factor are averaged over all sampled diagrams like it is done in an ordinary Monte Carlo simulation. On the other hand, the estimators for Green's functions and for $P(\mathbf{k},\tau)$ are normalized like the one-electron Green's function in Eq. 5.22. The errors can be estimated with the blocking method discussed in Sec. 4.1.1.

5.2.5 Algorithm

We are now ready to put all these considerations into an algorithm. Suppose the diagrammatic expansions of the one-electron-N-phonon Green's functions are given and that the updates, which fulfill ergodicity and detailed balance with respect to the diagram weights, have already been implemented. Before the DQMC simulation is started, one has to define certain parameters:

- τ_{max}: maximum allowed diagram length
- τ_{min}: minimum length of diagrams for which certain estimators (energy, effective mass, Z-factor) are collected
- n_{max}: maximum allowed diagram order
- N_{max}: maximum allowed number external phonon propagators
- $\{\tau_i\}$, $\{\delta\tau_i\}$: set of points at which one wants to evaluate the function $P(\mathbf{k},\tau)$ or any other $\tilde{G}_N(\mathbf{k},\tau;\mathbf{q}_1,\ldots,\mathbf{q}_N)$ and corresponding intervals surrounding those points

Furthermore, an initial diagram $\mathcal{D}_{init}(\tau_{init})$ needs to be defined, for example a zeroth-order diagram of length 1. At last, values for α, $\mathbf{k}$ and μ have to be fixed.

Figure 5.10 shows an example and the overall structure of the algorithm. For simplicity, it focuses only on the function $P(\mathbf{k},\tau)$ and one estimator, for example the energy. It doesn't include any error analysis and the points $\{\tau_i\}$ are assumed to be evenly distributed over $[0,\tau_{max}]$ and that they are the center of an interval of size $\delta\tau$ such that $\sum_i \tau_i\delta\tau = \tau_{max}$. The terms $p_{MC}(\mathcal{D}_n(\tau))$ and $e_{MC}(\mathcal{D}_n(\tau))$ correspond to the Green's function and energy estimator evaluated for the current diagram $\mathcal{D}_n(\tau)$ in the Markov chain. Figure 5.11 and 5.12 show the graphs of some $P(\mathbf{k},\tau)$ and $G(\mathbf{k},\tau)$. The exponential functions $e^{-(E_0^{MC_1}-\mu)\tau}$ and $Z_0^{MC_2}e^{-(E_0^{MC_2}-\mu)\tau}$ have been fitted to values $\tau > 15$. Energy estimates from the exponential fits are $E_0^{MC_1} = -5.55016$ and $E_0^{MC_2} = -5.54508$, respectively and from the direct MC estimator $E_0^{(est)} = -5.5529$.

Input : values for: α, μ, $\mathbf{k}$
constants: τ_{max}, τ_{min}, n_{max}, N_{max}, $\{\tau_i\}$, $\delta\tau$, I_0
initial diagram $\mathcal{D}_{init}(\tau_{init})$
update procedures $\{U_1, \ldots, U_k\}$
updates addressing probabilities $\{p_1, \ldots, p_k\}$
Output: estimator E_{MC}, $P(\mathbf{k}, \tau)$

$P^{(0)}_{MC}[\tau_{max}/\delta\tau]$;
$N_0 \leftarrow 0$;
$E^{(0)}_{MC} \leftarrow 0$;
$m \leftarrow 0$; `// counts all MC steps`
$c \leftarrow 0$; `// counts all samples taken for the estimator`
initialize diagram $\mathcal{D}_n(\tau) \leftarrow \mathcal{D}_{init}(\tau_{init})$;
do thermalization steps;
while *not enough samples* **do**
  choose an update U_i from $\{U_1, \ldots, U_k\}$ with probabilities $\{p_1, \ldots, p_k\}$;
  propose a new diagram $\mathcal{D}'_n(\tau')$ according to U_i;
  calculate acceptance ratio R;
  if $R \geq 1$ **then**
    $\mathcal{D}_n(\tau) \leftarrow \mathcal{D}'_n(\tau')$;
  else
    draw random uniform number r;
    if $r \leq R$ **then**
      $\mathcal{D}_n(\tau) \leftarrow \mathcal{D}'_n(\tau')$;
  end
  $m \leftarrow m + 1$;
  $j \leftarrow \inf\{k : k\delta\tau > \tau, k \in \mathbb{N}\}$;
  $P^{(m)}_{MC}[j] \leftarrow P^{(m-1)}_{MC}[j] + p_{MC}(\mathcal{D}_n(\tau))$;
  if $n = 0$ **then**
    $N_0 \leftarrow N_0 + 1$;
  if $\tau > \tau_{max}$ **then**
    $c \leftarrow c + 1$;
    $E^{(c)}_{MC} \leftarrow E^{(c-1)}_{MC} + e_{MC}(\mathcal{D}_n(\tau))$;
end
foreach $j = \{1, \ldots, \tau_{max}/\delta\tau\}$ **do**
  $P_{MC}[j] \leftarrow \frac{P^{(m)}_{MC}[j] I_0}{N_0 \delta\tau}$;
end
$E_{MC} \leftarrow \frac{E^{(c)}_{MC}}{c}$;
return P_{MC}, E_{MC};

FIGURE 5.10: DQMC algorithm for the function $P(\mathbf{k}, \tau)$ of the Fröhlich polaron.

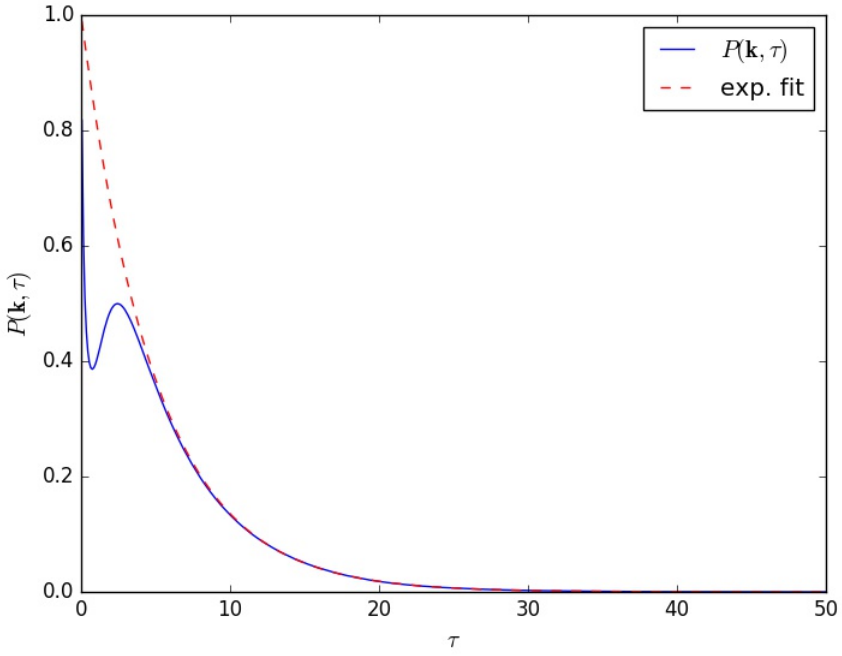

FIGURE 5.11: $P(\mathbf{0},\tau)$ and exponential fit for $\alpha = 5$, $\mathbf{k} = 0$ and $\mu = -5.75$.

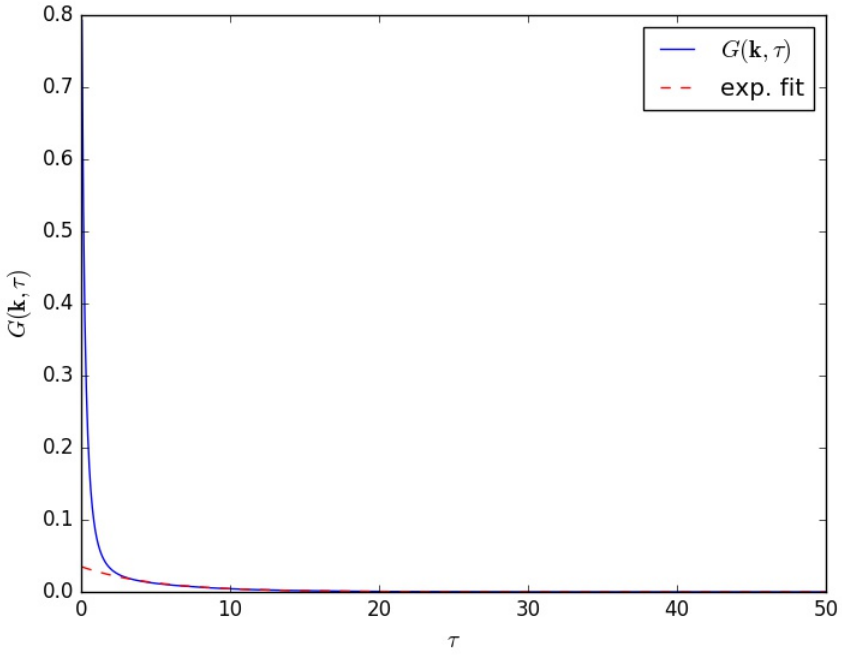

FIGURE 5.12: $G(\mathbf{0},\tau)$ and exponential fit for $\alpha = 5$, $\mathbf{k} = 0$ and $\mu = -5.75$.

Chapter 6

Results and Discussion

In [9] and [10], the Diagrammatic Quantum Monte Carlo method has been applied to the three dimensional Fröhlich polaron to obtain various quantities of interest. This thesis tried to reproduce these results as well as to produce new results corresponding to the two dimensional case using our own implementation of the DQMC algorithm. To obtain the results shown below, the MC estimators and updates discussed in the last Ch. 5 have been used. The implementation basically follows the algorithm described in Fig. 5.10 with some minor modifications and additions. Units are chosen such that $\hbar = \omega = m^* = 1$. All calculations were performed on the Vienna Scientific Cluster (VSC).

This chapter presents results for the 3D and 2D Fröhlich polaron calculated with the DQMC procedure. The results include ground state energies $E_0(\mathbf{0}, \alpha)$, effective masses $m_{pol}(\alpha)$, Z-factors $Z_0^{(N)}(\mathbf{k})$ and average number of phonons $\bar{N}(\mathbf{k})$ in the cloud of the polaron ground state as a function of the coupling constant α as well as the lowest energies as a function of the length k of the total wave vector $\mathbf{k}$ (polaron dispersion). The difference between the polaronic effects on 3D and 2D systems is shown and the results are compared to ones obtained analytically and to properties known exactly presented in Sec. 2.4.

6.1 Results

6.1.1 Ground state energy

At first the ground state energy $E_0(\mathbf{0}, \alpha)$ as a function of the coupling constant is examined. The total wave vector is therefore set to zero $\mathbf{k} = \mathbf{0}$ and the MC estimator for the energy from Eq. 5.31

$$\left\langle E_0(\mathbf{k}, \alpha) \right\rangle_{MC} = \frac{1}{M} \sum_{k=1}^{M} \frac{1}{\tau_k} \left(-n_k + \sum_i \epsilon(\mathbf{k}_i) \Delta\tau_i + \sum_j \Delta\tau_j \right) \tag{6.1}$$

is used to find the lowest energies for given α values. Figure 6.1 displays $E_0(\mathbf{0}, \alpha)$ for different coupling constants in 3D and 2D. Both graphs are compared to results obtained with Feynman's path integral approach. The values of the Feynman results

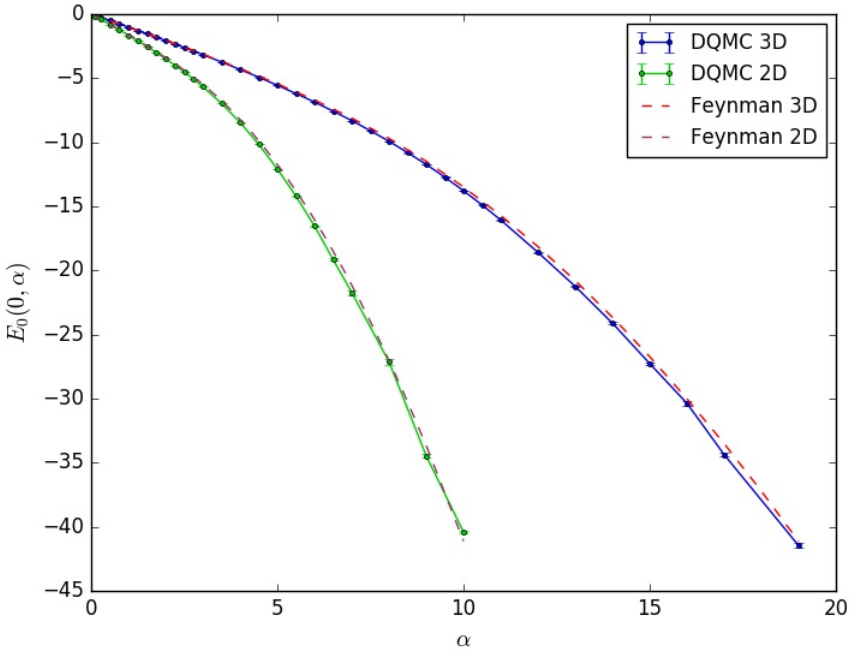

FIGURE 6.1: Ground state energy $E_0(\mathbf{0}, \alpha)$ vs. α in 2D and 3D.

for 3D are taken from [52] and then scaled to 2D with the exact scaling relations introduced in Sec. 2.4.5:

$$E_0^{2D}(\mathbf{0}, \alpha) = \frac{2}{3} E_0^{3D}\left(\mathbf{0}, \frac{3\pi}{4}\alpha\right), \tag{6.2}$$

This plot especially shows the remarkable accuracy and usefulness of Feynman's approach since it is of variational nature and therefore constitutes an upper bound for the polaron energy. Likewise, it is already seen that the polaron effect in two dimensions is stronger than in three. The corresponding data is listed in Tab. 6.1 (3D) and Tab. 6.2 (2D). Due to the nature of the scaling relations, values in the 2D case were read off directly from the plot. For $\alpha > 8$, they were calculated from the expansion in Eq. 2.118 and the scaling relation in Eq. 6.2.

Furthermore, the accuracy of the calculations has been evaluated using the exactly known expansion coefficients in the weak-coupling limit $\alpha \to 0$ and strong-coupling limit $\alpha \to \infty$. The expansions and their coefficients have been presented in Sec. 2.4.6 and are given by

$$E_0(\mathbf{0}, \alpha \to 0) = -q_1\alpha - q_2\alpha^2 + \mathcal{O}(\alpha^3), \tag{6.3}$$

$$\lim_{\alpha\to\infty} \frac{E_0(\mathbf{0}, \alpha)}{\alpha^2} = -\eta. \tag{6.4}$$

The results are displayed in Table 6.3.

α	E_0 DQMC	E_0 Feynman [52]	m_{pol} DQMC	m_{pol} Feynman [52]
1	-1.01526(122)	-1.0130308	1.19502(3)	1.1955147
2	-2.06973(114)	-2.0553559	1.46182(11)	1.4718919
3	-3.16762(118)	-3.1333335	1.84974(20)	1.8889540
4	-4.32490(211)	-4.2564809	2.45196(57)	2.5793104
5	-5.55297(296)	-5.4401445	3.47194(180)	3.8856197
6	-6.86647(287)	-6.7108710	5.41952(625)	6.8383564
7	-8.31039(309)	-8.1126875	9.7130(268)	14.394070
8	-9.92206(606)	-9.6953709	20.55(14)	31.569255
9	-11.72535(701)	-11.485786	46.90(78)	62.751527
10	-13.7820(136)	-13.490437	98.8(3.3)	111.81603
11	-16.0660(127)	-15.709808	158.2(4.6)	183.12497
12	-18.5943(240)	-18.143395	270.1(20.0)	281.62189
13	-21.2434(249)	-20.790681	/	412.78190
14	-24.1151(369)	-23.651278	/	582.58390
15	-27.2629(359)	-26.724904	/	797.49838

TABLE 6.1: Ground state energies $E_0(\mathbf{0}, \alpha)$ and effective masses $m_{pol}(\alpha)$ in 3D from the DQMC and Feynman method. Values in brackets stand for the uncertainty in the DQMC simulation, e.g $-1.01526(122)$ has a sample standard error of $1.22 * 10^{-3}$.

α	E_0 DQMC	E_0 Feynman [40, 52]	m_{pol} DQMC	m_{pol} Feynman [40, 52]
1	-1.64314(20)	-1.62664	1.57530(11)	1.6213
2	-3.48253(46)	-3.4002	3.01904(120)	3.50306
3	-5.66337(46)	-5.48136	8.94191(730)	15.6066
4	-8.45543(149)	-8.22536	52.108(341)	83.763
5	-12.08288(610)	-11.7398	229.3(7.8)	260.148
6	-16.5403(269)	-16.0485	601.9(46.0)	612.374
7	-21.7231(566)	-21.1579	/	1225.62
8	-27.1346(802)	-27.0381	/	2184.62
9	-34.4669(370)	-33.6643	/	/
10	-40.4139(379)	-41.1183	/	/

TABLE 6.2: Ground state energies $E_0(\mathbf{0}, \alpha)$ and effective masses $m_{pol}(\alpha)$ in 2D from the DQMC and Feynman method. Values in brackets stand for the uncertainty in the DQMC simulation, e.g $-1.64314(20)$ has a sample standard error of $2.0 * 10^{-4}$.

	q_1 exact	q_1 calc.	q_2 exact	q_2 calc.	η exact	η calc.
3D	1	1.00394	0.01592	0.01586 ($\alpha < 2$)	0.1085	0.10783 ($8 \leq \alpha < 15$)
2D	1.5708	1.5784	0.06397	0.06885 ($\alpha < 1$)	0.4047	0.4042 ($4 \leq \alpha < 8$)

TABLE 6.3: Exactly known vs. calculated expansion coefficients of $E_0(\mathbf{0}, \alpha)$ for the weak- and strong-coupling limit.

6.1.2 Effective mass

The effective mass of the Fröhlich polaron was obtained with the MC estimator from Eq. 5.36:

$$\left\langle \frac{1}{m_{pol}(\alpha)} \right\rangle_{MC} = \frac{1}{M} \sum_{k=1}^{M} \left(1 - \frac{\tau_k}{D} (\bar{\mathbf{k}}_k)^2 \right), \tag{6.5}$$

where D is the dimension of the system and $\bar{\mathbf{k}}_k$ is the average electronic wave vector of the current diagram k. Note that the estimator actually gives a value for the inverse effective mass so that its reciprocal must be taken. DQMC results are compared again to Feynman's variational technique. The Feynman results for three dimensions are taken once more from the paper by Rosenfelder et al. [52] and then scaled to two dimensions using the relation from Sec. 2.4.5

$$\frac{m_{pol}^{2D}(\alpha)}{m_{2D}^{*}} = \frac{m_{pol}^{3D}\left(\frac{3\pi}{4}\alpha\right)}{m_{3D}^{*}}. \tag{6.6}$$

Tables 6.1 and 6.2 show the calculated values for the effective polaron mass in comparison with Feynman's path integral approach. For large α values, the error in the Monte Carlo estimators became too big and so they have been omitted. The corresponding curves are plotted in Fig. 6.2.

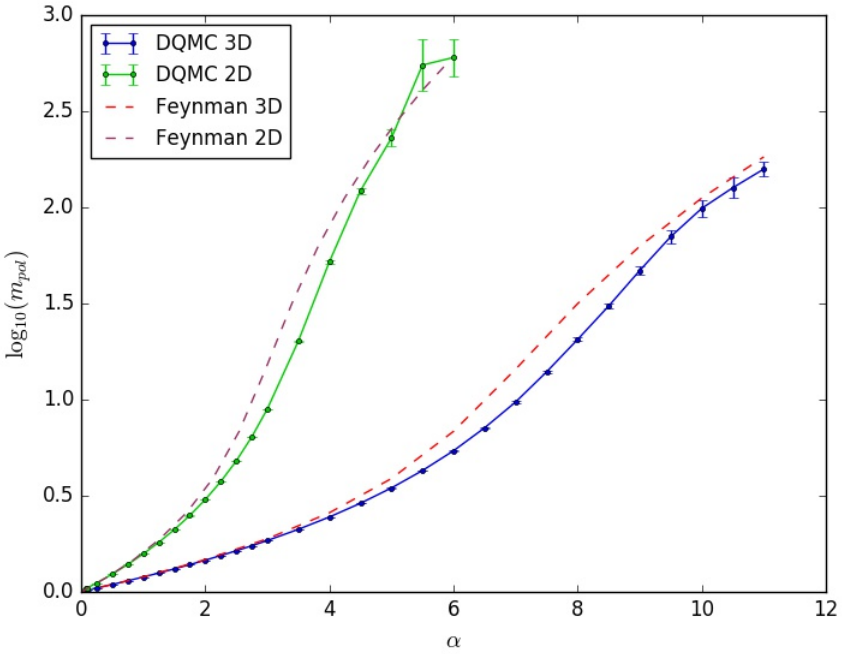

FIGURE 6.2: Logarithm of the effective polaron mass $m_{pol}(\alpha)$ as a function of α in 2D and 3D.

6.1.3 Z-factors and average number of phonons

The integrated Z-factor $Z_0^{(N)}(\mathbf{k})$ is defined as

$$Z_0^{(N)}(\mathbf{k}) = \int \frac{V_D}{(2\pi)^D} d\mathbf{q}_1 \cdots \int \frac{V_D}{(2\pi)^D} d\mathbf{q}_N |\left\langle pol(\mathbf{k})\right| a_{\mathbf{p}}^{\dagger} b_{\mathbf{q}_1}^{\dagger} \ldots b_{\mathbf{q}_N}^{\dagger} \left|vac\right\rangle|^2, \tag{6.7}$$

where $|pol(\mathbf{k})\rangle$ is the polaron state with the lowest energy for a given $\mathbf{k}$ value and $|vac\rangle$ is the vacuum state with no electron and no phonon present. It is readily estimated in the DQMC simulation using the MC estimator from Eq. 5.38

$$\left\langle Z_0^{(N)}(\mathbf{k}) \right\rangle_{MC} = \frac{1}{M} \sum_{k=1}^{M} \delta_{N_k,N}. \tag{6.8}$$

Since the $Z_0^{(N)}(\mathbf{k})$ sum up to 1, i.e.

$$\sum_{N=0}^{\infty} Z_0^{(N)}(\mathbf{k}) = 1, \tag{6.9}$$

it gives the probability of finding the polaronic state $|pol(\mathbf{k})\rangle$ in a state with N phonons. The Z-factor $Z_0^{(0)}(\mathbf{0})$ is therefore the contribution of the bare electron state to the ground state $|pol(\mathbf{0})\rangle$ of the polaron. Figure 6.3 shows how the bare electron Z-factor behaves with increasing coupling between the electron and the phonon field. If there is no coupling, i.e. $\alpha = 0$, then $Z_0^{(0)}(\mathbf{0}) = 1$ which means that there is no polaron and that the solution is basically a one-body object consisting of a single electron. When α is increased, the bare electron state loses importance because the polaron becomes more and more a many-body object, i.e. dressed with phonons. The polaronic effect is again seen to be stronger in 2D than in 3D.

In Fig. 6.4 and 6.5 the integrated Z-factors of the ground state as a function of the number of phonons N is plotted for different α values. This shows that the contribution of states with a higher number of phonons becomes more important when the coupling is increased. For a given α value, for example $\alpha = 6$ in Fig. 6.4 and 6.5, the polaron in 2D is surrounded on average by more phonons than in 3D ≈ 28 and ≈ 5, respectively. The distribution of the number of phonons in the cloud around the electron seems to approach a normal distribution with increasing coupling constant. It has a mean $\bar{N}(\mathbf{k})$ which is computed easily with

$$\hat{N}(\mathbf{k}) = \sum_{N=1}^{\infty} Z_0^{(N)}(\mathbf{k}) * N. \tag{6.10}$$

The average number of phonons in the polaron ground state $\bar{N}(\mathbf{0})$ is shown as a function of α in Figure 6.6.

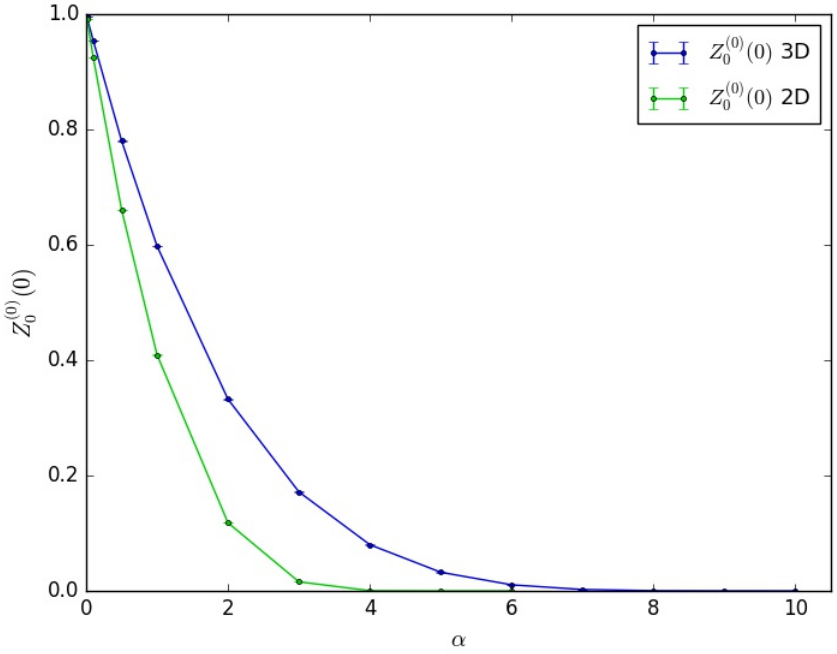

FIGURE 6.3: Bare-electron contribution $Z_0^{(0)}(\mathbf{0})$ to the polaron ground state as a function of α in 2D and 3D.

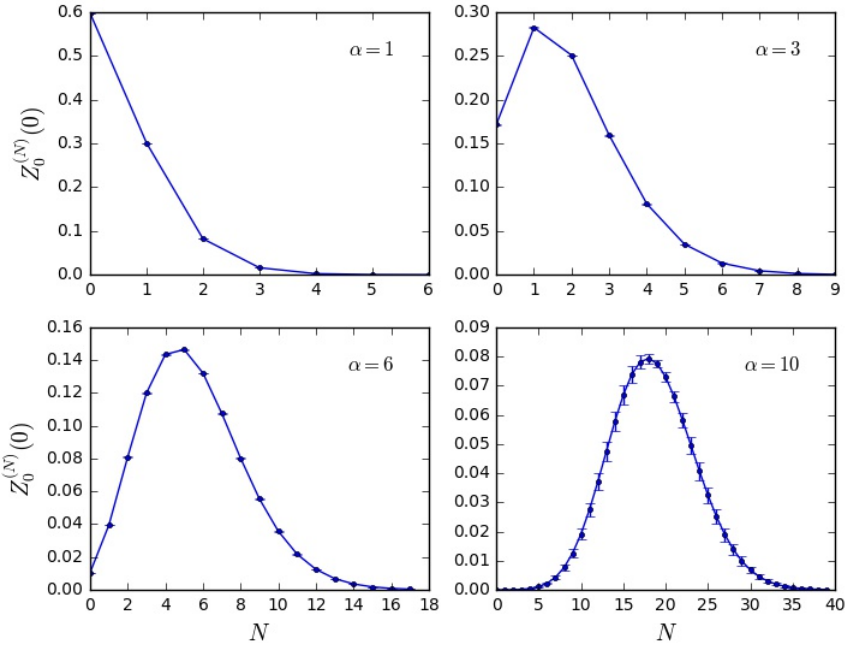

FIGURE 6.4: N-phonon contribution $Z_0^{(N)}(\mathbf{0})$ to the polaron ground state as a function of N in 3D for different coupling strengths α.

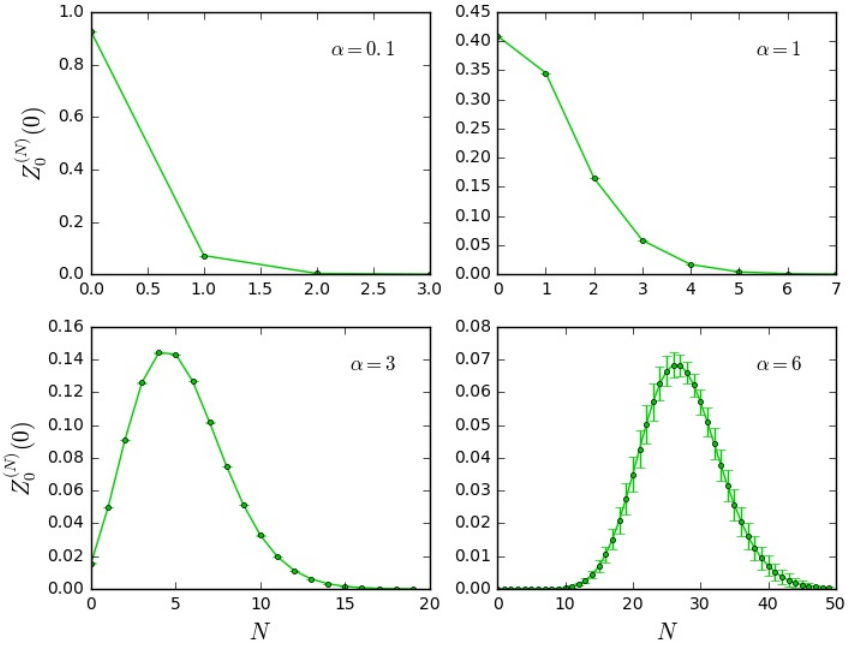

FIGURE 6.5: N-phonon contribution $Z_0^{(N)}(\mathbf{0})$ to the polaron ground state as a function of N in 2D for different coupling strengths α.

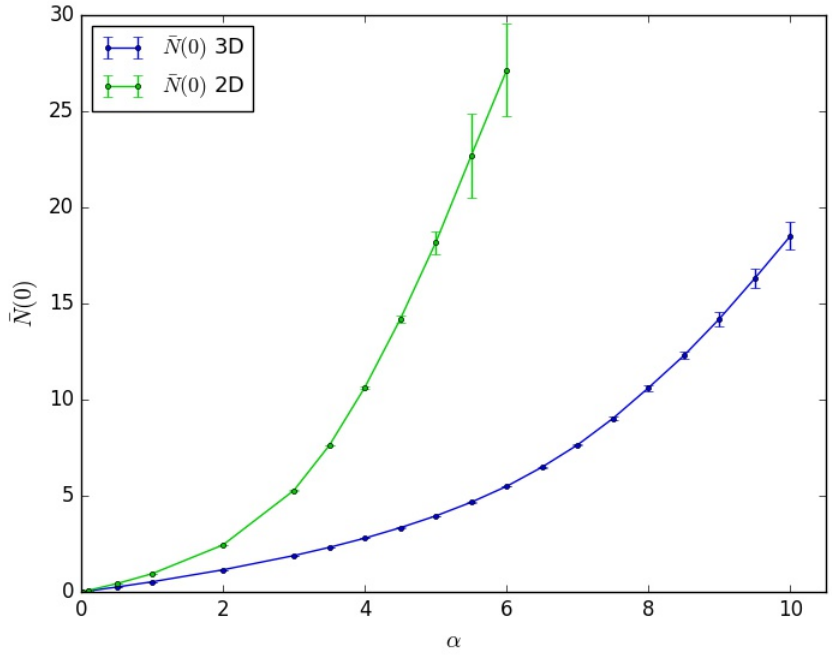

FIGURE 6.6: Average number of phonons $\bar{N}(\mathbf{0})$ in the polaron ground state as a function of α in 2D and 3D.

6.1.4 Polaron dispersion

One of the most interesting results are the polaron dispersion curves shown in Fig. 6.7 and 6.8. The plots display $E_0(\mathbf{k}, \alpha) - E_0(\mathbf{0}, \alpha)$ as a function of the total wave vector length k to make the comparison between different α values more apparent. $E_0(\mathbf{k}, \alpha)$ is the lowest energy eigenvalue of all eigenstates of the polaron corresponding to a given $\mathbf{k}$ and α value (see Eq. 2.76 and Sec. 3.4). The quantity $E_0(\mathbf{k}, \alpha) - E_0(\mathbf{0}, \alpha)$ simply shifts the polaron dispersion such that the ground state energy $E_0(\mathbf{0}, \alpha)$ is set to 0. The continuum edge $E_c(\alpha) = E_0(\mathbf{0}, \alpha) + \hbar\omega$ or in our units $E_c(\alpha) = E_0(\mathbf{0}, \alpha) + 1$ is also included (see Sec. 2.4.6).

In 3D, the polaron dispersion graph crosses the continuum edge at some finite $k_c(\alpha)$ as can be seen in Fig. 6.7. The following values have been obtained: $k_c(1) \approx 1.83$, $k_c(3) \approx 2.95$ and $k_c(5) \approx 4.825$. In 2D, the dispersion plot bends over at large k and approaches the continuum edge asymptotically as has been predicted in [36]. With increasing electron-phonon coupling, the dispersions become more flat regardless of the spatial dimension. It is also seen that $E_0(\mathbf{k}, \alpha)$ is indeed a strictly increasing function of k.

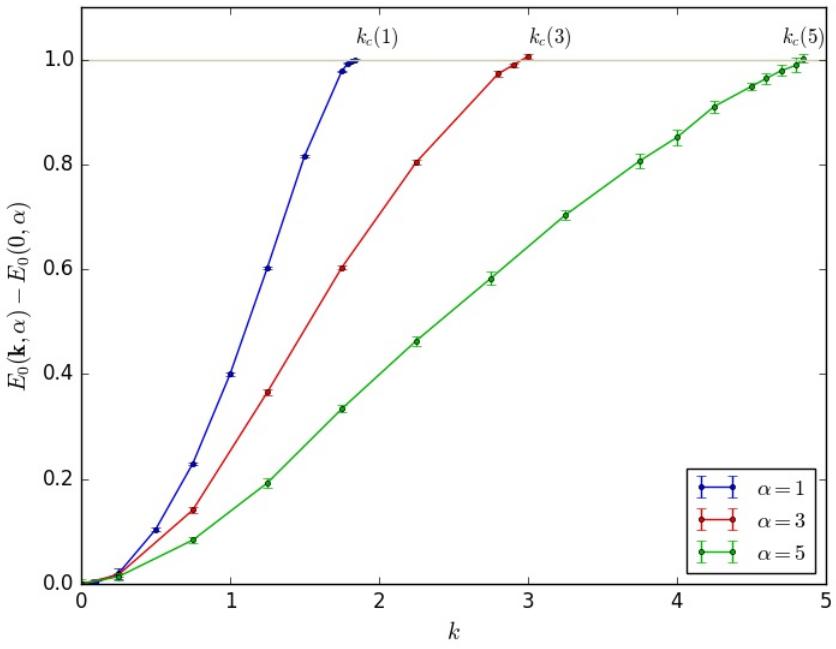

FIGURE 6.7: Shifted polaron dispersion $E_0(\mathbf{k}, \alpha) - E_0(\mathbf{0}, \alpha)$ for different coupling constants α in 3D. The grey line indicates the continuum edge $E_c(\alpha)$ and $k_c(\alpha)$ is the wave vector modulus k at which $E_0(\mathbf{k}, \alpha) = E_c(\alpha)$.

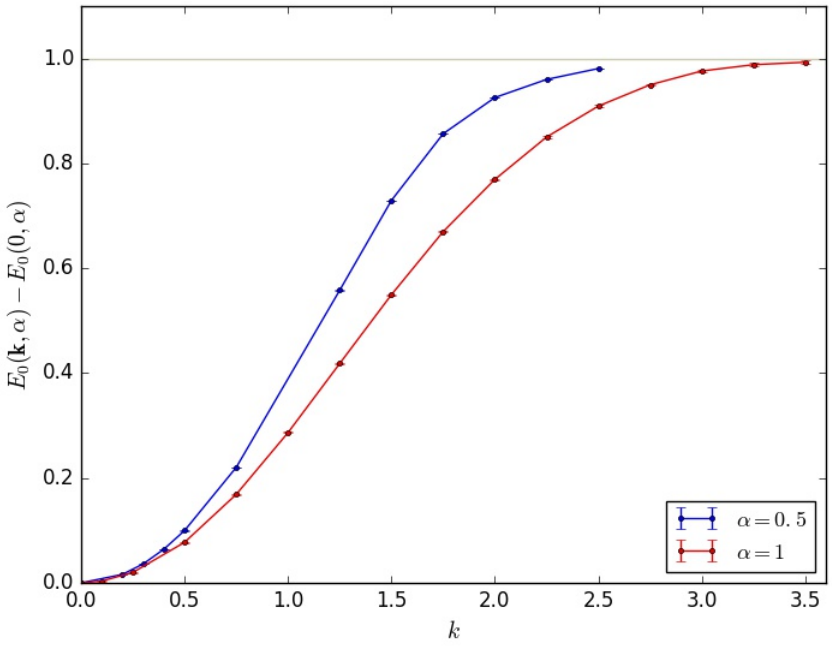

FIGURE 6.8: Shifted polaron dispersion $E_0(\mathbf{k},\alpha) - E_0(\mathbf{0},\alpha)$ for different coupling constants α in 2D. The grey line indicates the continuum edge.

6.2 Discussion

The discussion focuses mostly on the algorithmic part and on the implementation. The accuracy of our results and the comparison to other available DQMC data [9, 10] is mentioned only briefly. The physics are also discussed only shortly since it has been done already and can be found in papers, books and reviews about the Fröhlich polaron, for example in [25, 28, 31].

The Fröhlich Hamiltonian from Eq. 5.1 describes the interaction between a single electron and a phonon field. Its strength is determined by the coupling constant $\alpha \geq 0$. If there is no coupling between the electron and phonons, i.e. $\alpha = 0$, the interaction term from the Hamiltonian drops out and left is a simple operator describing a free Bloch electron and a free phonon field. The ground state energy of this system is then $E_0(\mathbf{0}, 0) = 0$ since it consists of an electron at rest and a phonon vaccum. This can be seen in Fig. 6.3. For $\alpha = 0$, the contribution of the bare electron state to the polaron ground state is $Z_0^{(0)}(\mathbf{0}) = 1$ which means they are the same. When the interaction is turned, i.e. $\alpha > 0$, the electron couples to the phonon field. The contribution of the bare electron state to the ground state of the polaron becomes less important because the polaron is now a many-body object (see Fig. 6.3). We say that the electron 'dresses' itself with a cloud of phonons. The stronger the coupling the more phonons will be in the cloud around the electron as

can be seen in Fig. 6.4, 6.5 and 6.6. The dressing of the electron with phonons increases the polaron effective mass (Fig.6.2) and lowers its ground state energy (Fig. 6.1) with respect to the effective mass and energy of a free Bloch electron.

In all our results presented in Sec. 6.1, it can be seen that the effects of the electron-phonon interaction are stronger in 2D than in 3D. The most interesting difference is shown in the dispersion relations in Fig. 6.7 and 6.8. In three spatial dimensions, the polaron dispersion crosses the continuum edge E_c at a finite value k_c, while in two dimensions, the dispersion bends over and approaches E_c asymptotically. Polarons with energies above the continuum edge have a finite life-time, even at zero temperature [53].

Our implementation of the DQMC algorithm for the 3D Fröhlich polaron seems to reproduce the results from other available DQMC data correctly. For example, our Fig. 5.5 of the one-electron Green's function $G(\mathbf{0}, \tau)$ for $\alpha = 2$ and the one presented in the paper by Prokof'ev *et al.* [9] seem to be nearly identical. The same goes for the graphs showing the ground state energy (Fig. 6.1), the effective polaron mass (Fig. 6.2), Z-factors (Fig. 6.3 and 6.4) and average number of phonons (Fig. 6.6) when compared to figures from the paper by Mishchenko *et al.* [10]. Unfortunately, we don't have the exact numerical data from those papers available at the moment which makes a more rigorous comparison difficult.

The Diagrammatic Quantum Monte Carlo method is a powerful algorithm which has proven to work in many applications and for many different systems. The Fröhlich polaron problem is a good way to get familiar with the DQMC technique. Its Green's functions have positive definite and convergent diagrammatic expansions so that one doesn't have to deal with the sign problem or use any resummation techniques. Also the topologies of the Feynman diagrams are simple, which makes the structure and implementation of the updates easy. Furthermore, a lot of properties and results for the Fröhlich polaron are already known. This allows for tests and accuracy evaluations of the DQMC method.

The implementation itself is quite straightforward once the Feynman diagrams and suitable updates are known. Especially, the algorithm and corresponding updates presented in Sec. 5.1 for the one-electron Green's function are not hard to turn into a working computer code. Retrieving the energy and bare electron Z-factor by fitting an exponential function to the Green's function at large τ values can be a bit tedious and also leaves room for errors. This is of course avoided by introducing the direct MC estimators. They also make it possible to use the well known error analysis from ordinary Monte Carlo simulations, which is very important for any stochastic calculations. One has to be aware that the local nature of these updates leads to correlation between generated diagrams. When the formula for the sample standard error given in Eq. 4.12 is used, the error will be underestimated by orders

of magnitude. The blocking method helps us to get reliable error bars but with the drawback that we have to take many samples. Particularly for increasing α values, the autocorrelation time becomes quite large so that the simulation has to run for a long time to get trustworthy error estimates. Additional and more sophisticated update procedures could make the sampling of the diagram space more efficient and may reduce the correlation between diagrams.

Introducing the one-electron-N-phonon Green's functions $G_N(\mathbf{k}, \tau)$ into the DQMC algorithm does not only allow us to use the direct MC estimators or to obtain interesting statistics on the phonon cloud around the electron (Fig. 6.4, 6.5 and 6.6) but it makes the calculations in the strong-coupling regime more efficient. The one-electron-0-phonon Green's function does not contribute much to the function $P(\mathbf{k}, \alpha)$ for large α as can be seen by comparing Fig. 5.11 and 5.12. Especially, long diagrams with large τ values, in which we are mainly interested, are rarely generated in simulations for $G_0(\mathbf{k}, \tau)$. This is where the $G_N(\mathbf{k}, \tau)$ functions and the $P(\mathbf{k}, \tau)$ function become important.

One of the major difficulties we came across was to get good results in the strong coupling regime, i.e. $\alpha > 10$ in 3D and $\alpha > 5$ in 2D. This can be seen in the graphs for the energy (Fig. 6.1), the effective mass (Fig. 6.2) and the Z-factors (Fig. 6.4 and 6.5). In the case of the Z-factor and the effective mass, the obvious problem is that the errors get too large with increasing coupling constant. The Z-factor estimates may be readily improved by using the circular diagram representation and the corresponding MC estimator described in the paper by Mishchenko *et al.* [10]. For the effective mass, the problem is inherent to its definition. It is defined as the inverse of the curvature of the polaron dispersion at the bottom of the energy band (see Eq. 5.32). For large α values, the energy band becomes more flat and accurately calculating the second derivative at $k = 0$ becomes more difficult. Another source for the large errors may be that the MC estimator for the effective mass is actually estimating the inverse effective mass. The polaron mass is increasing fast with increasing coupling between the electron and the phonon field. So its inverse gets very small leading to large errors in the estimator. One can try to bypass this problem by calculating $E_0(\mathbf{k}, \alpha)$ for small k values and use a difference quotient to obtain the effective mass. For this to work, the energy estimates would have to be given to a high accuracy. It has not been tried in this thesis.

Another problem is more subtle. The results in the strong coupling regime seem to depend significantly on the free parameter value μ which should be chosen slightly below the exact polaron energy. This is not the case for weak coupling. In the implementation used for the present thesis, μ is fixed before the simulation starts and it is not changed during runtime. This might be the problem. A solution could be to start with a μ value significantly below the expected true ground state and

then increase it slowly during the thermalization phase of the Markov chain.

Regarding the implementation, the code written for this thesis has not been parallelized. All calculations were performed on the Vienna Scientific Cluster 3 (VSC3). Each node on the cluster consists of 16 cores. A node was utilized by distributing a single DQMC simulation to every core, i.e. 16 simulations for different $\mathbf{k}$ and α values done simultaneously on one node.

Chapter 7

Summary and Outlook

This thesis has taken a closer look at the Diagrammatic Quantum Monte Carlo method for the Fröhlich polaron as described in [9, 10]. The main goal was to implement the DQMC algorithm and use it to obtain ground state energies, Z-factors, effective masses and dispersion curves for the three and two dimensional Fröhlich polaron presented in Ch. 6. The 3D results have been used to verify the correctness of our code as well as its accuracy by comparing them to exactly known expansions in the weak- and strong coupling limits (see Tab. 6.3). The 2D results are new to our knowledge or at least have not been obtained via the DQMC method.

The thesis started with an overview of the polaron problem in general including a derivation of the Fröhlich Hamilton operator (Ch. 2). In Chapter 3, Green's functions in many body physics and quantum field theory have been introduced. It was shown how to obtain a perturbation expansion of Green's functions and how they are related to Feynman diagrams before the diagrammatic expansion of the Fröhlich Hamiltonian was derived. Chapter 4 reviewed basic concepts of Monte Carlo simulations and Markov chains. This was followed by an introduction to the DQMC method. Maybe the most important chapter is Ch. 5. It tried to explain the DQMC algorithm for the Fröhlich polaron in detail and to give a step-by-step manual on how it can be implemented. Results have been presented and discussed in Ch. 6.

Future work on the DQMC method and specifically on the code written for this thesis can be devoted to either improve the code in terms of performance and accuracy of the results or to use it and apply it to different physical systems. For the latter, it is likely that some parts of the code would have to be changed, especially when the Feynman diagrams take on different forms as the ones for the Fröhlich polaron. An example where the diagram topology stays the same and where to our knowledge no DQMC algorithm has been applied, is a ripplonic polaron. Another interesting modification could be to use the diagrammatic expansion from the Fröhlich polaron but allow for a non-parabolic electron dispersion and for non-constant phonon dispersions as well as different phonon branches.

Bibliography

[1] H. Haken. *Quantenfeldtheorie des Festkörpers*. B. G. Teubner Verlag, 1973.

[2] W. Nolting. *Fundamentals of Many-body Physics*. Springer, 2009.

[3] G. Czycholl. *Theoretische Festkörperpyhsik Band 1*. 4th ed. Springer, 2016.

[4] F. Bloch. "Über die Quantenmechanik der Elektronen in Kristallgittern". In: *Zeitschrift für Physik* 52.7-8 (1929), pp. 555–600.

[5] J. Vlietinck. "Diagrammatic Monte Carlo study of polaron systems". PhD thesis. Universiteit Gent, 2014-2015.

[6] H. Fröhlich. "Electrons in lattice fields". In: *Advances in Physics* 3.11 (1998), pp. 325–361.

[7] R. P. Feynman. "Slow electrons in a polar crystal". In: *Physical Review* 97.3 (1955), pp. 660–665.

[8] A. S. Alexandrov and J. T. Devreese. *Advances in Polaron Physics*. Springer, 2010.

[9] N. V. Prokof'ev and B. V. Svistunov. "Polaron problem by Diagrammatic Quantum Monte Carlo". In: *Physical Review Letters* 81 (1998).

[10] A. S. Mishchenko, N. V. Prokof'ev, and A. Sakamoto B. V. Svistunov. "Diagrammatic quantum Monte Carlo study of the Fröhlich polaron". In: *Physical Review B* 62.10 (2000), pp. 6317–6336.

[11] N. V. Prokof'ev and B. V. Svistunov. "Fermi-polaron problem: Diagrammatic Monte Carlo method for divergent sign-alternating series". In: *Physical Review B* 77.020408 (2008).

[12] A. S. Mishchenko. "Diagrammatic Monte Carlo method as applied to the polaron problems". In: *Physics - Uspekhi* 48.9 (2005), pp. 887–902.

[13] J. Vlietinck, J. Ryckebusch, and K. Van Houcke. "Quasiparticle properties of an impurity in a Fermi gas". In: *Physical Review B* 87.115133 (2013).

[14] J. Vlietinck, J. Ryckebusch, and K. Van Houcke. "Diagrammatic Monte Carlo study of the Fermi polaron in two dimensions". In: *Physical Review B* 89.085119 (2014).

[15] J. Vlietinck et al. "Diagrammatic Monte Carlo study of the acoustic and the Bose-Einstein condensate polaron". In: *New J. Phys.* 17.033023 (2015).

[16] L. Landau. "Über die Bewegung der Elektronen im Kristallgitter". In: *Phys. Z. Sowjet.* 3 (1933), p. 664.

[17] E. I. Rashba. "Polarons". In: *Encyclopedia of Condensed Matter Physics* 4 (2005), pp. 347–355.

[18] S. I. Pekar. "Local quantum states of an electron in an ideal ionic crystal". In: *Zh. Eksp. Teor. Fiz.* 16 (1946), p. 341.

[19] S. I. Pekar. "Autolocalization of the electron in a dielectric inertially polarizing medium". In: *Zh. Eksp. Teor. Fiz.* 16 (1946), p. 335.

[20] S. I. Pekar and M. F. Deigen. "The quantum states and the optical transitions of an electron in a polaron and in a color center in a crystal". In: *Zh. Eksp. Teor. Fiz.* 18.6 (1948), pp. 481–486.

[21] S. I. Pekar and L. Landau. "Effective mass of a polaron". In: *Zh. Eksp. Teor. Fiz.* 18.5 (1949), pp. 419–423.

[22] B. Gerlach and H. Löwen. "Analytical properties of polaron systems or: Do polaronic phase transitions exist or not?" In: *Reviews of Modern Physics* 63.1 (1991).

[23] H. Fröhich, H. Pelzer, and S. Zienau. "Properties of slow electrons in polar materials". In: *Philosophical Magazine Series 7* 41.314 (1950), pp. 221–242.

[24] F. M. Peeters, Wu Xiaoguang, and J. T. Devreese. "Ground state energy of a polaron in n dimensions". In: *Physical Review B* 33.6 (1986), pp. 3926–3934.

[25] J. Appel. *Solid State Physics - Advances in Research and Application*. Vol. 21. Academic Press Inc., 1968, pp. 193–391.

[26] T. Holstein. In: *Annals of Physics* 8 (1959), pp. 325–342.

[27] T. Holstein. In: *Annals of Physics* 8 (1959), pp. 343–389.

[28] C. G. Kuper and G. D. Whitfield. *Polarons and Excitons*. Plenum Press, 1963.

[29] T. K. Mitra, A. Chatterjee, and S. Mukhopadhyay. "Polarons". In: *Physics Reports (Review Section of Physics Letters)* 153.2&3 (1987), pp. 91–207.

[30] R. P. Feynman. *Statistical Mechanics - A set of lectures*. W. A. Benjamin, Inc., 1972.

[31] J. T. Devreese. "Polaron Physics in 2D and 3D". In: *Physica Scripta* T25 (1989), pp. 309–315.

[32] T-D. Lee, F. E. Low, and D. Pines. "The motion of slow electrons in a polar crystal". In: *Phys. Rev.* 90.2 (1953), pp. 297–302.

[33] M. Gurari. "Self energy of slow electrons in polar materials". In: *Phil. Mag.* 44 (1953), pp. 329–336.

[34] S. V. Tiablikov. In: *Zh. Eksp. i Teor. Fiz.* 22 (1952), p. 325.

[35] T-D. Lee and D. Pines. "The motion of slow electrons in polar crystals". In: *Phys. Rev.* 88 (1952), p. 960.

[36] B. Gerlach, F. Kalina, and M. Smondyrev. "On the LO-polaron dispersion in D dimensions". In: *phys. stat. sol.* 237.1 (2003), pp. 204–214.

[37] W. Xiaoguang and F. M. Peeters. "Exact and approximate results for the ground-state energy of a Frohlich polaron in two dimensions". In: *Physical Review B* 31.6 (1985), pp. 3420–3426.

[38] R. Evrard. "On the excited states of the polaron". In: *Physics Letters* 14.4 (1965), pp. 295–296.

[39] G. R. Allcock. In: *Advances in Physics* 5.20 (1956), pp. 412–451.

[40] F. M. Peeters and J. T. Devreese. In: *Physical Review B* 36.8 (1987), pp. 4442–4445.

[41] G. Whitfield and R. Puff. In: *Physical Review* 139.1A (1965), pp. 338–342.

[42] A. L. Fetter and J. D. Walecka. *Quantum Theory of Many-Particle Systems*. McGraw-Hill Book Company, 1971.

[43] R. D. Mattuck. *A Guide to Feynman Diagrams in the Many-Body Problem*. Dover Publications Inc., 1992.

[44] J. Ellis. In: (2016). arXiv:1601.05437 [hep-ph].

[45] D. Marchand. "Polaron Physics beyond the Holstein model". PhD thesis. The University of British Columbia, 2011.

[46] J. Gubernatis, N. Kawashima, and P. Werner. *Quantum Monte Carlo Methods*. Cambridge University Press, 2016.

[47] J. T. Titantah, C. Pierleoni, and S. Ciuchi. In: *Physical Review Letters* 87.20 (2001).

[48] J. M. Thijssen. *Computational Physics*. Cambridge University Press, 2007.

[49] N. Metropolis et al. In: *The Journal of Chemical Physics* 21.6 (1953), pp. 1087–1092.

[50] K. Van Houcke et al. In: *Physics Procedia* 6 (2010), pp. 95–105.

[51] C. M. Bishop. *Pattern Recognition and Machine Learning*. Springer, 2006.

[52] R. Rosenfelder and A. W. Schreiber. In: *Physics Letters A* 284 (2001), pp. 63–71.

[53] G. Whitfield and R. D. Puff. In: *Physics Letters* 10.1 (1964), pp. 9–10.